Available online at www.sciencedirect.com
SCIENCE DIRECT®
Nuclear Physics A 765 (2006) 126–187
NUCLEAR PHYSICS A

# Global study of nuclear structure functions

S.A. Kulagin [a,*], R. Petti [b]

[a] *Institute for Nuclear Research, 117312 Moscow, Russia*
[b] *CERN, CH-1211 Genéve 23, Switzerland*

Received 18 February 2005; received in revised form 17 October 2005; accepted 19 October 2005

Available online 14 November 2005

**Abstract**

We present the results of a phenomenological study of unpolarized nuclear structure functions for a wide kinematical region of $x$ and $Q^2$. As a basis of our phenomenology we develop a model which takes into account a number of different nuclear effects including nuclear shadowing, Fermi motion and binding, nuclear pion excess and off-shell correction to bound nucleon structure functions. Within this approach we perform a statistical analysis of available data on the ratio of the nuclear structure functions $F_2$ for different nuclei in the range from the deuteron to the lead. We express the off-shell effect and the effective scattering amplitude describing nuclear shadowing in terms of few parameters which are common to all nuclei and have a clear physical interpretation. The parameters are then extracted from statistical analysis of data. As a result, we obtain an excellent overall agreement between our calculations and data in the entire kinematical region of $x$ and $Q^2$. We discuss a number of applications of our model which include the calculation of the deuteron structure functions, nuclear valence and sea quark distributions and nuclear structure functions for neutrino charged-current scattering.


## 1. Introduction

The lepton Deep Inelastic Scattering (DIS) has been since long time a powerful tool to probe the structure of hadrons and nuclei at small and intermediate scales. After the discovery of the parton structure of nucleons, DIS remains to be the primary source of experimental information on the distribution of quark and gluon fields in the nucleon and nuclei and a valuable tool to test predictions of QCD. New data from high-intensity electron (Jefferson Laboratory) and neu-

* Corresponding author.
*E-mail addresses:* kulagin@ms2.inr.ac.ru (S.A. Kulagin), roberto.petti@cern.ch (R. Petti).

0375-9474/$ – see front matter 
doi:10.1016/j.nuclphysa.2005.10.011

trino (NuMI at Fermilab and JPARC in Japan) beams will allow in future to further extend our knowledge of the nucleon and nuclear structure from high-precision experiments.

The role of nuclei in DIS studies is dual. First, it should be noted that the study of nuclei at small space–time scales is interesting by itself and it can provide valuable insights into the origin of nuclear force and properties of hadrons in nuclear medium. On the other hand the nuclear data often serve as the source of information on hadrons otherwise not directly accessible. A typical example is the extraction of the neutron structure function which is usually obtained from deuterium and proton data in a wide kinematic region. This procedure requires, in turn, a detailed knowledge of nuclear effects in order to control the corresponding systematic uncertainties. Another example is the determination of nuclear parton distribution functions which are universal high-momentum transfer characteristics of complex nuclei.

Significant nuclear effects were discovered in charged lepton DIS experiments [1–13]. These observations rule out a simple picture of a nucleus as a system of quasi-free nucleons and indicate that the nuclear environment plays an important role even at energies and momenta much larger than those involved in typical nuclear ground state processes. The study of nuclei is therefore directly related to the interpretation of high-energy physics from hadron colliders to fixed target experiments. The measurements of nucleus–nucleus and proton–nucleus interactions at RHIC [15] and LHC [16] will help to clarify the nuclear modifications of the parton distributions, as well as to define the initial conditions towards the studies of new states of matter in heavy ion collisions.

The understanding of nuclear effects is particularly relevant for neutrino physics, where the tiny cross section with matter requires the use of heavy nuclear targets in order to collect a significant number of interactions. The presence of an axial-vector component in the weak current and the quark flavour selection differentiate neutrinos from charged leptons and imply a more complex description of nuclear effects in neutrino scattering. The role of nuclear corrections to neutrino structure functions has been recently emphasized [17] after the NuTeV collaboration reported a deviation from the Standard Model prediction for the value of the weak mixing angle ($\sin^2\theta_W$) measured in neutrino DIS [18]. One of the original motivations of the present work is indeed related to the extraction of the weak mixing angle from neutrino DIS data of the NOMAD experiment [19]. It must be remarked that nuclear effects are important not only in the determination of electroweak parameters, but also for the understanding of neutrino masses and mixing. The recent high-intensity NuMI [20] and JPARC [21] neutrino facilities offer the possibility to perform a detailed study of nuclear effects in neutrino interactions on a relatively short time scale. The construction of a future neutrino factory [22] would then allow to reach the ultimate precision of the neutrino probe.

The main experimental information on nuclear structure functions comes from charged-lepton scattering DIS experiments performed at CERN [2–8], SLAC [9,10], FNAL [11,12] and recently at JLab [13,23]. The measurements usually refer to the ratio $\mathcal{R}_2$ of the structure function $F_2$ of two nuclei (usually a complex nucleus to deuterium). Additional data from the Drell–Yan reaction of protons off nuclear targets are also available [14]. From the studies of data on the ratio $\mathcal{R}_2$ one can separate a few regions of characteristic nuclear effects: depletion of nuclear structure functions at small Bjorken $x$ ($x < 0.05$) known as shadowing region; a small enhancement of nuclear structure functions for $0.1 < x < 0.3$ (antishadowing); depletion with a minimum around $x = 0.6$–$0.7$ followed by a rise at large $x$ (known as "EMC effect" after the name of the experiment which discovered it). It is interesting to note that a clear $Q^2$ dependence has been reported only in the shadowing region, while for $0.1 < x < 0.6$ $\mathcal{R}_2$ is almost $Q^2$ independent. However, the data available on the $Q^2$ dependence of nuclear effects are still scarce. One of the

main drawbacks of all existing data is the strong correlation between $x$ and $Q^2$ resulting from the kinematics of fixed (stationary) target experiments. As a result, significant regions of the $(x, Q^2)$ plane are still uncovered in DIS experiments.

Many different theoretical models have been proposed to explain the basic features of data (for a detailed summary of the current understanding of nuclear corrections we refer to recent reviews and references cited therein [24–27], see also discussion in Section 4 of this paper). The modelling is important to derive some insights on the underlying physics of observed phenomena. However, consistent and quantitative description of nuclear effects in DIS in a wide kinematical region of $x$ and $Q^2$ and for a wide range of nuclei are clearly needed. In this paper we perform a quantitative study of data aiming to develop a model of nuclear DIS applicable in the analysis of existing data and in the interpretation of future experiments. In order to describe nuclear data over a wide kinematical region we take into account many effects including nuclear shadowing, nuclear pion excess, Fermi motion, nuclear binding and off-shell corrections to bound nucleon structure functions. It should be noted that if some effects, such as Fermi motion and nuclear binding, are well constrained by other studies or data, the remaining ones are less known. The main example is the off-shell correction which describes the modification of structure functions of bound nucleons in nuclear environment. We study this effect phenomenologically by parameterizing the off-shell correction to the nucleon structure function in terms of a few parameters which are fixed from statistical analysis of nuclear data, together with the corresponding uncertainties. It is worth to emphasize that these parameters are universal, i.e. common for all nuclei, since they are related to the nucleon structure. In a certain sense the off-shell correction can be considered as a new structure function which describes the response of the nucleon parton distributions to the variation of the nucleon invariant mass. Even if this structure function is not accessible for free proton and neutron, it can be probed in nuclear reactions.

It should be also emphasized that different nuclear effects in different kinematical regions of $x$ are correlated by DIS sum rules. For example, the light-cone momentum sum rule links bound nucleon and pion contributions to DIS. We use this requirement in order to constrain mesonic contributions to nuclear structure functions. Another example is the baryon number sum rule which links shadowing and off-shell corrections. In our approach the off-shell effect provides the mechanism of cancellation of a negative nuclear-shadowing contribution to the normalization of nuclear valence quark distributions.

After fixing the parameters of our model, we compute predictions for a number of applications. In particular, we discuss nuclear valence and sea quarks at high $Q^2$ and compute nuclear corrections to neutrino structure functions. These subjects will be treated more extensively in future publications.

The paper is organized as follows. In Section 2 we briefly summarize the DIS kinematics for electron (muon) and neutrino scattering and introduce notations used in this paper. Section 3 provides information on the nucleon structure functions and parton distributions necessary for our analysis. Section 4 is devoted to the theoretical framework to treat different nuclear corrections in our studies. In particular, in Section 4.1 we examine the derivation of nuclear structure functions in the approximation of incoherent scattering off bound nucleons and nuclear pions (Section 4.1.3), the off-shell effects in the structure functions and quark distributions (Section 4.1.6) and coherent nuclear effects leading to nuclear shadowing and antishadowing (Section 4.2). In Section 5 we discuss in detail the nuclear input which is used in our analysis (Sections 5.1 to 5.3), the model of off-shell effects (Section 5.4) and effective scattering amplitude (Section 5.5). The analysis of data is described in Sections 5.6 and 5.7. In Section 6 we present the results obtained from our fits to nuclear data. The $Q^2$ and $A$ dependence of nuclear

effects are discussed in Sections 6.4 to 6.5. In Section 7 we apply our approach to study nuclear parton distributions (Section 7.1) and neutrino structure functions (Section 7.2). In Appendix A we provide the details of the integration in nuclear convolution and in Appendix B the multiple scattering coefficients are given.

## 2. Kinematics of lepton inelastic scattering

Consider the scattering of a *charged lepton* (electron or muon) off a nucleon with the four-momentum $p = (E_p, \boldsymbol{p})$ and mass $M$. The scattering matrix element to leading order in the electromagnetic coupling constant $\alpha = e^2/4\pi \approx 1/137$ is determined by the standard one-photon exchange process. In inclusive scattering, the final hadronic state is not detected and the differential cross section is fully given by hadronic tensor $W_{\mu\nu}$, which is the sum of hadronic matrix elements of the electromagnetic current $J^{\rm em}_\mu$ over all final hadronic states (see, e.g., [28])

$$W_{\mu\nu}(p,q) = \frac{1}{4\pi}\sum_n (2\pi)^4 \delta(p+q-p_n)\langle p|J^{\rm em}_\mu(0)|n\rangle\langle n|J^{\rm em}_\nu(0)|p\rangle, \tag{1}$$

where $q$ is four-momentum transfer to the target.

We do not consider the polarization effects and assume the averaging over the target and beam polarizations. Then only the symmetric part of the hadronic tensor contributes to the cross section. Because of the conservation of electromagnetic current, time reversal invariance and parity conservation in electromagnetic interaction, the symmetric hadronic tensor has only 2 independent Lorentz structures (see, e.g., [28])

$$W_{\mu\nu}(p,q) = -\tilde{g}_{\mu\nu} F_1 + \tilde{p}_\mu \tilde{p}_\nu \frac{F_2}{p\cdot q}, \tag{2}$$

where $F_{1,2}$ are Lorentz-invariant structure functions, and, for simplicity, we use the following notations:

$$\tilde{g}_{\mu\nu} = g_{\mu\nu} - \frac{q_\mu q_\nu}{q^2}, \tag{3a}$$

$$\tilde{p}_\mu = p_\mu - q_\mu \frac{p\cdot q}{q^2}. \tag{3b}$$

We use the normalization of states $\langle p|p'\rangle = 2E_{\boldsymbol{p}}(2\pi)^3\delta(\boldsymbol{p}-\boldsymbol{p}')$ for both bosons and fermions. With this normalization the hadronic tensor and the structure functions $F_{1,2}$ are dimensionless.

The structure functions are the functions of two independent invariant variables. In deep inelastic regime the Bjorken variable $x = Q^2/(2p\cdot q)$ and four-momentum transfer squared $Q^2 = -q^2$ are usually used as the variables the structure functions depend on.

The polarization averaged differential cross section is determined by the structure functions $F_{1,2}$. In terms of the variables $x$ and $Q^2$ the cross section reads

$$\frac{{\rm d}^2\sigma}{{\rm d}x\,{\rm d}Q^2} = \frac{4\pi\alpha^2}{xQ^4}\left[\left(1-y-\frac{(Mxy)^2}{Q^2}\right)F_2 + xy^2\left(1-\frac{2m_l^2}{Q^2}\right)F_1\right], \tag{4}$$

where $y = p\cdot q/p\cdot k$. The variable $y$ is not independent variable and related to $x$ and $Q^2$ via the equation $xy = Q^2/(2p\cdot k)$. The lepton mass term is kept in Eq. (4) for the sake of completeness. Although it is negligible in electron deep inelastic scattering, it might be relevant for muon scattering at small momentum transfer or for $\tau$ lepton scattering.

The structure functions $F_{1,2}$ can be related to the virtual photon helicity cross sections by projecting Eq. (1) onto the states with definite photon polarizations. These states are described by the photon polation vectors. In the reference frame, in which the momentum transfer is along the $z$-axis, $q = (q_0, \mathbf{0}_\perp, q_z)$, $q_z = -|\boldsymbol{q}|$ the photon polarization vectors are

$$e_\pm = (0, 1, \pm i, 0)/\sqrt{2}, \tag{5a}$$

$$e_0 = (q_z, \mathbf{0}_\perp, q_0)/Q, \tag{5b}$$

where $Q = \sqrt{Q^2}$. The polarization vectors $e_+$ and $e_-$ describe transversely polarized states with helicities $+1$ and $-1$, respectively (right- and left-polarized photons). The vector $e_0$ corresponds to the longitudinally polarized (scalar) virtual photons. The polarization vectors are orthogonal to momentum transfer, $e_\pm \cdot q = e_0 \cdot q = 0$, and obey the orthogonality and the normalization conditions, $e_\pm \cdot e_0 = 0$, $e_\pm^* \cdot e_\pm = -1$, $e_0^2 = 1$.

The helicity structure functions are

$$W_\pm = e_\pm^{\mu\,*} W_{\mu\nu} e_\pm^\nu = F_1, \tag{6a}$$

$$W_0 = e_0^{\mu *} W_{\mu\nu} e_0^\nu = \gamma^2 F_2/(2x) - F_1, \tag{6b}$$

where $\gamma = |\boldsymbol{q}|/q_0 = (1 + 4x^2M^2/Q^2)^{1/2}$. In applications the transverse and the longitudinal structure functions are commonly used

$$F_T = x(W_+ + W_-) = 2x F_1, \tag{7a}$$

$$F_L = 2x W_0 = \gamma^2 F_2 - 2x F_1. \tag{7b}$$

Let us briefly consider the scattering of (anti)neutrino. In the Standard Model neutrino can either couple to charged $W^\pm$ bosons or to neutral $Z$ boson. In the former case interaction is driven by *charged curent* (CC) $J_\mu^\pm = V_\mu^\pm - A_\mu^\pm$ with $V_\mu^\pm$ and $A_\mu^\pm$ the charged components of the vector and axial-vector current. The interaction with $Z$ boson is described by the *neutral current* (NC) which is the superposition of the isovector weak left current and electromagnetic current $J_\mu^0 = \sqrt{2}(V_\mu^3 - A_\mu^3 - 2\sin^2\theta_W J_\mu^{\rm em})$, where $\theta_W$ is the Weinberg weak mixing angle.

The hadronic tensor for CC or NC interaction is given by Eq. (1) with the electromagnetic current replaced by the corresponding weak current. The Lorentz decomposition of hadronic tensor is different for neutrino case and includes additional terms compared to Eq. (2). For example, for CC neutrino interaction we have[1] (see, e.g., [28])

$$W_{\mu\lambda}^\pm = -\tilde{g}_{\mu\lambda} F_1^{W^\pm} + \tilde{p}_\mu \tilde{p}_\lambda \frac{F_2^{W^\pm}}{p\cdot q} + i\varepsilon_{\mu\lambda}(p,q)\frac{F_3^{W^\pm}}{2p\cdot q} + \frac{q_\mu q_\lambda}{Q^2} F_4^{W^\pm} + \frac{q_\mu p_\lambda + q_\lambda p_\mu}{p\cdot q} F_5^{W^\pm}, \tag{8}$$

where we denote $\varepsilon_{\mu\lambda}(a,b) = \varepsilon_{\mu\lambda\alpha\beta} a^\alpha b^\beta$. The first two terms with $F_1$ and $F_2$ in Eq. (8) are similar to those in charged-lepton scattering and appear due to VV and AA interactions in Eq. (1). The term with $F_3$ describes parity-violating VA and AV interference. The terms $F_4$ and $F_5$ are present because the axial current does not conserve. The contributions from the structure functions $F_4$

[1] The tensor $W_{\mu\lambda}^+$ corresponds to interaction mediated by $W^+$ boson and describes neutrino CC scattering while $W_{\mu\lambda}^+$ describes antineutrino. It should also be remarked that the neutrino and antineutrino NC structure functions are identical, since neutrino and antineutrino in NC scattering couple to the same hadronic NC. This is not the case for CC neutrino and antineutrino structure functions.

and $F_5$ to the neutrino production cross section are suppressed by a small ratio $m_l^2/(ME)$ (these terms vanish in the NC cross section). It was also shown that $F_4 = 0$ and $2xF_5 = F_2$ in the leading order and in the limit of massless quarks (Albright–Jarlskog relations [29]). Recently it was argued that the second of these relations survives the higher order and the target mass corrections in massless QCD, while the relation for $F_4$ should be replaced by $F_4 = F_2/(2x) - F_1$ [30].

The relations between the helicity structure functions and the structure functions $F_{1,2,3}$ in the neutrino scattering are

$$W_\pm = F_1 \pm \gamma F_3, \tag{9a}$$

$$W_0 = \gamma^2 F_2/(2x) - F_1. \tag{9b}$$

The definition of $F_{T,L}$ by Eq. (7) also apply in this case. One observes from Eqs. (9) that the structure function $F_3$ determines the left–right asymmetry in the transverse helicity structure functions.

## 3. Nucleon structure functions

The structure functions remain important observables to probe QCD structure of proton and neutron and nuclei. In this section we briefly review the characteristics of nucleon structure functions necessary for our analysis.

### 3.1. QCD perturbative regime

In the region of $Q^2$ large compared to the nucleon scale the structure functions can be analyzed in perturbative QCD. A working tool of this analysis is the operator product expansion (OPE) [31]. Using the OPE, the contributions from different quark-gluon operators to hadronic tensor can be ordered according to their *twist*. For the DIS structure functions this leads to the expansion in inverse powers of $Q^2$:

$$F_a\big(x, Q^2\big) = F_a^{LT}\big(x, Q^2\big) + \frac{H_a(x, Q^2)}{Q^2} + \mathcal{O}\big(1/Q^4\big), \tag{10}$$

where $a$ labels the type of the structure function ($a = T, 2, 3$). The first term is the leading twist (LT) contribution and $H_a$ are the twist-4 contributions (higher twist, HT).

The *leading twist* contribution is directly related to the distributions of quarks and gluons inside the nucleon, the parton distribution functions (PDFs) via the DIS factorization theorem as a convolution with coefficient functions (for more detail see, e.g., Ref. [32] and references therein). The coefficient functions depend on the process and the type of the structure function but are independent of the target. These functions are computable as power series in $\alpha_S$. The parton distributions are independent of the process but do depend on the target.

The PDFs have non-perturbative origin and cannot be calculated in perturbative QCD. However, the $Q^2$ dependence of the PDFs can be handled using QCD perturbation theory, and is governed by the well-known DGLAP evolution equations with the kernel given by the splitting functions [33].

The one-loop (NLO) coefficient and splitting functions have been computed since long time [34]. The two-loop (NNLO) coefficient functions [35] and the corresponding splitting functions [36] are now also available. In our analysis of nuclear data we use both the coefficient functions and the PDFs to NNLO approximation calculated in $\overline{\text{MS}}$ scheme using the factorization and the renormalization scales set to $Q^2$.

The HT components involve interactions between quarks and gluons and lack simple probabilistic interpretation.

It must be noted that the twist expansion was derived in the massless limit. If a finite mass for the nucleon target is considered, the new terms arise in Eq. (10) that mix operators of different spin, leading to additional power terms of kinematical origin—the so-called *target mass corrections* (TMC). If the parameter $x^2M^2/Q^2$ is small, the TMC series can be absorbed in the leading twist term [37]. Therefore, Eq. (10) remains valid with the LT terms replaced by

$$F_T^{\rm TMC}(x,Q^2) = \frac{x^2}{\xi^2\gamma}F_T^{\rm LT}(\xi,Q^2) + \frac{2x^3M^2}{Q^2\gamma^2}\int\limits_\xi^1 \frac{{\rm d}z}{z^2}F_2^{\rm LT}(z,Q^2), \tag{11a}$$

$$F_2^{\rm TMC}(x,Q^2) = \frac{x^2}{\xi^2\gamma^3}F_2^{\rm LT}(\xi,Q^2) + \frac{6x^3M^2}{Q^2\gamma^4}\int\limits_\xi^1 \frac{{\rm d}z}{z^2}F_2^{\rm LT}(z,Q^2), \tag{11b}$$

$$xF_3^{\rm TMC}(x,Q^2) = \frac{x^2}{\xi^2\gamma^2}\xi F_3^{\rm LT}(\xi,Q^2) + \frac{2x^3M^2}{Q^2\gamma^3}\int\limits_\xi^1 \frac{{\rm d}z}{z^2}zF_3^{\rm LT}(z,Q^2), \tag{11c}$$

where $\gamma = (1+4x^2M^2/Q^2)^{1/2}$ and $\xi = 2x/(1+\gamma)$ is the Nachtmann variable [38].

However, it must be remarked that the derivation of [37] was given in the zeroth order in $\alpha_S$, assuming that the target quarks are on-shell and neglecting the transverse degrees of freedom. Furthermore, Eqs. (11) suffer the so-called threshold problem. Indeed, it follows from Eqs. (11) that the target mass corrected inelastic structure functions $F_2^{\rm TMC}$ remain finite as $x\to 1$ even if the LT terms vanish in this limit. Clearly, the region $x$ close to 1 is beyond the applicability of Eqs. (11). However, in the applications to nuclear structure functions at large $x$ it is important to meet the threshold condition. One possible way to deal with this problem is to expand Eqs. (11) in power series in $Q^{-2}$ and keep a finite number of terms. In particular, keeping the LT and the $1/Q^2$ term we have

$$F_T^{\rm TMC}(x,Q^2) = F_T^{\rm LT}(x,Q^2) + \frac{x^3M^2}{Q^2}\left(2\int\limits_x^1 \frac{{\rm d}z}{z^2}F_2^{\rm LT}(z,Q^2) - \frac{\partial}{\partial x}F_T^{\rm LT}(x,Q^2)\right), \tag{12a}$$

$$F_2^{\rm TMC}(x,Q^2) = \left(1-\frac{4x^2M^2}{Q^2}\right)F_2^{\rm LT}(x,Q^2) + \frac{x^3M^2}{Q^2}\left(6\int\limits_x^1 \frac{{\rm d}z}{z^2}F_2^{\rm LT}(z,Q^2) - \frac{\partial}{\partial x}F_2^{\rm LT}(x,Q^2)\right), \tag{12b}$$

$$xF_3^{\rm TMC}(x,Q^2) = \left(1-\frac{2x^2M^2}{Q^2}\right)xF_3^{\rm LT}(x,Q^2) + \frac{x^3M^2}{Q^2}\left(2\int\limits_x^1 \frac{{\rm d}z}{z^2}zF_3^{\rm LT}(z,Q^2) - \frac{\partial}{\partial x}\left(xF_3^{\rm LT}(x,Q^2)\right)\right). \tag{12c}$$

In this approximation the structure functions have a correct threshold behavior and vanish in the limit of $x \to 1$, provided that the LT terms and their derivatives vanish in this limit.

In general, the target mass corrections should also be applied to the HT terms in the higher order terms in the twist expansion (10). In this paper we only consider twist 2 and 4 terms. For consistency we do not consider $1/Q^4$ terms in Eqs. (11), (12) and do not apply TMC to HT terms. We also note, that the extrapolation of the target mass corrections to off-shell region $p^2 \neq M^2$ is important in the treatment of the nuclear effects and will be discussed in Section 4.1.6.

### *3.2. Structure function phenomenology*

The twist expansion and PDFs as universal, process-independent characteristics of the target are at the basis of extensive QCD phenomenology of high-energy processes. In phenomenological studies, the PDFs are extracted from QCD global fits. A number of such analyses are available [39–41]. In our studies of nuclear data described in Sections 5.6 to 6.5 we use the results by Alekhin [39] who provides the set of the nucleon PDFs obtained with the coefficient and splitting functions calculated to the NNLO approximation.[2] Furthermore, the HT terms and the PDF uncertainties have also been evaluated in [39].

It should be also remarked that the twist expansion and perturbative QCD apparently breaks down at low $Q^2$. Furthermore, the conservation of electromagnetic current requires the structure function $F_2$ to vanish as $Q^2$ for $Q^2 \to 0$. The data seem to indicate the presence of a transition region between perturbative and non-perturbative regimes at $Q^2$ about 1 GeV$^2$. In our studies of nuclear effects in the structure functions some data points at small $x$ are in the low-$Q^2$ region. In order to match low-$Q$ and high-$Q$ regions we apply spline interpolations for the structure functions which obeys the current conservation requirements.

## 4. Nuclear structure functions

In this section we describe a theoretical framework which will be the basis of phenomenological studies of nuclear DIS data discussed in Sections 5 to 6.

The mechanisms of nuclear DIS appear to be different for small and large Bjorken $x$ as viewed from the laboratory system. The physics scale for this separation comes from the comparison of a characteristic DIS time, which is also known as Ioffe length $L_I = 1/(Mx)$ (see, e.g., Ref. [28]), and an average distance between bound nucleons in nuclei which is about 1.5 Fm. At large $x > 0.1$ the characteristic DIS time is smaller than average internucleon distance. This observation justifies the use of the incoherent approximation for the nuclear Compton amplitude in this region. It was realized long ago that the nucleon momentum distribution (*Fermi motion*) is important effect even in the scaling limit and results in the enhancement of nuclear structure functions at large Bjorken $x$ [43]. After discovery of the EMC effect [1] the calculation of nuclear DIS in impulse approximation was revisited [44,46,48–50] and effect of *nuclear binding* was emphasised which explains a significant part of the observed dip in the EMC ratio at $x \sim 0.6$ (for a review of the EMC effect and more references see [25–27]).

Effects beyond the impulse approximation are important. It should be noted that because of binding, the nucleons do not carry all of the light-cone momentum of the nucleus and the mo-

[2] In our analysis we use PDFs obtained from new fits optimized in the low $Q^2$ region and including additional data with respect to [39]. This extraction of PDFs also takes into account the nuclear effects in the deuterium data as described in the present paper (see Section 5.7). Results from the new fits will be reported elsewhere.

mentum sum rule is violated in the impulse approximation. A natural way to correct this problem is to explicitly consider the pion contribution to the structure functions [54] which balances missing momentum. Several calculations of the *pion correction* to nuclear structure functions have been performed in different approaches and approximations [55]. Although all calculations predict some enhancement at small $x$, the concrete predictions are model-dependent. In this paper we calculate nuclear pion correction following the approach of Ref. [47] in which the pion contribution was constrained using the equations of motion for interacting pion–nucleon system. By using the light-cone momentum balance equation we effectively constrain the contribution from all mesonic fields responsible for nuclear binding.

It should be noted that bound nucleons are off-shell particles and their structure functions can be different from those of free nucleons. *Off-shell effects* in nuclear DIS were discussed in a number of papers [45,46,48,50,51,53]. It was shown that, because of spin $1/2$, the off-shell nucleon is characterized by the increased number of structure functions which depend on the nucleon virtuality as an additional variable [48–51]. However, in the vicinity of the mass shell (which is the relevant case for nuclei) the off-shell nucleon can still be described by the same number of structure functions as the on-shell nucleon [48–50]. Nevertheless, the off-shell dependence of structure functions remains an important effect through which the modification of the internal structure of the bound nucleon in nuclear environment can be assessed. It should be also emphasized that the off-shell effect provides the specific mechanism of balancing a negative contribution to the nuclear baryon number sum rule from nuclear shadowing effect (for details see Sections 6.1 and 6.2). In Section 4.1 we discuss the derivation of the nuclear structure functions in the presence of off-shell effects with the full consideration of the nucleon spin. The treatment of the off-shell effect in the parton distributions is discussed in more detail in Sections 4.1.6 and 5.4.

In the small-$x$ region the space–time picture of DIS is different. For $x \ll 0.1$ the characteristic DIS time is large on the nuclear scale, the nuclear DIS becomes "stretched" in time and in the longitudinal direction. The process can be viewed as the intermediate boson first fluctuates into a quark pair which can form a complex configuration (hadronic or quark-gluon) which then scatters off the target. As an average time of life of such fluctuation is large compared to average distance between bound nucleons, the photon interaction with nuclear targets resembles hadronic properties [57,58]. In particular, since hadron scattering amplitudes are almost imaginary at high energy, the double scattering correction to the DIS cross section is negative leading to nuclear *shadowing* effect, similar to that in hadron scattering [56]. Nuclear shadowing in DIS was subject to intensive studies [60] (for a review of nuclear shadowing and more references see, e.g., [24,27]). In the present paper we treat nuclear shadowing effect in a semi-phenomenological approach by introducing phenomenological amplitude which describes interaction of hadronic component of the intermediate boson with the nucleon and consider the propagation of this state in nuclear environment using multiple scattering theory. Details are discussed in Section 4.2.

Summarizing we write the nuclear structure functions as the sum of incoherent and coherent contributions

$$F_a^A = F_a^{p/A} + F_a^{n/A} + F_a^{\pi/A} + \delta F_a^A, \tag{13}$$

where $F_a^{p/A}$, $F_a^{n/A}$, $F_a^{\pi/A}$ denote the contributions to the structure function of type $a$ from bound protons, neutrons, and nuclear pions, respectively. The last term in Eq. (13) is a correction due to nuclear coherent interaction. The exact meaning of all these terms will be explained in the following sections.

### 4.1. Incoherent scattering approximation

The DIS hadronic tensor is given by the imaginary part of the virtual photon Compton amplitude in the forward direction. In the incoherent scattering regime (large $x$) taking into account the nucleon spin the nuclear hadronic tensor can be written as (see also [47–49])

$$W^A_{\mu\nu}(P_A,q)=\sum_{\tau=p,n}\int [\mathrm{d}p]\,\mathrm{Tr}\big[\hat{\mathcal{W}}^\tau_{\mu\nu}(p,q)\mathcal{A}^\tau(p;A)\big], \tag{14}$$

where the sum is taken over the protons and neutrons, Tr is taken in the nucleon Dirac space and the integration is performed over the nucleon four-momentum, $[\mathrm{d}p]=\mathrm{d}^4p/(2\pi)^4$. In Eq. (14) $\mathcal{A}^\tau(p;A)$ is the imaginary part of the proton ($\tau=p$) or the neuteron ($\tau=n$) propagator in the nucleus

$$\mathcal{A}^\tau_{\alpha\beta}(p;A)=\int \mathrm{d}t\,\mathrm{d}^3\boldsymbol{r}\,e^{ip_0t-i\boldsymbol{p}\cdot\boldsymbol{r}}\langle A|\bar{\Psi}^\tau_\beta(t,\boldsymbol{r})\,\Psi^\tau_\alpha(0)|A\rangle \tag{15}$$

with $\Psi^\tau_\alpha(t,\boldsymbol{r})$ the nucleon field operator and $\alpha$ and $\beta$ the Dirac spinor indeces. The off-shell nucleon electromagnetic tensor $\hat{\mathcal{W}}_{\mu\nu}(p,q)$ is the matrix in the Dirac space. On the mass shell $p^2=M^2$, averaging $\hat{\mathcal{W}}_{\mu\nu}(p,q)$ over the nucleon polarizations we obtain the nucleon tensor (2)

$$W^\tau_{\mu\nu}(p,q)=\frac{1}{2}\,\mathrm{Tr}\big[(\not{p}+M)\hat{\mathcal{W}}^\tau_{\mu\nu}(p,q)\big]. \tag{16}$$

In off-shell region, the Lorentz tensor structure of $\hat{\mathcal{W}}_{\mu\nu}$ is more involved than the corresponding structure of the on-shell nucleon tensor. In order to establish the tensor structure of $\hat{\mathcal{W}}_{\mu\nu}$ we expand the latter in terms of a complete set of Dirac matrices $\{I,\gamma^\alpha,\sigma^{\alpha\beta},\gamma^\alpha\gamma_5,\gamma_5\}$. The various coefficients in this expansion must be constructed from the vectors $p$ and $q$, and from the symmetric tensor $g_{\alpha\beta}$ and the antisymmetric tensor $\varepsilon_{\mu\nu\alpha\beta}$. For the symmetric part of $\hat{\mathcal{W}}_{\mu\nu}$ we keep only those terms which are even under time-reversal and parity transformations, since only such terms can contribute to $F_{1,2}$. Keeping only current-conserving terms we have 7 independent Lorentz–Dirac structures which can be written as [48,51]

$$\begin{aligned}2\hat{\mathcal{W}}^{\mathrm{sym}}_{\mu\nu}(p,q)=&-\tilde{g}_{\mu\nu}\left(\frac{f_1^{(0)}}{M}+\frac{f_1^{(1)}\not{p}}{M^2}+\frac{f_1^{(2)}\not{q}}{p\cdot q}\right)\\&+\frac{\tilde{p}_\mu\tilde{p}_\nu}{p\cdot q}\left(\frac{f_2^{(0)}}{M}+\frac{f_2^{(1)}\not{p}}{M^2}+\frac{f_2^{(2)}\not{q}}{p\cdot q}\right)+\frac{f_2^{(3)}}{p\cdot q}\,\tilde{p}_{\{\mu}\tilde{g}_{\nu\}\alpha}\gamma^\alpha,\end{aligned} \tag{17}$$

where $\tilde{g}_{\mu\nu}$ and $\tilde{p}_\mu$ are given by Eq. (3). The curly braces in the last term denote symmetryzation over Lorentz indeces, i.e. $a_{\{\mu}b_{\nu\}}=\frac{1}{2}(a_\mu b_\nu+a_\nu b_\mu)$. The coefficients $f_i^{(j)}$ in Eq. (17) are the dimensionless Lorentz-invariant functions of $x$, $Q^2$ and the nucleon offshellness $p^2$.

Similar analysis can also be applied to the antisymmetric part of $\hat{\mathcal{W}}_{\mu\nu}$ for the neutrino scattering. This term is described by the structure functions $F_3$ in Eq. (8). For off-shell nucleon the result can be written as [50]

$$2\hat{\mathcal{W}}^{\mathrm{asym}}_{\mu\nu}(p,q)=\frac{i\,\varepsilon_{\mu\nu\alpha\beta}}{2\,p\cdot q}\,q^\alpha\left[\left(\frac{f_3^{(0)}}{M}+\frac{f_3^{(1)}\not{p}}{M^2}+\frac{f_3^{(2)}\not{q}}{p\cdot q}\right)p^\beta+f_3^{(3)}\gamma^\beta\right], \tag{18}$$

where the coefficients $f_3^{(j)}$ are dimensionless Lorentz-invariant functions of $x$, $Q^2$ and $p^2$.

By substituting Eqs. (17) and (18) into Eq. (16) one observes that at $p^2 = M^2$ Eqs. (2) and (8) are recovered with the nucleon structure functions given by

$$F_1 = f_1^{(0)} + f_1^{(1)} + f_1^{(2)}, \tag{19a}$$

$$F_2 = f_2^{(0)} + f_2^{(1)} + f_2^{(2)} + f_2^{(3)}, \tag{19b}$$

$$F_3 = f_3^{(0)} + f_3^{(1)} + f_3^{(2)} + f_3^{(3)}. \tag{19c}$$

It should be noted that the Dirac equation is the underlying reason of simplification of the Lorentz structure of the hadronic tensor of the on-shell nucleon.

One important observation which follows from this analysis is that Eq. (14) does not factorize into completely separate nuclear and nucleon parts. The off-shell nucleon is described by 7 independent structure functions in the symmetric $P$-even hadronic tensor ($f_1^{(i)}$ and $f_2^{(i)}$) and 4 independent structure functions $f_3^{(i)}$ in the $P$-odd antisymmetric hadronic tensor. These functions depend on $p^2$ as an additional variable and weighted in Eq. (14) with generally different nuclear distributions.

Clearly, the fact that we have to deal with unknown functions not present for the on-shell nucleon introduces additional uncertainty in the calculation of nuclear structure functions. However, in practice it may be quite sufficient to treat nuclei as non-relativistic systems. In this limit the nuclear hadronic tensor considerably simplifies, as will be discussed in the next section.

*4.1.1. The limit of weak nuclear binding*

Let us now discuss Eq. (14) in the limit of weak nuclear binding. We assume that the nucleus is a non-relativistic system with small characteristic momentum and energy of bound nucleons, $|\boldsymbol{p}| \ll M$, $|p_0 - M| \gg M$. The antinucleon degrees of freedom are neglected in this approximation. A non-relativistic approximation to Eq. (14) is derived using the relation between the relativistic four-component nucleon field $\Psi$ and the non-relativistic two-component operator $\psi$ (for simplicity we suppress the isospin index $\tau$)

$$\Psi(\boldsymbol{p}, t) = e^{-iMt} \begin{pmatrix} (1 - \boldsymbol{p}^2/8M^2)\,\psi(\boldsymbol{p}, t) \\ (\boldsymbol{\sigma}\cdot\boldsymbol{p}/2M)\,\psi(\boldsymbol{p}, t) \end{pmatrix}, \tag{20}$$

where the nucleon operators are taken in a mixed $(\boldsymbol{p}, t)$ representation. The renormalization operator $1 - \boldsymbol{p}^2/(8M^2)$ is introduced to provide a correct normalization of non-relativistic nucleon field $\psi$, i.e. the operator $\psi^\dagger\psi$ is normalized to the nucleon number to order $\boldsymbol{p}^2/M^2$.

In order to make the non-relativistic reduction of Eq. (14), we separate the nucleon mass from the energy $p_0$ and write the four-momentum of the bound nucleon as $p = (M + \varepsilon, \boldsymbol{p})$. We then substitute Eq. (20) into Eq. (14) and reduce the four-dimensional Dirac basis to the two-dimensional spin matrices. In this way we examine all Lorentz–Dirac structures in Eqs. (17) and (18) and keep the terms to order $\varepsilon/M$ and $\boldsymbol{p}^2/M^2$. The result can be summarized as follows:

$$\frac{1}{M_A}\,\mathrm{Tr}\big(\mathcal{A}(p; A)\,\hat{\mathcal{W}}_{\mu\nu}(p, q)\big) = \frac{1}{M + \varepsilon}\,\mathcal{P}(\varepsilon, \boldsymbol{p})\,W_{\mu\nu}(p, q), \tag{21}$$

where $M_A$ is the mass of a nucleus $A$ and

$$\mathcal{P}(\varepsilon, \boldsymbol{p}) = \int \mathrm{d}t\, \exp(-i\varepsilon t)\langle A|\psi^\dagger(\boldsymbol{p}, t)\psi(\boldsymbol{p}, 0)|A\rangle/\langle A|A\rangle \tag{22}$$

is the non-relativistic nuclear spectral function normalized to the number of nucleons in the corresponding isospin state

$$\int [\mathrm{d}p]\, \mathcal{P}^{p,n}(\varepsilon, \boldsymbol{p}) = (Z, N). \tag{23}$$

Note that the factor $M_A$ in the left side of (21) is absorbed in the normalization of nuclear states $\langle A|A\rangle$ in Eq. (22). The hadronic tensor $W_{\mu\nu}(p,q)$ in Eq. (21) is given by Eq. (2) with the structure functions

$$F_1\big(x, Q^2, p^2\big) = f_1^{(0)}\left(1 + \frac{p^2 - M^2}{2M^2}\right) + f_1^{(1)}\frac{p^2}{M^2} + f_1^{(2)}, \tag{24a}$$

$$F_2\big(x, Q^2, p^2\big) = f_2^{(0)}\left(1 + \frac{p^2 - M^2}{2M^2}\right) + f_2^{(1)}\frac{p^2}{M^2} + f_2^{(2)} + f_2^{(3)}, \tag{24b}$$

$$F_3\big(x, Q^2, p^2\big) = f_3^{(0)}\left(1 + \frac{p^2 - M^2}{2M^2}\right) + f_3^{(1)}\frac{p^2}{M^2} + f_3^{(2)} + f_3^{(3)}. \tag{24c}$$

From Eq. (21) we obtain a non-relativistic approximation to the nuclear hadronic tensor (14)

$$\frac{W^A_{\mu\nu}(P_A, q)}{M_A} = \sum_{\tau=p,n}\int \frac{[\mathrm{d}p]}{M+\varepsilon}\mathcal{P}^{\tau}(\varepsilon, \boldsymbol{p})\, W^{\tau}_{\mu\nu}(p,q), \tag{25}$$

which is a basic equation for further analysis of nuclear DIS.

A few comments are in order. It should be emphasized that the non-relativistic limit is taken with respect to the nucleon momentum. In the derivation of Eq. (21) we keep terms to order $\boldsymbol{p}^2/M^2$ and $\varepsilon/M$ and neglect the higher-order terms. Furthermore, Eq. (21) is valid for arbitrary momentum transfer $q$. Note the factorization of the high-energy amplitude $W_{\mu\nu}$ from the spectral function $\mathcal{P}$ which describes the low-energy part of the problem. In the vicinity of the mass shell the hadronic tensor involves the same number of independent structure functions as on the mass shell. Therefore the problem of "splitting" of structure functions in the off-shell region (i.e. the problem of additional nucleon structure functions) can be avoided in this region. Eqs. (24) give the nucleon structure functions in the off-shell region in the vicinity of the mass-shell and it is easy to see that Eqs. (24) reduce to Eqs. (19) at $p^2 = M^2$ thus assuring a correct on-shell limit.

Let us extract the relations between the nuclear and the nucleon structure functions from Eq. (25). Nuclear structure functions are given by Eq. (2) with $p$ replaced by $P_A$ and $x$ by $x_A = Q^2/(2M_A q_0)$. However, it is convenient to consider the nuclear structure functions as the functions of the variable $x = Q^2/(2Mq_0)$ instead of the "natural" nuclear scaling variable $x_A$. We then define $F^A_{T,L}(x, Q^2) = F^A_{T,L}(x_A, Q^2)$ and $xF^A_3(x, Q^2) = x_A F^A_3(x_A, Q^2)$. In order to separate the structure functions we contract the both sides of Eq. (25) with the virtual photon polarization vectors (5) and consider the helicity structure functions. As a result we have

$$F^A_T\big(x, Q^2\big) = \sum_{\tau=p,n}\int [\mathrm{d}p]\mathcal{P}^{\tau}(\varepsilon, \boldsymbol{p})\left(1 + \frac{\gamma p_z}{M}\right)\left(F^{\tau}_T + \frac{2x'^2\boldsymbol{p}^2_{\perp}}{Q^2}F^{\tau}_2\right), \tag{26a}$$

$$F^A_L\big(x, Q^2\big) = \sum_{\tau=p,n}\int [\mathrm{d}p]\mathcal{P}^{\tau}(\varepsilon, \boldsymbol{p})\left(1 + \frac{\gamma p_z}{M}\right)\left(F^{\tau}_L + \frac{4x'^2\boldsymbol{p}^2_{\perp}}{Q^2}F^{\tau}_2\right), \tag{26b}$$

where in the integrand $F^{\tau}_a$ with $a = T, L, 2$ are the structure functions of bound proton ($\tau = p$) and neutron ($\tau = n$) with the four-momentum $p = (M + \varepsilon, \boldsymbol{p})$, $x' = Q^2/(2p\cdot q) = x/[1 + (\varepsilon +$

$\gamma p_z)/M]$ is the Bjorken variable for the bound nucleon and $\boldsymbol{p}_\perp$ is the transverse component of the nucleon momentum with respect to the momentum transfer. The off-shell nucleon structure functions depend on $x'$, momentum transfer square $Q^2$ and the virtuality $p^2 = (M+\varepsilon)^2 - \boldsymbol{p}^2$ as additional variable. In Eq. (26) the off-shell transverse and longitudinal structure functions are given by equations similar to (7) with $M^2$ replaced by $p^2$, i.e. $F_T = 2x' F_1$, $F_L = \gamma'^2 F_2 - F_T$ with $\gamma'^2 = 1 + 4x'^2 p^2/Q^2$. Using Eqs. (26) we have for the nuclear structure function $F_2^A$

$$\gamma^2 F_2^A\big(x, Q^2\big) = \sum_{\tau=p,n} \int [\mathrm{d}p] \mathcal{P}^\tau(\varepsilon, \boldsymbol{p}) \left(1 + \frac{\gamma p_z}{M}\right) \left(\gamma'^2 + \frac{6x'^2 \boldsymbol{p}_\perp^2}{Q^2}\right) F_2^\tau. \tag{27}$$

The nuclear structure function $F_3$ can be extracted from the left-right asymmetry in the helicity amplitudes, Eq. (9). We have [50]

$$x F_3^A\big(x, Q^2\big) = \sum_{\tau=p,n} \int [\mathrm{d}p] \mathcal{P}^\tau(\varepsilon, \boldsymbol{p}) \left(1 + \frac{p_z}{\gamma M}\right) x' F_3^\tau. \tag{28}$$

Eqs. (26) to (28) allow us to compute the structure functions of a generic nucleus as a convolution of nuclear spectral function, which describes the distribution of the bound nucleons over momentum and separation energy, with the bound proton and neutron structure functions.

We also comment that the transverse motion of the bound nucleon in the target rest frame causes the mixture of different structure functions in Eqs. (26a) and (26b) to order $Q^{-2}$ (note $\boldsymbol{p}_\perp^2$ terms in these equations). This effect on the ratio $F_L^A/F_T^A$ was recently discussed in [52].

*4.1.2. Convolution representation*

If $Q^2$ is high enough to neglect power terms in (26)–(28) then these equations can be written as two-dimensional convolution. For example, for the structure function $F_2$ we have

$$F_2^A\big(x, Q^2\big) = \int\limits_{y>x} \mathrm{d}y\, \mathrm{d}v \big[ f_{p/A}(y, v) F_2^p\big(x/y, Q^2, v\big) + f_{n/A}(y, v) F_2^n\big(x/y, Q^2, v\big)\big], \tag{29}$$

where $f_{p/A}(y, v)$ and $f_{n/A}(y, v)$ are the proton and the neutron distributions over the fraction of light-cone momentum $y$ and the virtuality $v = p^2$. The proton (neutron) distribution function is given in terms of the proton (neutron) spectral function as follows [47,48]

$$f(y, v) = \int [\mathrm{d}p] \mathcal{P}(\varepsilon, \boldsymbol{p}) \left(1 + \frac{p_z}{M}\right) \delta\left(y - 1 - \frac{\varepsilon + p_z}{M}\right) \delta\big(v - p^2\big). \tag{30}$$

The distribution functions are normalized to the number of bound protons (neutrons), as follows from Eq. (23). Equations similar to (29) hold for other structure functions with the same nucleon distribution functions. If we further neglect off-shell effects in the structure functions, Eq. (29) reduces to the familiar one-dimensional convolution.

It is instructive to calculate the average nucleon light-cone momentum $\langle y \rangle_N$ per one nucleon. Using Eq. (30) we have

$$\langle y \rangle_N = 1 + \frac{\langle \varepsilon \rangle + \frac{2}{3}\langle T \rangle}{M}, \tag{31}$$

where $\langle \varepsilon \rangle$ and $\langle T \rangle$ are the average nucleon separation and kinetic energies. Because of binding effect we have $\langle y \rangle_N < 1$ (using our nuclear spectral function from Section 5.2 we have for iron $\langle y \rangle_N = 0.966$). The missing nuclear light-cone momentum apparently should be carried by fields

responsible for nuclear binding. In our approach the missing light-cone momentum is balanced by nuclear pion field. Note that this situation is qualitatively similar to the balance of light-cone momentum in the nucleon in which about a half of the nucleon momentum is carried by gluons. However, in nuclear case the fraction of pion light-cone momentum is much smaller because the nuclei are weakly-bound systems. The scattering from nuclear pions is discussed below.

*4.1.3. Pion contribution to nuclear structure functions*

The lepton can scatter off virtual pions which are exchanged by bound nucleons. The pion correction to nuclear hadronic tensor can be written as follows (see, e.g., [47])

$$W_{\mu\nu}^{\pi/A}(P_A,q)=\frac{1}{2}\sum_{\pi}\int[\mathrm{d}k]D_{\pi/A}(k)W_{\mu\nu}^{\pi}(k,q), \tag{32}$$

where $W_{\mu\nu}^{\pi}(k,q)$ is hadronic tensor of a pion with four-momentum $k$ and the function $D_{\pi/A}$ describes the distribution of pions in a nucleus and the sum is taken over different types of pions. The distribution $D_{\pi/A}$ can be expressed in terms of the pion propagator in a nucleus as

$$D_{\pi/A}(k)=\int \mathrm{d}^4x\exp(ik\cdot x)\langle A|\varphi_i(x)\varphi_i(0)|A\rangle, \tag{33}$$

where $\varphi_i$ is the pion field operator in the corresponding isospin state. The $\pi^0$ state is described by real pseudoscalar field $\varphi_3$, while the charged pion states are described by the complex pseudoscalar fields $(\varphi_1\pm\varphi_2)/\sqrt{2}$. The factor $1/2$ in Eq. (32) is because of the chosen representation of the pion field operator in Eq. (33) in which $\varphi$ is real (particle and antiparticle are identical).

In the further discussion of pion effect it is convenient to consider the normalized pion distribution, i.e. independent of normalization of the target state. We define this as follows

$$\mathcal{D}_{\pi/A}(k)=\int \mathrm{d}t\exp(ik_0t)\langle A|\varphi^*(\boldsymbol{k},t)\varphi(\boldsymbol{k},0)|A\rangle/\langle A|A\rangle, \tag{34}$$

$$\varphi(\boldsymbol{k},t)=\int \mathrm{d}^3\boldsymbol{r}\,\exp(i\boldsymbol{k}\cdot\boldsymbol{r})\varphi(\boldsymbol{r},t), \tag{35}$$

where $\varphi(\boldsymbol{k},t)$ is the pion field operator in momentum representation. Using translational invariance it is easy to verify that $\mathcal{D}_{\pi/A}(k)=D_{\pi/A}(k)/(2M_A)$ in the nucleus rest frame.

In order to extract the pion contribution to nuclear structure functions we contract both sides of Eq. (32) with the photon polarization vectors. Assuming that the hadronic tensor for off-shell pions is given by Eq. (2) we obtain from Eq. (32)

$$F_T^{\pi/A}\big(x,Q^2\big)=\sum_{\pi}\int[\mathrm{d}k]\mathcal{D}_{\pi/A}(k)\big(k_0+\gamma k_z\big)\bigg(F_T^{\pi}+\frac{2x'^2\boldsymbol{k}_\perp^2}{Q^2}F_2^{\pi}\bigg), \tag{36a}$$

$$F_L^{\pi/A}\big(x,Q^2\big)=\sum_{\pi}\int[\mathrm{d}k]\mathcal{D}_{\pi/A}(k)\big(k_0+\gamma k_z\big)\bigg(F_L^{\pi}+\frac{4x'^2\boldsymbol{k}_\perp^2}{Q^2}F_2^{\pi}\bigg), \tag{36b}$$

$$\gamma^2F_2^{\pi/A}\big(x,Q^2\big)=\sum_{\pi}\int[\mathrm{d}k]\mathcal{D}_{\pi/A}(k)\big(k_0+\gamma k_z\big)\bigg(\gamma'^2+\frac{6x'^2\boldsymbol{k}_\perp^2}{Q^2}\bigg)F_2^{\pi}, \tag{36c}$$

$$xF_3^{\pi/A}\big(x,Q^2\big)=\sum_{\pi}\int[\mathrm{d}k]\mathcal{D}_{\pi/A}(k)\big(k_0+k_z/\gamma\big)x'F_3^{\pi}, \tag{36d}$$

where $F_a^{\pi/A}$ denotes the pion correction to the nuclear structure function $F_a^A$. In the integrand $F_a^{\pi}$ are the structure functions of virtual pion with four-momentum $k$, $\boldsymbol{k}_\perp$ is transverse component

of the pion momentum relative to the direction of momentum transfer and $x' = Q^2/(2k\cdot q)$ is the pion Bjorken variable. The pion structure functions in Eqs. (36) depend on $x'$, $Q^2$ and pion invariant mass $k^2 = k_0^2 - \boldsymbol{k}^2$ as an additional variable. The transverse and longitudinal structure functions are related to $F_1$ and $F_2$ as $F_T = 2x'F_1$, $F_L = \gamma'^2 F_2 - F_T$ with $\gamma'^2 = 1 + 4x'^2k^2/Q^2$. The mixture of the structure functions $F_T$ and $F_L$ in Eqs. (36) is because of transverse motion of nuclear pions, similar to the corresponding effect in Eqs. (26) for bound nucleons.

At high $Q^2$ Eqs. (36) can be written in a convolution form. For example, pion correction to $F_2$ can be written as

$$F_2^{\pi/A}\big(x, Q^2\big) = \sum_{\pi} \int\limits_{x<y} \mathrm{d}y\,\mathrm{d}v\, f_{\pi/A}(y, v) F_2^{\pi}\big(x/y, Q^2, v\big), \tag{37}$$

$$f_{\pi/A}(y, v) = 2yM \int [\mathrm{d}k] \mathcal{D}_{\pi/A}(k) \delta\bigg(y - \frac{k_0 + k_z}{M}\bigg)\delta\big(v - k^2\big). \tag{38}$$

Similar equations hold for other structure functions in Eqs. (36). If one neglects the off-shell dependence of the pion structure functions then Eq. (37) reduces to the standard one-dimensional convolution with the pion light-cone distribution which is given by Eq. (38) integrated over $v$. We note that the distribution function by Eq. (38) is antisymmetric function, $f_{\pi/A}(-y) = -f_{\pi/A}(y)$. This property allows us to derive the sum rules for the odd moments of the pion distribution function which will be discussed in more detail in Section 5.3. Note that beyond the leading order approximation the gluonic effects should also be considered.

*4.1.4. Application to the deuteron*

So far the discussion did not refer to particular nuclear target. In this section we apply the discussed formalism to the *deuteron*. The deuteron is an isoscalar bound state of the proton and the neutron. The residual nuclear system is, therefore, the proton or neutron and the spectral function is given in terms of the deuteron wave function $\Psi_D(\boldsymbol{p})$

$$\mathcal{P}^{p,n}(\varepsilon, \boldsymbol{p}) = 2\pi\delta\bigg(\varepsilon - \varepsilon_D + \frac{\boldsymbol{p}^2}{2M}\bigg)\big|\Psi_D(\boldsymbol{p})\big|^2, \tag{39}$$

where $\varepsilon_D = M_D - 2M$ and $\boldsymbol{p}^2/2M$ are the deuteron binding energy and the spectator nucleon recoil energy, respectively. The deuteron structure functions then become

$$F_T^D\big(x, Q^2\big) = \int \frac{\mathrm{d}^3\boldsymbol{p}}{(2\pi)^3}\big|\Psi_D(\boldsymbol{p})\big|^2\bigg(1 + \frac{\gamma p_z}{M}\bigg)\bigg(F_T^N + \frac{2x'^2\boldsymbol{p}_\perp^2}{Q^2}F_2^N\bigg), \tag{40a}$$

$$F_L^D\big(x, Q^2\big) = \int \frac{\mathrm{d}^3\boldsymbol{p}}{(2\pi)^3}\big|\Psi_D(\boldsymbol{p})\big|^2\bigg(1 + \frac{\gamma p_z}{M}\bigg)\bigg(F_L^N + \frac{2x'^2\boldsymbol{p}_\perp^2}{Q^2}F_2^N\bigg), \tag{40b}$$

$$\gamma^2 F_2^D\big(x, Q^2\big) = \int \frac{\mathrm{d}^3\boldsymbol{p}}{(2\pi)^3}\big|\Psi_D(\boldsymbol{p})\big|^2\bigg(1 + \frac{\gamma p_z}{M}\bigg)\bigg(\gamma'^2 + \frac{6x'^2\boldsymbol{p}_\perp^2}{Q^2}\bigg)F_2^N, \tag{40c}$$

$$xF_3^D\big(x, Q^2\big) = \int \frac{\mathrm{d}^3\boldsymbol{p}}{(2\pi)^3}\big|\Psi_D(\boldsymbol{p})\big|^2\bigg(1 + \frac{p_z}{\gamma M}\bigg)x'F_3^N, \tag{40d}$$

where $F_a^N = (F_a^p + F_a^n)/2$ with $a = T, 2, 3$ are the structure functions of the isoscalar nucleon. The variables of these structure functions are similar to those of Eqs. (26)–(28) and we do not write them explicitly.

*4.1.5. Application to complex nuclei*

Unlike the deuteron, the spectral function of complex nuclei does not reduce to the ground state wave function but includes, generally infinite, set of excited residual states (this can be seen directly from Eq. (22) by inserting the complete set of intermediate states). Furthermore, complex nuclei typically have different numbers of protons and neutrons and, in contrast to the deuteron case, the calculation of nuclear structure functions requires both the isoscalar and the isovector contributions. In order to take into account this effect we explicitly separate the isoscalar and the isovector contributions to Eqs. (26)–(28). To this end we consider generic integrand in the convolution formulas and write

$$\sum_{\tau=p,n} \mathcal{P}^{\tau} F_a^{\tau} = \mathcal{P}^{p+n} F_a^N + \mathcal{P}^{p-n} F_a^{p-n}/2, \tag{41}$$

where we denote $\mathcal{P}^{p\pm n} = \mathcal{P}^p \pm \mathcal{P}^n$ and $F_a^N = \frac{1}{2}(F_a^p + F_a^n)$ and $F_a^{p-n} = F_a^p - F_a^n$ for the structure function of type $a$.

In an isoscalar nucleus with equal number of protons and neutrons Eq. (41) is dominated by the isoscalar contribution and one generally assumes $\mathcal{P}^{p-n} = 0$. However, it must be remarked that this equation is violated by a number of effects even in the isoscalar nucleus. The finite difference between the proton and neutron spectral functions is generated by the Coulomb interaction and isospin-dependent effects in the nucleon–nucleon interaction. The discussion of these effects goes beyond the scope of this paper and we leave them for future studies. Instead we focus on the neutron excess effect for heavy nuclei.

We write the isoscalar and isovector spectral functions in terms of reduced functions $\mathcal{P}_0$ and $\mathcal{P}_1$ as

$$\mathcal{P}^{p+n} = A\mathcal{P}_0, \tag{42a}$$

$$\mathcal{P}^{p-n} = (Z-N)\mathcal{P}_1. \tag{42b}$$

The functions $\mathcal{P}_0$ and $\mathcal{P}_1$ are normalized to unity as follows from Eq. (23). These spectral functions are quite different. The function $\mathcal{P}_0$ involves the averaging over all isoscalar intermediate states. The function $\mathcal{P}_1$ probes the isovector component in a nucleus and its strength is peaked about the Fermi surface as argued in Section 5.2. The model spectral functions $\mathcal{P}_0$ and $\mathcal{P}_1$, which are used in this paper, are discussed in Section 5.2.

Using Eqs. (41) and (42) we can write each of the structure function $a = T, 2, 3$ as

$$F_a^A = A\langle F_a^N\rangle_0 + \frac{Z-N}{2}\langle F_a^{p-n}\rangle_1, \tag{43}$$

where the averaging $\langle F_a\rangle_{0,1}$ denotes the integration in Eqs. (26)–(28) with the reduced spectral functions $\mathcal{P}_0$ and $\mathcal{P}_1$, respectively.

We conclude this section by commenting that data are sometimes naively corrected for the neutron excess effect neglecting Fermi motion and binding effects (as well as any other nuclear effects) in the isovector and the isoscalar distributions. As follows from the present discussion, the Fermi motion and binding effects are quite different in the isoscalar and the isovector distributions in heavy nuclei. If neglected, this effect may cause an additional systematic uncertainty in data and a distortion of final results.

*4.1.6. Off-shell effects*

The bound proton and neutron are off-mass-shell and their structure functions differ from those of the free proton and neutron. The off-shell nucleon structure functions depend on the

nucleon virtuality $p^2$ as an additional variable. Therefore, the off-shell effects in the structure functions are closely related to the target mass corrections. Target mass effects in the off-shell nucleon can be of two different kinds. First, similarly to the on-shell nucleon, we have to take into account the kinematical target mass dependence due to the finite $p^2/Q^2$ ratio. We assume that this effect is described by Eqs. (11), where the nucleon mass squared is replaced by $p^2$ (this leads in turn to the modification of the parameter $\gamma$ and the variable $\xi$ in the off-shell region). Furthermore, the dependence on $p^2$ appears already at leading twist (LT) at the PDF level as was argued in [46,48,50,51]. Thus off-shell effects in the LT structure functions can be viewed as a measure of the nucleon's modification inside nuclear medium.

Since we treat nuclei as non-relativistic systems it would be enough to consider the off-shell effect as a correction. We expand the nucleon LT structure functions in the vicinity of the mass shell in series in $p^2-M^2$. Keeping only the linear term we have for $F_2$

$$F_2\big(x, Q^2, p^2\big) = F_2\big(x, Q^2\big)\left(1 + \delta f_2\big(x, Q^2\big)\,\frac{p^2-M^2}{M^2}\right), \tag{44}$$

$$\delta f_2\big(x, Q^2\big) = \frac{\partial \ln F_2(x, Q^2, p^2)}{\partial \ln p^2}, \tag{45}$$

where the first term is the structure function of the on-mass-shell nucleon and the derivative is evaluated at $p^2 = M^2$. Similar expressions can be written for the other structure functions.

The function $\delta f_2$ can be related to the corresponding off-shell functions for the nucleon parton distributions. The necessary relation can be obtained by writing $F_2$ in terms of a convolution of the parton distributions with the corresponding coefficient function according to the given order in $\alpha_S$. In order to simplify discussion and illustrate this relation we can consider the simple leading order expression of $F_2$

$$F_2 = x\sum e_i^2(q_i + \bar{q}_i), \tag{46}$$

where $e_i$ and $q_i$ ($\bar{q}_i$) are the charge and the distribution of (anti)quarks of the type $i$ and the sum is taken over different types of quarks. The off-shell function for the parton distribution $q(x)$ is defined similarly to Eq. (45), $\delta f_q = \partial \ln q/\partial \ln p^2$. Then from Eq. (46) we have a relation

$$F_2(x)\delta f_2(x) = x\sum e_q^2\big[q(x)\delta f_q(x) + \bar{q}(x)\delta f_{\bar{q}}(x)\big]. \tag{47}$$

One can conclude from Eq. (47) that at large $x$, where the antiquark distributions can be neglected, $\delta f_2$ is dominated by quarks. For simplicity we neglect the isospin effect and assume $\delta f_u = \delta f_d = \delta f_q$, then $\delta f_2 = \delta f_q$ at large $x$. At small $x$ both, the quark and the antiquark contributions, have to be taken into account.

Off-shell effects in nucleon structure functions were discussed in [48,50] using the spectral representation of the quark distributions in the nucleon with four-momentum $p$

$$q\big(x, p^2\big) = \int \mathrm{d}s \int^{t_{\max}} \mathrm{d}t\, D_{q/N}\big(s, t, x, p^2\big). \tag{48}$$

The integration in Eq. (48) is taken over the mass spectrum of spectator states $s$ and the quark virtuality $t = k^2$ with the kinematical maximum $t_{\max} = x[p^2 - s/(1-x)]$ for the given $s$ and $p^2$. The invariant spectral density $D_{q/N}$ measures the probability to find in a nucleon with momentum $p$, a quark with light-cone momentum $x$ and virtuality $t$ and the remnant system in a state with invariant mass $s$.

We conclude from Eq. (48) that the $p^2$ dependence of quark distributions can have two sources: the $p^2$ term in $t_{\max}$ (kinematical off-shell dependence), and the $p^2$ dependence of the quark spectral function $D_{q/N}$ (dynamical off-shell dependence). The kinematical off-shell effect causes a negative correction to the bound nucleon structure functions that results in an enhanced EMC effect, as first noticed in [46,48]. However, if only the kinematical off-shell effects are taken into account the number of valence quarks in the nucleon would change with $p^2$. It can be seen directly from Eq. (48) that the normalization of the quark distribution decreases as $p^2$ decreases, provided that the spectral density is positively defined. This observation indicates that off-shell effect of dynamical origin must also be present. A method to estimate the dynamical off-shell effects minimizing the model dependence was suggested in [48], in which the conservation of the valence quark number in off-shell nucleon was used as a constraint. A partial cancellation between the kinematical and dynamical off-shell effects was found in [48,50]. However, the off-shell effect in the structure functions remains an important correction. In this paper we treat the function $\delta f_2$ phenomenologically and fix it from nuclear data as discussed in more detail in Section 5.

### *4.2. Coherent nuclear effects*

Nuclear shadowing effect was extensively discussed in the literature. A recent paper [24] provides a review of both data and theoretical models of nuclear shadowing.

It appears to be a common wisdom that nuclear shadowing is a result of coherent interaction of hadronic component of virtual photon with target nucleus. The structure functions at small $x$ can be presented as a superposition of contributions from different hadronic states. We consider the helicity structure functions $W_0$ and $W_\pm$, as defined in Eq. (6), that will allow us to discuss nuclear effects in charged-lepton and neutrino interactions on the same ground. We have

$$W_h = \sum_v w_v \sigma_h^v(s), \tag{49}$$

where $\sigma_h^v(s)$ is the total cross section of scattering of the hadronic state $v$ with the given helicity $h = 0, \pm 1$ off the target nucleon (or nucleus) with the center-of-mass energy $s = Q^2(1/x-1) + M^2$ and the quantities $w_v$ describe the weight of different hadronic states.

At low $Q^2$ the vector meson dominance model (VMD) was proved to be a good tool to evaluate nuclear corrections to the structure functions [58]. In this model the structure functions are approximated by contributions from a few vector-meson states. The weights for the electromagnetic current are $w_v = Q^2/(\pi f_v^2)(1 + Q^2/m_v^2)^{-2}$ with $f_v$ the photon–meson coupling constants and $m_v$ the vector meson mass. Usually only the lowest mass vector mesons ($\rho^0$, $\omega$, $\phi$) are important at low $Q^2 \lesssim 1$ GeV$^2$. The VMD structure functions have strong $Q^2$ dependence and decrease as $Q^{-2}$ at high $Q$. In the generalized versions of VMD, the higher-mass states including continuum have also been considered that made it possible to apply the model at higher $Q^2$ (see, e.g., [24]).

In this paper we approximate the sum over hadronic states in Eq. (49) by a factorized form

$$W_h\big(x, Q^2\big) = w_h\big(x, Q^2\big)\bar{\sigma}_h(s), \tag{50}$$

where $\bar{\sigma}_h$ is an *effective* cross section corresponding to helicity $h$ averaged over hadronic configurations and $w_h$ is remaining normalization factor. At low $Q^2$ the quantity $\bar{\sigma}_h$ corresponds to the average over a few vector meson states. As $Q^2$ increases, the averaging in (50) involves the rising number of active hadronic configurations. Since the relative weight of higher-mass

states increases with $Q^2$ and the cross section decreases with the mass, one can qualitatively conclude that $\bar{\sigma}_h$ should decrease with $Q^2$. In the approach adopted in this paper we will treat $\bar{\sigma}_h$ phenomenologically.

In this paper we are concerned with the relative effect of nuclear interactions

$$\delta\mathcal{R}_h\big(x, Q^2, A/N\big) = \delta W_h^A\big(x, Q^2\big)/W_h^N\big(x, Q^2\big), \tag{51}$$

where $\delta W_h^A$ is the nuclear structure function of helicity $h$ subtracted incoherent contribution (cf. Eq. (13)). Assuming that the weight factors are not affected by nuclear effects, from Eq. (50) we conclude that the relative nuclear correction to the structure functions equals the corresponding correction to the effective cross section

$$\delta\mathcal{R}_h(A/N) = \delta\bar{\sigma}_h^A/\bar{\sigma}_h^N, \tag{52}$$

where $\delta\bar{\sigma}^A$, similar to $\delta W^A$, is the nuclear cross section subtracted incoherent contribution. The problem of calculation of nuclear corrections to structure functions at small $x$ thus reduces to the calculation of multiple scattering effects on effective hadronic cross section.

*4.2.1. Application to the deuteron*

We now consider this effect in application to the deuteron. In order to calculate the shadowing correction we consider hadron elastic scattering amplitude $a(s,k)$ with $s$ the center-of-mass energy and $k$ the momentum transfer. We choose the normalization of the amplitude such that the optical theorem reads $\mathrm{Im}\,a(s,0) = \sigma(s)/2$ and parametrize the scattering amplitude as $a = (i+\alpha)(\sigma/2)\exp(-Bk^2/2)$, where the exponent describes the dependence on momentum transfer.[3] The hadron–deuteron scattering amplitude in forward direction can be written as [56]

$$a^D = a^p + a^n + \delta a^D, \quad \delta a^D = i a^p a^n \mathcal{C}_2^D, \tag{53}$$

where $a^p$ and $a^n$ are the scattering amplitudes off the proton and the neutron and $\delta a^D$ the double scattering correction. $\mathcal{C}_2^D$ can be written in terms of the deuteron wave function as

$$\mathcal{C}_2^D = \frac{1}{(2\pi)^2}\int \mathrm{d}^2\boldsymbol{k}_\perp\, S_D(\boldsymbol{k}_\perp, k_L) e^{-B\boldsymbol{k}_\perp^2}, \tag{54}$$

$$S_D(\boldsymbol{k}) = \int \mathrm{d}^3\boldsymbol{r}\, e^{i\boldsymbol{k}\cdot\boldsymbol{r}}\big|\Psi_D(\boldsymbol{r})\big|^2. \tag{55}$$

Note that Eq. (53) is the scattering amplidude of an off-shell hadron with four-momentum $q$. For this reason there appears a finite longitudinal momentum transfer $k_L = Mx(1+m^2/Q^2)$, which accounts for a finite longitudinal correlation length of a virtual hadron ($k_L = 0$ for the scattering of on-shell particles).

We apply Eqs. (52) and (53) in order to calculate coherent nuclear effects for different structure functions. It should be remarked that helicity conserves in multiple scattering interactions and the scattering matrix is diagonal in helicity basis. For this reason the multiple scattering corrections involve the amplitudes with the same helicity. We also assume no isospin effect, i.e. the effective scattering amplitudes of the given helicity are equal for the proton and the neutron. Let us first discuss the transverse structure function $F_T$. The relative shadowing correction to the transverse structure function is

$$\delta\mathcal{R}_T\big(x, Q^2, D/N\big) = \sigma_T\big(\alpha_T^2 - 1\big)\mathcal{C}_2^D/2, \tag{56}$$

[3] Such dependence is confirmed experimentally and for low mass vector mesons the value of the parameter $B$ is between 4 and 10 GeV$^2$ depending on $Q^2$ (see, e.g., [58]).

where $\sigma_T$ and $\alpha_T$ are parameters of effective scattering amplitude of transversaly polarized virtual photon. A particular model of the scattering amplitude used in our analysis is discussed in Section 5.5.

Relation similar to Eq. (56) holds in the longitudinal channel. It follows from Eq. (50) that the ratio $R = F_L/F_T$ equals the corresponding ratio of the cross sections $\sigma_L/\sigma_T$ provided that the normalization factor $w(x, Q^2)$ is independent of helicity. This holds in the VMD for low-mass mesons and we also assume that this is approximately true for the contribution from higher-mass states. Thus using Eq. (56) and assuming $\alpha_L = \alpha_T$ we find that the relative shadowing corrections for longitudinal and transverse structure functions is simply determined by $R$

$$\frac{\delta\mathcal{R}_L(x, Q^2, D/N)}{\delta\mathcal{R}_T(x, Q^2, D/N)} = R\big(x, Q^2\big), \tag{57}$$

where $R(x, Q^2)$ is calculated for the nucleon.

Eqs. (56) and (57) allow us to compute the nuclear shadowing effect for the structure function $F_2$ in terms of the corresponding correction to $F_T$. Indeed, recalling Eqs. (7) we have

$$\delta\mathcal{R}_2(D/N) = \frac{\delta\mathcal{R}_T(D/N) + R\delta\mathcal{R}_L(D/N)}{1+R}. \tag{58}$$

Taking into account (57) we find the factor $(1 + R^2)/(1 + R)$ difference between shadowing effect for $F_2$ and $F_T$.

Let us discuss the shadowing effect for the structure function $xF_3$. This structure function is given by the left–right asymmetry in helicity structure functions $W_+ - W_-$. Therefore, in this case the problem reduces to computing the multiple scattering effect for the difference of the corresponding scattering amplitudes. We denote $\Delta a = a_+ - a_-$. The non-zero difference $\Delta a$ is generated because of vector–axial vector current transitions in the hadronic tensor. The double scattering correction to $\Delta a$ can readily be derived from Eq. (53)

$$\delta\Delta a^D = 2i\,\Delta a\, a_T \mathcal{C}_2^D, \tag{59}$$

where we denote $a_T = (a_+ + a_-)/2$. It follows from Eq. (59) that the relative shadowing effect for the cross section asymmetry is determined by the cross section $\sigma_T$. Using Eqs. (53) and (59) we find

$$\frac{\delta\mathcal{R}_\Delta(D/N)}{\delta\mathcal{R}_T(D/N)} = 2\frac{1-\alpha_\Delta\alpha_T}{1-\alpha_T^2}. \tag{60}$$

We observe from this equation that the shadowing effect is enhanced for the cross section asymmetry by the factor of 2 with respect to the shadowing effect for the cross section $\sigma_T$ if we neglect the effect of real part of the amplitudes [61]. To clarify the origin of this enhancement we consider a somewhat simplified VMD model with the single vector meson ($\rho$ meson) and the axial-vector meson ($a_1$ meson). In this model the structure functions $F_L$ and $F_T$ in charged-current scattering are determined by the diagonal vector–vector and axial vector–axial vector transitions $VN \to VN$ and $AN \to AN$, while the structure function $F_3$ is driven by the off-diagonal transitions $VN \to AN$ and $AN \to VN$. The cross section of the off-diagonal transitions is much smaller than the cross sections of the direct processes. For this reason, $xF_3 \ll F_2$ at small $x$. However, the nuclear multiple scattering corrections to off-diagonal process $V \to A$ are determined by a strong cross section of the diagonal processes $V \to V$ and $A \to A$. This becomes clear if we consider the double scattering term for the off-diagonal nuclear amplitude. To this order the nuclear scattering proceeds via two steps: the off-diagonal scattering from one

nucleon followed by the diagonal scattering from the second nucleon. The off-diagonal scattering can be interchanged with the diagonal scattering that leads to the factor of 2 enhancement, which appears to have the combinatorial origin.

*4.2.2. Application to complex nuclei*

We now turn to the discussion of the shadowing effect in complex nuclei. We apply the Glauber–Gribov multiple scattering theory to calculate the multiple scattering effect on effective cross sections. Let $a^A$ be the nuclear scattering amplitude in forward direction. We will assume no isospin dependence of the scattering amplitude, i.e. $a^p = a^n$. Then $a^A$ can be written as (see, e.g., [58] and references therein)

$$a^A = A\,a + \delta a^A, \quad \delta a^A = i a^2 \mathcal{C}_2^A(a), \tag{61}$$

where $a$ is the corresponding nucleon amplitude and $\mathcal{C}_2^A$ incorporates the multiple scattering effects and read as follows

$$\mathcal{C}_2^A(a) = \int\limits_{z_1<z_2} \mathrm{d}^2\boldsymbol{b}\,\mathrm{d}z_1\,\mathrm{d}z_2\,\rho_A(\boldsymbol{b},z_1)\rho_A(\boldsymbol{b},z_2)\exp\Big[\,i\int\limits_{z_1}^{z_2}\mathrm{d}z'\,\big(a\,\rho_A(\boldsymbol{b},z') - k_L\big)\Big]. \tag{62}$$

Here $\rho_A$ is the nucleon density distribution normalized to the number of nucleons $A$ and the integration is performed along the collision axis, which is chosen to be $z$-axis, and over the transverse positions of nucleons (impact parameter $\boldsymbol{b}$). If only the double scattering approximation is considered then the exponential factor in Eq. (62) should be omitted. The exponential factor in Eq. (62) accounts for multiple scattering effects (see, e.g., [58]).

We note that Eqs. (61) and (62) were derived assuming that the wave function factorizes into the product of the single particle wave functions and neglecting short-range correlation effects between bound nucleons (optical approximation). We comment in this respect that the correlations are relevant only if the coherence length $L_c = 1/k_L$ is comparable to the short-range repulsive part of the nucleon–nucleon force, which is about 0.5 fm. This takes place at relatively large $x$, for which shadowing effect is small (see discussion in Ref. [24]).

The transverse momentum dependence of elastic scattering amplitudes was also neglected, since the transverse size of the meson-nucleon amplitude in the impact parameter space is of order $B^{-1/2}$, much smaller than the radius of the nucleus.

We first discuss multiple scattering correction to the transverse structure function. The relative shadowing correction is determined by effective scattering amplitude $a_T$ of transversely polarized virtual photon

$$\delta\mathcal{R}_T(A/N) = \sigma_T\,\mathrm{Re}(i+\alpha_T)^2\mathcal{C}_2^A(a_T)/2. \tag{63}$$

If the real part of the amplitude is small then multiple scattering correction is negative because of destructive interference of forward scattering amplitudes on the upstream nucleons that causes *shadowing* of virtual hadron interactions. It should be also noted that if the real part is large then the interference in the double scattering term is constructive that would lead to antishadowing effect.

If the coherence length of hadronic fluctuation is small compared to average nuclear radius, $L_c \ll R_A$, then the oscillating factor in Eq. (62) suppresses multiple scattering effect. The onset point of coherent nuclear effects can be estimated by comparing the coherence length of hadronic fluctuation $L_c$ with the averaged distance between bound nucleons in the nucleus $r_{\mathrm{NN}}$. The coherent nuclear effects take place if the coherence length is large enough $L_c > r_{\mathrm{NN}}$. Since for

any mass $m^2$ of intermediate hadronic state $L_c < (Mx)^{-1}$ the region of coherent nuclear effects is limited to small $x$ for any $Q^2$, $x < (Mr_{\rm NN})^{-1}$. Nuclear shadowing saturates if the coherence length $L_c$ exceeds average nuclear radius that happens at small $x$ and the condition $L_c \sim R_A$ defines the transition region with strong $x$ dependence of the shadowing correction.

The rate of multiple scattering interactions is controlled by mean free path of hadronic fluctuation in a nucleus $(\rho_A\sigma)^{-1}$. If this is small enough compared with nuclear radius, which is the case for heavy nuclei, then multiple scattering effects are important.

It can be easily seen from Eqs. (61) and (62) that if the dependence of $\mathcal{C}_2^A$ on the scattering amplitude can be neglected, then Eq. (57) generalizes to complex nuclei. This corresponds to the case when the double scattering saturates the multiple scattering corrections. Generally, for heavy nuclei Eq. (57) should be replaced by

$$\frac{\delta\mathcal{R}_L(x,Q^2,A/N)}{\delta\mathcal{R}_T(x,Q^2,A/N)} = R\big(x,Q^2\big)\frac{\mathrm{Re}[(i+\alpha_L)^2\mathcal{C}_2^A(a_L)]}{\mathrm{Re}[(i+\alpha_T)^2\mathcal{C}_2^A(a_T)]}, \tag{64}$$

with $a_L$ and $a_T$ the effective scattering amplitudes for longitudinally and transversely polarized photons. The relation between the nuclear shadowing effect for $F_2$ and $F_T$ in heavy nuclei can be derived from Eqs. (58), (63) and (64).

We now discuss the multiple scattering corrections to the right–left asymmetry in the helicity scattering amplitudes and the generalization of Eq. (60) to heavy nuclei. The multiple scattering correction to the difference $\Delta a = a_+ - a_-$, as follows from Eqs. (61) and (62), can be written as

$$\delta\Delta a^A = i\big[a_+^2\mathcal{C}_2^A(a_+) - a_-^2\mathcal{C}_2^A(a_-)\big], \tag{65}$$

where $a_\pm$ are the corresponding nucleon amplitudes. We now use the fact that $|\Delta a| \ll |a_T|$, where $a_T = \frac{1}{2}(a_+ + a_-)$ is the amplitude averaged over the transverse polarizations of the intermediate boson, and expand Eq. (65) in $\Delta a$ keeping only the linear term. We have

$$\delta\Delta a^A = 2i\,\Delta a\,a_T\mathcal{C}_2^A(a_T) - \Delta a\,a_T^2\mathcal{C}_3^A(a_T), \tag{66}$$

where

$$\begin{aligned}\mathcal{C}_3^A(a) &= -i\,\partial\mathcal{C}_2^A(a)/\partial a\\ &= \int\limits_{z_1<z_2<z_3} \mathrm{d}^2\boldsymbol{b}\,\mathrm{d}z_1\mathrm{d}z_2\,\mathrm{d}z_3\,\rho_A(\boldsymbol{b},z_1)\rho_A(\boldsymbol{b},z_2)\rho_A(\boldsymbol{b},z_3)\\ &\quad\times\exp\bigg[i\int\limits_{z_1}^{z_3}\mathrm{d}z'\big(a\,\rho_A(\boldsymbol{b},z') - k_L\big)\bigg].\end{aligned} \tag{67}$$

The first term in the right side of Eq. (66) is similar to that in Eq. (59). This term is driven by the double scattering term (the quadratic $\rho_A^2$ term). However, the higher order multiple scattering terms also contribute to (66) through non-linear effects in $\mathcal{C}_2^A$ and $\mathcal{C}_3^A$. Note in this respect that the expantion of the term $\mathcal{C}_3^A$ in the multiple scattering series starts from the tripple scattering term $\rho_A^3$. The analytical expressions for $\mathcal{C}_2^A$ and $\mathcal{C}_3^A$ calculated for uniform density distribution, which is used in our analysis described in Section 5.7, are given in Appendix B.

Using Eq. (66) it is straightforward to compute the relative multiple scattering correction to the cross section asymmetry $\delta\mathcal{R}_\Delta(A/N) = \delta\Delta\sigma^A/\Delta\sigma$ that also determines the nuclear shadowing effect for the structure function $F_3$. The resulting expression for $\delta\mathcal{R}_\Delta(A/N)$ is somewhat cumbersome in general case and we do not give it explicitly here. It should be noted that

$\delta\mathcal{R}_\Delta(A/N)$ does not depend on the cross section asymmetry $\Delta\sigma$ for the nucleon but does depend on $\alpha_\Delta = \mathrm{Re}\,\Delta a/\mathrm{Im}\,\Delta a$. If we keep only the double scattering term then $\delta\mathcal{R}_\Delta(A/N)$ is given by Eq. (60) also in the case of complex nuclei. However, this relation is violated by higher order scattering terms.

## 5. Description of the model

In the following we discuss in detail the model which is used to describe nuclear structure functions. The model incorporates the treatment of both the coherent and incoherent processes as described in Section 4. We use the model nuclear spectral function calculated in a many-body approach (Section 5.2). The model pion distribution function is constrained by light-cone momentum conservation and equations of motion of pion field (Section 5.3). The nuclear shadowing effect is described in terms of effective scattering amplitude of intermediate hadronic states of virtual boson off the nucleon (see Section 4.2). In order to describe data on nuclear structure functions we explicitly introduce an off-shell correction to the nucleon structure functions, which provides a measure of the modification of the nucleon structure in the nuclear environment. This effect and the effective scattering amplitude are treated phenomenologically in terms of few universal parameters, common for all nuclei, which are extracted from nuclear DIS data in a wide kinematic range of $x$ and $Q^2$. The parameterizations of the off-shell effect and of the effective amplitude are discussed in Sections 5.4 and 5.5. Sections 5.6 to 5.7.3 describe the analysis of data and our main results.

### 5.1. Deuteron wave function

Nuclear spectral function $\mathcal{P}$ describes the probability to find the nucleon with the momentum $\boldsymbol{p}$ and the (non-relativistic) energy $\varepsilon$ in the ground state of the nucleus. We first discuss the *deuteron* for which the spectral function is determined by the wave function (see Eq. (39)). The deuteron wave function is the superposition of $s$- and $d$-wave states. In the momentum space it can be written as follows

$$\Psi_{D,m}(\boldsymbol{p}) = \sqrt{2\pi^2}\left(\psi_0(p) - \psi_2(p)\frac{S_{12}(\hat{\boldsymbol{p}})}{\sqrt{8}}\right)\chi_{1m}, \tag{68}$$

where $\psi_0$ and $\psi_2$ are respectively the $s$- and $d$-wave function in the momentum space,[4] $m$ is the projection of the total angular momentum on the spin quantization axis, $\chi_{1m}$ is the spin 1 wave function with $S_z = m$, and $S_{12}(\hat{\boldsymbol{p}})$ is the tensor operator

$$S_{12}(\hat{\boldsymbol{p}}) = 3(\boldsymbol{\sigma}_1\cdot\hat{\boldsymbol{p}})(\boldsymbol{\sigma}_2\cdot\hat{\boldsymbol{p}}) - \boldsymbol{\sigma}_1\cdot\boldsymbol{\sigma}_2, \tag{69}$$

where $\hat{\boldsymbol{p}} = \boldsymbol{p}/|\boldsymbol{p}|$ and $\boldsymbol{\sigma}_1$ and $\boldsymbol{\sigma}_2$ are the Pauli matrices acting on the spin variables of the bound proton and neutron, respectively. The momentum distribution in the deuteron is given by the wave function squared

$$\left|\Psi_{D,m}(\boldsymbol{p})\right|^2 = 2\pi^2\left[\psi_0^2(p) + \psi_2^2(p) - \chi_{1m}^\dagger S_{12}\chi_{1m}\left(\frac{\psi_0(p)\psi_2(p)}{\sqrt{2}} + \frac{\psi_2^2(p)}{4}\right)\right], \tag{70}$$

[4] In terms of the standard wave functions in the coordinate space $u(r)$ and $w(r)$ the functions $\psi_0$ and $\psi_2$ are $\psi_0(p) = (2/\pi)^{1/2}\int \mathrm{d}r\, r j_0(rp)u(r)$ and $\psi_2(p) = (2/\pi)^{1/2}\int \mathrm{d}r\, r j_2(rp)w(r)$, where $j_0$ and $j_2$ are the spherical Bessel functions. Note also a different sign of the $d$-wave term in Eq. (68) with respect to the wave function in the coordinate space.

where the last term in the right side appears due to the tensor operator (69). This term vanishes after averaging over the deuteron polarizations, which is the case for the present paper. The normalization of the wave function is

$$\int_0^\infty \mathrm{d}p\, p^2\big(\psi_0^2(p)+\psi_2^2(p)\big)=1. \tag{71}$$

In order to study the sensitivity of our result to the choice of the deuteron wave function we used the Bonn [62] and the Paris [63] wave functions.

### 5.2. Nuclear spectral function

The nuclear spectral function can formally be written as a sum over the set of excited residual states. This can be seen directly from Eq. (22) by inserting the complete set of intermediate states. For simplicity we suppress the explicit notations for different isospin states and write

$$\mathcal{P}(\varepsilon,\boldsymbol{p})=2\pi\sum_n\big|\langle(A-1)_n,-\boldsymbol{p}\big|\psi(\boldsymbol{p})|A\rangle\big|^2\delta\big(\varepsilon+E_n^{A-1}+E_R-E_0^A\big). \tag{72}$$

Here the sum runs over the quantum numbers of the states of $A-1$ nucleons, which include the bound states as well as the continuum states, $E_n^{A-1}$ and $E_0^A$ are respectively the energy of the residual nucleus (in the recoil nucleus rest frame) and the ground state energy of the target nucleus. The residual system balances momentum of the removed nucleon and acquires the recoil energy $E_R=\boldsymbol{p}^2/2M_{A-1}$.

The nuclear spectral function determines the rate of nucleon removal reactions such as $(e,e'p)$ that makes it possible to extract the spectral function from experimental data. For low separation energies (for $|\varepsilon|<\varepsilon_F\sim 30$–$50$ MeV) the experimentally observed spectrum is similar to that predicted by the mean-field model [64]. The mean-field model spectral function $\mathcal{P}_{\rm MF}$ is given by the wave functions and energies of the occupied levels in the mean field [65]. The mean-field picture gives a good approximation to experimentally observed spectrum in $(e,e'p)$ reactions in the vicinity of the Fermi level, where the excitation energies of the residual nucleus are small [64]. As nuclear excitation energy becomes higher the mean-field model becomes less accurate. The peaks corresponding to the single-particle levels acquire a finite width (fragmentation of deep-hole states). Furthermore, the high-energy and high-momentum components of nuclear spectrum cannot be described in the mean-field model and driven by correlation effects in nuclear ground state as witnessed by numerous studies (for a review see [66]). We denote the contribution to the spectral function which absorbs the correlation effects as $\mathcal{P}_{\rm cor}(\varepsilon,\boldsymbol{p})$.

In this paper we consider a phenomenological model of the spectral function which incorporates both the single particle nature of the spectrum at low energy and high-energy and high-momentum components due to NN-correlations in the ground state. We first discuss the isoscalar spectral function which we write as

$$\mathcal{P}_0(\varepsilon,\boldsymbol{p})=\mathcal{P}_{\rm MF}(\varepsilon,\boldsymbol{p})+\mathcal{P}_{\rm cor}(\varepsilon,\boldsymbol{p}). \tag{73}$$

The low-energy part is described by the mean-field spectral function for which we use an approximate expression motivated by closure, i.e. the sum over occupied levels is substituted by its average value:

$$\mathcal{P}_{\rm MF}(\varepsilon,\boldsymbol{p})=2\pi\, n_{\rm MF}(\boldsymbol{p})\delta\big(\varepsilon+E^{(1)}+E_R(\boldsymbol{p})\big), \tag{74}$$

with $E_R(\boldsymbol{p})$ the recoil energy of residual nucleus, $E^{(1)} = E^{A-1} - E_0^A$ the nucleon separation energy averaged over single-particle levels, and $n_{\rm MF}(\boldsymbol{p})$ the corresponding part of the nucleon momentum distribution. Note that $\mathcal{P}_{\rm MF}$ is not normalized to the number of nucleons since a part of the strength is taken by the correlation term $\mathcal{P}_{\rm cor}$.

The correlated part of the spectral function $\mathcal{P}_{\rm cor}$ is determined by excited states in (72) with one or more nucleons in the continuum. Following [67] we assume that $\mathcal{P}_{\rm cor}$ at high momentum and high separation energy is dominated by ground state configurations with a correlated nucleon–nucleon pair and remaining $A-2$ nucleons moving with low center-of-mass momentum

$$|A-1,-\boldsymbol{p}\rangle \approx \psi^{\dagger}(\boldsymbol{p}_1)\big|(A-2)^*,\boldsymbol{p}_2\big\rangle\delta(\boldsymbol{p}_1+\boldsymbol{p}_2+\boldsymbol{p}). \tag{75}$$

The corresponding matrix element in Eq. (72) can thus be parametrized in terms of the wave function of the nucleon–nucleon pair embeded into nuclear environment. We assume factorization into relative and center-of-mass motion of the pair [67]

$$\big\langle(A-2)^*,\boldsymbol{p}_2\big|\psi(\boldsymbol{p}_1)\psi(\boldsymbol{p})|A\rangle \approx C_2\psi_{\rm rel}(\boldsymbol{k})\psi_{\rm CM}^{A-2}(\boldsymbol{p}_{\rm CM})\delta(\boldsymbol{p}_1+\boldsymbol{p}_2+\boldsymbol{p}), \tag{76}$$

where $\psi_{\rm rel}$ is the wave function of the relative motion in the nucleon–nucleon pair with relative momentum $\boldsymbol{k} = (\boldsymbol{p}-\boldsymbol{p}_1)/2$ and $\psi_{\rm CM}$ is the wave function of center-of-mass (CM) motion of the pair in the field of $A-2$ nucleons, $\boldsymbol{p}_{\rm CM} = \boldsymbol{p}_1 + \boldsymbol{p}$. The CM wave function $\psi_{\rm CM}$ generally depends on the quantum numbers of the state of $A-2$ nucleons, however the corresponding dependence of the $\psi_{\rm rel}$ is assumed to be weak. Both the wave functions, $\psi_{\rm rel}$ and $\psi_{\rm CM}$, are assumed to be normalized to unity. The normalization factor $C_2$ describes the weight of the two-nucleon correlated part in the full spectral function.

Using Eq. (76) we sum over the spectrum of states of $A-2$ nucleons and obtain an approximate expression for $\mathcal{P}_{\rm cor}$ in terms of convolution of the relative and the CM momentum distributions

$$\begin{aligned}\mathcal{P}_{\rm cor}(\varepsilon,\boldsymbol{p}) = 2\pi C_2^2 \int \mathrm{d}^3\boldsymbol{p}_1\,\mathrm{d}^3\boldsymbol{p}_2\, n_{\rm rel}(\boldsymbol{k}) n_{\rm CM}(\boldsymbol{p}_2)\delta(\boldsymbol{p}_1+\boldsymbol{p}_2+\boldsymbol{p}) \\ \times\,\delta\left(\varepsilon + \frac{\boldsymbol{p}_1^2}{2M} + \frac{\boldsymbol{p}_2^2}{2M_{A-2}} + E^{(2)}\right).\end{aligned} \tag{77}$$

Here $n_{\rm rel}$ and $n_{\rm CM}$ are the relative and the CM momentum distributions, respectively, and $E^{(2)} = E^{A-2} - E_0^A$ is the energy needed to separate two nucleons from the ground state averaged over configurations of $A-2$ nucleons with low excitation energy. Note that the minimum two-nucleon separation energy $E^{(2)} = E_0^{A-2} - E_0^A$ is of order 20 MeV for medium-range nuclei like $^{56}$Fe.

We can further simplify Eq. (77) if the momentum $p$ is high enough and $|\boldsymbol{p}| \gg |\boldsymbol{p}_2|$. This allows us to take the relative momentum distribution out of the integral over the CM momentum at the point $\boldsymbol{k} = \boldsymbol{p}$. Then we have

$$\mathcal{P}_{\rm cor}(\varepsilon,\boldsymbol{p}) = 2\pi C_2^2 n_{\rm rel}(\boldsymbol{p})\left\langle\delta\left(\varepsilon + \frac{\boldsymbol{p}^2}{2M} + \frac{\boldsymbol{p}\cdot\boldsymbol{p}_2}{M} + \frac{\boldsymbol{p}_2^2}{2M_*} + E^{(2)}\right)\right\rangle_{\rm CM}, \tag{78}$$

where the averaging is done with respect to the CM motion of the correlated pair and $M_* = M(A-2)/(A-1)$ is effective mass of the system of the residual nucleus of $A-2$ nucleons and the nucleon with momentum $\boldsymbol{p}_1$. In this approximation the high momentum part of nuclear momentum distribution is determined by relative momentum distribution in the correlated nucleon–nucleon pair embedded into nuclear environment, $n_{\rm cor}(\boldsymbol{p}) = C_2^2 n_{\rm rel}(\boldsymbol{p})$. The energy

spectrum predicted by Eq. (78) is a broad peak with the maximum at $\varepsilon \sim -\boldsymbol{p}^2/2M$ and effective width $|\boldsymbol{p}|\bar{p}_{\rm CM}/M$ with $\bar{p}_{\rm CM}$ an average CM momentum.

We perform the averaging over the CM motion of the NN pair in the field of other $A-2$ nucleons assuming that the CM momentum distribution is given by a Gaussian

$$n_{\rm CM}(\boldsymbol{p}_{\rm CM}) = (\alpha/\pi)^{3/2}\exp\bigl(-\alpha \boldsymbol{p}_{\rm CM}^2\bigr). \tag{79}$$

The parameter $\alpha$ is related to the averaged CM momentum of the nucleon–nucleon pair, $\alpha = \frac{3}{2}\langle \boldsymbol{p}_{\rm CM}^2\rangle^{-1}$. The latter can be estimated from the balance of the overall nucleus momentum [67], $\langle(\sum \boldsymbol{p}_i)^2\rangle = 0$, where the sum is taken over all bound nucleons and the expectation value is performed with respect to the intrinsic wave function of the nucleus. This gives $\langle \boldsymbol{p}_{\rm CM}^2\rangle = 2\langle \boldsymbol{p}^2\rangle(A-2)/(A-1)$, with $\langle \boldsymbol{p}^2\rangle$ the mean value of the squared single nucleon momentum. We consider configurations in which characteristic CM momenta are small. For this reason we should also exclude the high-momentum part in estimating $\langle \boldsymbol{p}^2\rangle$ and we will assume that this quantity is given by averaging over mean-field configurations.

Using Eq. (79) we integrate over the CM momentum in (78) and the result reads,

$$\mathcal{P}_{\rm cor}(\varepsilon, \boldsymbol{p}) = n_{\rm cor}(\boldsymbol{p})\frac{2M}{p}\sqrt{\alpha\pi}\bigl[\exp\bigl(-\alpha p_{\rm min}^2\bigr) - \exp\bigl(-\alpha p_{\rm max}^2\bigr)\bigr], \tag{80}$$

where $p = |\boldsymbol{p}|$, $p_{\rm min}$ and $p_{\rm max}$ are respectively the minimum and the maximum CM momenta allowed by the energy–momentum conservation in Eq. (77) for the given $\varepsilon$ and $\boldsymbol{p}$,

$$p_{\rm max} = M_* p/M + p_T, \tag{81a}$$

$$p_{\rm min} = |M_* p/M - p_T|, \tag{81b}$$

where $p_T = (2M_*(|\varepsilon| - E_{\rm th}))^{1/2}$ and $E_{\rm th} = E^{(2)} + E_R(\boldsymbol{p})$. The latter is the threshold value of the nucleon separation energy for discussed configurations. Note that in our notations $\varepsilon < 0$. We also remark that $p_T$ has the meaning of the maximum CM momentum in the correlated NN-pair in the direction transverse to $\boldsymbol{p}$ for the given $\varepsilon$ and $p$ [69].

In numerical evaluations we use the parameterizations for $n_{\rm MF}(A, \boldsymbol{p})$ and $n_{\rm cor}(A, \boldsymbol{p})$ of [67] which fit nicely the results of many-body calculation of nuclear momentum distribution. It follows from this calculation that low-momentum part incorporates about 80% of the total normalization of the spectral function while the other 20% are taken by the high-momentum part. The momentum distributions are presented in [67] for a limited range of nuclei. In order to evaluate the momentum distributions for other values of the nucleus mass number $A$, we interpolate the values of the momentum distributions for each value of momentum $|\boldsymbol{p}|$. For the parameter $E^{(2)}$ we take the two-nucleon separation energy, i.e. the difference $E_0^{A-2} - E_0^A$ between the ground state energies (note that $E^{(2)} > 0$). The remaining parameter $E^{(1)}$ of $\mathcal{P}_{\rm MF}$ is fixed using the Koltun sum rule [70], which is exact relation for non-relativistic systems with two-body forces

$$\langle\varepsilon\rangle + \langle T\rangle = 2\varepsilon_B, \tag{82}$$

where $\varepsilon_B = E_0^A/A$ is nuclear binding energy per bound nucleon and $\langle\varepsilon\rangle$ and $\langle T\rangle$ are the nucleon separation and kinetic energies averaged with the full spectral function

$$\langle\varepsilon\rangle = A^{-1}\int [{\rm d}p]\mathcal{P}(\varepsilon, \boldsymbol{p})\varepsilon, \tag{83a}$$

$$\langle T\rangle = A^{-1}\int [{\rm d}p]\mathcal{P}(\varepsilon, \boldsymbol{p})\frac{\boldsymbol{p}^2}{2M}. \tag{83b}$$

The function $\mathcal{P}_1$ describes the isovector component in a nucleus (see Eqs. (42)). In calculating $\mathcal{P}_1$ we assume that the correlation part of the spectral function $\mathcal{P}_{\rm cor}$ is mainly isoscalar and cancels out in the $p-n$ difference. Then $\mathcal{P}^{p-n}$ is determined by the difference of the mean-field configurations for protons and neutrons. If we further neglect small differences between the energy levels of protons and neutrons then $\mathcal{P}^{p-n}$ is determined by the difference in the occupation numbers of single-particle levels for protons and neutrons. In a complex nucleus the deep levels are usually occupied and their contribution cancel out in $\mathcal{P}_1$. The Fermi level has a large degeneracy factor and the occupation numbers for protons and neutrons are different. We then conclude that the difference $\mathcal{P}^{p-n}$ is saturated by the Fermi level and

$$\mathcal{P}_1 = \left|\phi_F(\boldsymbol{p})\right|^2 \delta(\varepsilon - \varepsilon_F), \tag{84}$$

where $\varepsilon_F$ and $\phi_F$ are the energy and the wave function of the Fermi level (we have neglected the recoil of the $A-1$ nucleus).

The isovector correction is usually relevant for heavy-weight nuclei in which there exists a considerable neutron excess over protons. For such nuclei the Fermi gas model is supposed to be a reasonable approximation and we use this model in numerical applications. In this model $|\phi_F(p)|^2 \propto \delta(p_F - p)$, where $p_F$ is the Fermi momentum which is determined by average nucleon density $\rho = 4p_F^2/(6\pi^2)$. The normalization coefficient can be found from condition (23), according to which $\mathcal{P}_1$ is normalized to unity. As a result we have

$$\mathcal{P}_1^{\rm FG} = \delta(p - p_F)\delta(\varepsilon - \varepsilon_F)/\big(4\pi p_F^2\big). \tag{85}$$

### *5.3. Nuclear pion distribution function*

In calculating the pion effect in nuclear structure functions the relevant quantity is the distribution of pion excess in a nucleus since the nucleon pion cloud effect is taken into account in the nucleon structure functions. The inspection of Eqs. (37) and (38) suggests that the pion correction is located at small $x < p_F/M$, which is also confirmed by model calculations. In this region a good approximation is to neglect $x^2/Q^2$ terms in Eqs. (36) as well as target mass corrections to structure functions. We also assume no off-shell dependence of pion structure function and base our discussion on convolution approximation by Eqs. (37) and (38).

Before doing model calculations it is important to realize that the pion distribution function is constrained by a number of sum rules. The first moment of (38) gives an average pion light-cone momentum

$$\langle y\rangle_\pi = \int {\rm d}y\, y f_{\pi/A}(y) = \big\langle\theta^\pi_{++}\big\rangle/M, \tag{86}$$

where $\theta^\pi_{++} = (\partial_0\varphi)^2 + (\partial_z\varphi)^2$ is the light-cone component of pion energy–momentum tensor. In Eq. (86) we assume the sum over different pion states and the averaging means $\langle\mathcal{O}\rangle = \int {\rm d}^3\boldsymbol{r}\langle A|\mathcal{O}(\boldsymbol{r})|A\rangle/\langle A|A\rangle$ for any operator $\mathcal{O}$. It is also useful to consider the average $y^{-1}$ which is proportional to $\varphi^2$ averaged over nuclear ground state:

$$\big\langle y^{-1}\big\rangle_\pi = \int {\rm d}y\, y^{-1} f_{\pi/A}(y) = M\big\langle\varphi^2\big\rangle. \tag{87}$$

The pion and nucleon fractions of nuclear light-cone momentum are related by the momentum balance equation

$$\langle y\rangle_\pi + \langle y\rangle_N = \frac{M_A}{AM}. \tag{88}$$

Eq. (88), although being intuitively obvious, can formally be derived in a meson-nucleon field-theoretic model of nuclear Hamiltonian [47]. Several constraints on nuclear pion distribution $\mathcal{D}_{\pi/A}(k)$ can be obtained in this model using the equations of motion for pion and nucleon operators and energy–momentum conservation condition. In particular, for a model nuclear Hamiltonian with nucleons and pions with pseudo-scalar interaction we obtain the following relations [47]

$$m_\pi^2\langle\varphi^2\rangle = \varepsilon_B + \langle T\rangle, \tag{89a}$$

$$\langle(\partial_0\varphi)^2\rangle = \varepsilon_B - \tfrac{1}{2}\big(\langle\varepsilon\rangle + \langle T\rangle\big), \tag{89b}$$

$$\langle(\nabla\varphi)^2\rangle = -\tfrac{3}{2}\langle\varepsilon\rangle - \tfrac{1}{2}\langle T\rangle. \tag{89c}$$

A few comments are in order. Pion field in nuclei is mainly generated by nucleon sources. Time variation of the pion field describes retardation effects in the nucleon–nucleon interaction. In a non-relativistic system this effect is small since typical energy variations are small compared to the pion mass. We, therefore, take the static approximation $\partial_0\varphi = 0$. Then Eq. (89b) is equivalent to the Koltun sum rule (82). In the static approximation for the pion energy–momentum tensor we have $\langle\theta^\pi_{++}\rangle = \frac{1}{3}\langle(\nabla\varphi)^2\rangle$. Then using Eq. (31) we conclude that Eqs. (89c) and (88) are equivalent. For this reason only Eq. (89a) gives independent constraint.

We use the constraints on average pion light-cone momentum $y$ and $1/y$ which follow from Eqs. (89a) and (88) in order to evaluate the pion contribution to nuclear structure functions. It should be remarked that in this approach by using momentum balance equation (88) we effectively take into account the contributions from all mesons. In order to quantitatively evaluate the pion effect in the structure functions we use a model distribution

$$f_{\pi/A}(y) = C\,y(1-y)^n, \tag{90}$$

which is motivated by the asymptotics of pion distribution function at small and large $y$. The normalization constant $C$ and the exponent $n$ are fixed from Eqs. (88) and (87) using Eqs. (31) and (89a). The nucleon average separation and kinetic energies are calculated with the spectral function described in Section 5.2.

### *5.4. Parameterization of off-shell effects*

The off-shell effect in the structure function $F_2$ is described by Eq. (45). In the analysis of data, described in detail in Section 5.7, we consider a phenomenological model of the off-shell function $\delta f_2(x, Q^2)$. In order to choose an appropriate model we first note that function (45) describes the relative off-shell effect on the LT structure function and we expect that $Q^2$-independent $\delta f_2$ is a good approximation. We also note that off-shell effects are constrained by the normalization of nuclear valence quark distribution (see Section 6.1). For this reason we anticipate that $\delta f_2(x)$ should have at least one zero. Moreover, the analysis of nuclear pion correction as discussed in Section 5.3 suggest that $\delta f_2(x)$ can have two zeros. These motivate us to choose the following simple parameterization for the off-shell function:

$$\delta f_2(x) = C_N(x - x_1)(x - x_0)(h - x), \tag{91}$$

where $C_N$ is an overall normalization constant and $0 < x_1 < x_0 < 1$ and $h > 1$. The analysis of data indicates that the parameters $h$ and $x_0$ are fully correlated and suggests $h = 1 + x_0$. After imposing such condition then expression (91) has only three independent parameters. We use this model to describe off-shell effects in the analysis of Section 5.7.2.

### 5.5. Effective scattering amplitude

As discussed in Section 4.2, the coherent multiple-scattering nuclear effects are determined by effective (averaged over hadronic configurations of the intermediate boson) scattering ampliudes $a_h$ for different helicities $h = \pm 1, 0$. The amplitudes $a_h = \bar{\sigma}_h(i + \alpha_h)/2$ are parametrized in terms of effective cross section $\bar{\sigma}$ and the Re / Im ratio $\alpha$. For the unpolarized case, which is considered in this paper, the relevant amplitudes are the average transverse $a_T = (a_+ + a_-)/2$ and the longitudinal $a_L$ amplitudes. One can qualitatively expect that $\bar{\sigma}_T$ descreases with $Q^2$ since the relative weight of higher mass states increases with $Q^2$ and the cross section decreases with the meson mass (see Section 4.2). In order to parametrize effective transverse cross section we use then the following expression

$$\bar{\sigma}_T = \sigma_1 + \frac{\sigma_0 - \sigma_1}{(1 + Q^2/Q_0^2)}. \tag{92}$$

The parameter $\sigma_0$ describes the cross section at small $Q^2$, while $\sigma_1$ corresponds to high-$Q^2$ regime. The choice of both these parameters will be discussed in detail in Section 5.7.1. The free parameter $Q_0^2$ describes the transition between low- and high-$Q^2$ regions. We note that in the discussed approach we only consider relative corrections to the effective cross section and for this reason the analysis is not very sensitive to the detailed modelling of such cross section. The presence of non-zero real part of the amplitude is required by both theoretical arguments and phenomenology. The choice of $\alpha_T$ in our analysis will be discussed in Section 5.7.1.

In order to fix the effective amplitude in the longitudinal channel we use the relation $a_L/a_T = R = F_L/F_T$ with $R$ calculated using the PDFs and the structure functions of Ref. [39] as discussed in Section 3 (see also Section 4.2).

The $C$-odd asymmetry $\Delta a = a_+ - a_-$ in the scattering amplitude of left- and right-polarized virtual boson does not affect the structure functions $F_1$ and $F_2$. However, $\Delta a$ is relevant for $F_3$ and affects the normalization of nuclear valence number as described in Section 6.1. It should be noted that the relative nuclear shadowing correction to $F_3$ does not depend on the cross section asymmetry $\Delta\sigma$ but does depend on $\alpha_\Delta = \mathrm{Re}\,\Delta a/\mathrm{Im}\,\Delta a$ as explained in Section 4.2.2. In order to fix $\alpha_\Delta$ we use the approach based on Regge phenomenology of high-energy hadronic amplitudes and approximate $\Delta a$ by the $\omega$-reggeon pole, a simple proper contribution to the $C$-odd amplitude. The energy dependence and Re / Im ratio of the Regge pole is fully determined by its intercept which is about 0.5 that leads to $\alpha_\Delta = 1$ [71]. We use this value in the calculation of nuclear shadowing correction to the valence quark distribution in Section 6.1.

### 5.6. Nuclear data

Table 1 summarizes the list of experimental data used in this paper. They include both muon (EMC, NMC, BCDMS, FNAL E665) and electron (SLAC E139, E140) scattering on a variety of targets: $p$, D, $^4$He, $^7$Li, $^9$Be, $^{12}$C, $^{27}$Al, $^{40}$Ca, $^{56}$Fe, $^{63}$Cu, $^{108}$Ag, $^{119}$Sn, $^{197}$Au, $^{207}$Pb. For each target and kinematic region, we select the most precise and recent data and we do not use earlier results characterized by larger uncertainties, since their contribution to the present analysis would be negligible.[5] Most of the data come from NMC for the small $x$ region and SLAC E139 for the region $x > 0.1$.

[5] Note also that the addition of unnecessary data points with large uncertainties can produce an artificial reduction of the $\chi^2$ of fits.

Table 1
List of nuclear data used in the analysis. See text for details

| Experiment | Targets | # of points | $x$ range | $Q^2$ range [GeV$^2$] |
|---|---|---|---|---|
| NMC [2] | D/$p$ | 12 | $7.0\times10^{-3}$–0.70 | 4.0 |
| NMC [4] | $^4$He/D | 18 | $3.5\times10^{-3}$–0.65 | 0.77–44.0 |
| NMC [3] | $^7$Li/D | 24 | $1.4\times10^{-4}$–0.65 | 0.034–39.0 |
| NMC [5] | $^9$Be/$^{12}$C | 15 | $1.25\times10^{-2}$–0.70 | 3.4–66.7 |
| NMC [3] | $^{12}$C/D | 24 | $1.5\times10^{-4}$–0.65 | 0.035–41.0 |
| NMC [4] | $^{12}$C/$^7$Li | 25 | $8.5\times10^{-3}$–0.60 | 0.8–17.0 |
| NMC [5] | $^{27}$Al/C | 15 | $1.25\times10^{-2}$–0.70 | 3.4–63.9 |
| NMC [4] | $^{40}$Ca/D | 18 | $3.5\times10^{-3}$–0.65 | 0.6–41.0 |
| NMC [4] | $^{40}$Ca/$^7$Li | 25 | $8.5\times10^{-3}$–0.60 | 0.8–17.0 |
| NMC [4] | $^{40}$Ca/$^{12}$C | 25 | $8.5\times10^{-3}$–0.60 | 0.8–17.0 |
| NMC [5] | $^{56}$Fe/$^{12}$C | 15 | $1.25\times10^{-2}$–0.70 | 3.4–66.6 |
| EMC [7] | $^{63}$Cu/D | 10 | $1.5\times10^{-2}$–0.61 | 3.3–46.4 |
| NMC [6] | $^{119}$Sn/$^{12}$C | 161 | $1.25\times10^{-2}$–0.70 | 1.3–110.0 |
| NMC [5] | $^{207}$Pb/$^{12}$C | 15 | $1.25\times10^{-2}$–0.70 | 3.4–66.1 |
| E139 [10] | He/D | 21 | 0.125–0.88 | 2.0–10.0 |
| E139 [10] | $^9$Be/D | 21 | 0.125–0.88 | 2.0–10.0 |
| E139 [10] | $^{12}$C/D | 17 | 0.205–0.80 | 3.5–10.0 |
| E139 [10] | $^{27}$Al/D | 21 | 0.125–0.88 | 2.0–10.0 |
| E139 [10] | $^{40}$Ca/D | 17 | 0.205–0.80 | 3.5–10.0 |
| E139 [10] | $^{56}$Fe/D | 23 | 0.084–0.88 | 2.0–10.0 |
| E139 [10] | $^{108}$Ag/D | 17 | 0.205–0.80 | 3.5–10.0 |
| E139 [10] | $^{197}$Au/D | 22 | 0.125–0.88 | 2.0–10.0 |
| E140 [9] | $^{56}$Fe/D | 8 | 0.200–0.50 | 1.0–5.0 |
| E140 [9] | $^{197}$Au/D | 1 | 0.200 | 1.0 |
| BCDMS [8] | $^{56}$Fe/D | 10 | 0.07–0.65 | 17.0–113.0 |
| E665 [11] | D/$p$ | 21 | $2.0\times10^{-5}$–0.25 | 0.005–35.6.0 |
| E665 [12] | $^{207}$Ca/$^{12}$C | 10 | $1.2\times10^{-4}$–0.027 | 0.15–7.9 |
| E665 [12] | $^{207}$Pb/D | 10 | $1.2\times10^{-4}$–0.027 | 0.15–7.9 |
| E665 [12] | $^{207}$Pb/$^{12}$C | 10 | $1.2\times10^{-4}$–0.027 | 0.15–7.9 |

We note that, since all available nuclear data are provided by fixed-target experiments, there is always an implicit correlation between $x$ and $Q^2$ in data points. Usually low-$x$ regions also correspond to low-$Q^2$ values. As described in the following, this reduces the possibility to test the $Q^2$ dependence of the model in a complete way.

### 5.7. Extraction of parameters

The numerical values of the parameters in the model are determined from the data listed in Table 1[6] with two main steps. Initially, we verify the consistency of our model with $F_2$ data from charged-lepton scattering, without imposing specific constraints. We then discuss in detail the deconvolution of different physical effects which contribute to the overall nuclear modification of the structure functions.

[6] We note that D/$p$ data were not used in our fits. We compare our predictions with these data in Section 6.5.

It must be noted that the extraction of parameters responsible for nuclear effects is correlated with the determination of PDFs (see Section 3.2), which requires both the proton and deuterium data to obtain the distributions of $d$ and $u$ quarks. Nuclear effects can significantly affect extraction of parton densities. In principle, using our approach it would be possible to extract simultaneously the proton PDFs and the parameters responsible for nuclear effects (such as off-shell correction and effective cross section) by applying QCD analysis to the extended set of data including nuclear data. However, in order to limit correlations we follow a different approach.

The parameters of the model are extracted only from the measured ratios $\mathcal{R}_2(A'/A) = F_2^{A'}/F_2^A$, where $A'$ and $A$ are two different nuclei (usually the denominator corresponds to deuterium). The description of the nucleon structure functions largely cancels in the ratios, thus effectively removing the correlation with PDFs. In order to verify this we applied an iterative procedure. We first extracted the parameters using PDFs obtained without our nuclear corrections. Then we repeated the procedure after updating the PDF extraction using the information on nuclear effects in deuterium from the previous step (Section 3.2). Results indicated that the fitted parameters were stable, demonstrating the absence of strong correlations.

Nuclear data are usually available in bins of $x$ ($\Delta x$), while only the average $\bar{Q}^2$ in each bin is provided. We perform a fit to the experimental data with MINUIT [72] by minimizing $\chi^2 = \sum(\mathcal{R}_2^{\rm exp} - \mathcal{R}_2^{\rm th})^2/\sigma^2(\mathcal{R}_2^{\rm exp})$, where $\sigma^2(\mathcal{R}_2^{\rm exp})$ represents the uncertainty on the measurements and the sum includes all data points. For each experimental point, the model is evaluated at the given average $\bar{Q}^2$ and integrated over the size of the $x$ bin:[7]

$$\mathcal{R}_2^{\rm th}\big(x, \bar{Q}^2, A'/A\big) = \frac{\int_{x-\Delta x/2}^{x+\Delta x/2} F_2^{A'}(x', \bar{Q}^2)\,{\rm d}x'}{\int_{x-\Delta x/2}^{x+\Delta x/2} F_2^{A}(x', \bar{Q}^2)\,{\rm d}x'}. \tag{93}$$

Both the normalization and point-to-point uncorrelated uncertainties, as published by experiments, are taken into account. We would like to emphasize that the lack of knowledge of the experimental $Q^2$ distribution in the $x$ bins can potentially result in a mismatch between data and predictions in the regions where a significant $Q^2$ dependence is present. As discussed in the following, this increases the systematic uncertainties of the calculation from the measured parameters at $x > 0.70$ and $x < 0.05$.

As explained in Section 3.2, we use a phenomenological extrapolation of free nucleon structure functions for $Q^2 < 1.0$ GeV$^2$ and, in general, nuclear corrections to structure functions can be calculated at low $Q^2$. However, we restrict the fits to extract the free parameters of our model to the data with $Q^2 \geqslant 1.0$ GeV$^2$ in order to reduce systematic uncertainties on the parameters. We then validate our predictions against the data points with $Q^2 < 1.0$ GeV$^2$, which are included in all comparisons shown in the following.

### *5.7.1. Choice of fixed parameters*

We start our fits by treating $\sigma_0$ and $\sigma_1$, the asymptotic values of the effective transverse cross section in Eq. (92), and the real part of the effective scattering amplitude $\alpha_T = {\rm Re}\,a_T/{\rm Im}\,a_T$ (Section 4.2.1) as additional free parameters. This procedure allows a preliminary estimate of their correlation with the remaining parameters and a consistency check with the expected values.

[7] In a few cases, in which the explicit $Q^2$ dependence is provided, the model is averaged over the corresponding $Q^2$ bins.

The best fit value obtained for $\sigma_1$ is consistent with zero. By setting $\sigma_1 \neq 0$ we can still obtain an acceptable description of data provided $\sigma_1 < 1.0$ mb (at 90%CL), due to the (anti)correlation of $\sigma_1$ with $Q_0^2$ in Eq. (92). After verifying that the correlation between $\sigma_1$ and the off-shell parameters in Eq. (91) is negligible, we then fix $\sigma_1 = 0$ in all our fits.

We note that a non-vanishing shadowing correction at large $Q^2$ affects the normalization of the valence quark number per nucleon (Section 6.1). In this respect we have two possible constraints at large $Q^2$. The first condition is to require the conservation of the overall valence number in nuclei through a balance between the shadowing and the off-shell corrections. As a second choice, it is also possible to explicitly impose the off-shell effect to conserve the valence quark number of the off-shell nucleon. This implies that both the off-shell and the shadowing effects conserve independently the normalization of valence quark distribution. In our approach, initially we do not assume any specific normalization constraint. Instead, we verify a posteriori the magnitude of the renormalization introduced by the off-shell effect (Section 6.1) and its balance with the shadowing correction. We then use the normalization condition for nuclear valence number to further bound some of the parameters. This procedure will be discussed in more detail in Sections 5.7.2 and 6.1.

The fits to DIS data on nuclear targets show a strong (positive) correlation between $\sigma_0$ and $\alpha_T$. In addition, the value of $\sigma_0$ is also correlated with $Q_0^2$ so that it is not possible to unambiguously disentangle the three parameters from the fits. If we fix $\alpha_T = 0$ we obtain $\sigma_0 = 36$ mb from data. However, data clearly prefer $\alpha_T \neq 0$, with a somewhat lower value of $\sigma_0$. The best fit solution corresponds to $\alpha_T = -0.179 \pm 0.038$(stat) and $\Delta\chi^2 \sim 29$ with respect to the fit with fixed $\alpha_T = 0$. This can be interpreted as the evidence for a sizeable real part in the effective scattering amplitude. If we impose $\sigma_0 = 27$ mb, as expected from VMD model by averaging over $\rho^0$, $\omega$ and $\phi$ vector mesons, we obtain $\alpha_T = -0.182 \pm 0.037$(stat). Note that this is in a good agreement with the analysis of $\rho^0$ photoproduction experiments [59] at low-$Q^2$. Since we require our phenomenological model to correctly reproduce the photoproduction limit, we fix $\sigma_0 = 27$ mb and $\alpha_T = -0.20$ according to [59].

In our model we use the pionic parton distributions extracted from real pion scattering data [42] to approximate the structure functions of virtual pions in nuclei. To this end we perform fits with and without the pionic sea distributions and we find a significantly better description of data in the latter case. Therefore we only consider the valence contribution to the pionic structure functions in the following.

### *5.7.2. Results*

In our model we assume three main free parameters: $C_N$, $x_0$ and $Q_0^2$ (see Sections 5.4 and 5.5). In addition, the off-shell function $\delta f_2(x)$ is characterized by the presence of a second zero, $x_1$. This specific feature has important consequences, as it is discussed in Section 6.2. Since the parameter $x_1$ turns out to be strongly correlated with $C_N$ and $Q_0^2$, we perform several fits with different fixed values of $x_1$ in the range $0.030 \leqslant x_1 \leqslant 0.065$ and we evaluate the corresponding effect on the normalization of the valence quarks at large $Q^2$. Among the fits with comparable $\chi^2$ with respect to data, we choose a fixed value $x_1 = 0.050$, since this value provides a good cancellation between off-shell and shadowing corrections in the normalization for all nuclei (see Section 6.1 for details).

In order to test our hypothesis about the universality of parameters in Eqs. (91) and (92), we perform independent fits to different sub-sets of nuclei (from $^4$He to $^{207}$Pb) and we compare the corresponding values of the parameters with the ones obtained from a combined fit to all data. As can be seen from Table 2, the results are compatible within uncertainties, thus allowing a unified

Table 2
Values of the parameters extracted from independent fits to different sub-sets of data with $Q^2 > 1.0\ \mathrm{GeV}^2$. Uncertainties are startistical only. The column on the right gives the $\chi^2$ from each fit and the corresponding number of degrees of freedom. The last row shows the result of the global fit

| Data set | $C_N$ | $x_0$ | $Q_0^2$ [GeV$^2$] | $\chi^2$/d.o.f. |
|---|---|---|---|---|
| $^4$He/D | $6.17 \pm 1.29$ | $0.456 \pm 0.033$ | $1.30 \pm 0.30$ | 16.0/35 |
| $^7$Li/D; $^9$Be/D | $7.65 \pm 0.92$ | $0.435 \pm 0.022$ | $0.80 \pm 0.30$ | 35.1/35 |
| $^{12}$C/D | $9.38 \pm 0.76$ | $0.449 \pm 0.012$ | $1.20 \pm 0.21$ | 23.8/31 |
| $^{27}$Al/D; $^{27}$Al/$^{12}$C | $7.39 \pm 0.86$ | $0.470 \pm 0.016$ | $3.60 \pm 2.41$ | 15.1/33 |
| $^{40}$Ca/D; $^{40}$Ca/$^{12}$C | $7.09 \pm 0.79$ | $0.482 \pm 0.016$ | $1.67 \pm 0.15$ | 56.8/58 |
| $^{56}$Fe/D; $^{63}$Cu/D; $^{56}$Fe/$^{12}$C | $8.28 \pm 0.53$ | $0.449 \pm 0.009$ | $1.39 \pm 0.30$ | 55.6/63 |
| $^{108}$Ag/D; $^{119}$Sn/$^{12}$C | $9.61 \pm 1.29$ | $0.448 \pm 0.018$ | $1.41 \pm 0.34$ | 21.0/29 |
| $^{197}$Au/D; $^{207}$Pb/D; $^{207}$Pb/$^{12}$C | $8.52 \pm 0.87$ | $0.387 \pm 0.026$ | $1.31 \pm 0.37$ | 18.2/42 |
| All data | $8.10 \pm 0.30$ | $0.448 \pm 0.005$ | $1.43 \pm 0.06$ | 458.9/556 |

Table 3
Correlation coefficients between the nuclear parameters from the global combined fit

| $C_{ij}$ | $j = C_N$ | $j = x_0$ | $j = Q_0^2$ |
|---|---|---|---|
| $i = C_N$ | 1.000 | −0.067 | −0.127 |
| $i = x_0$ | −0.067 | 1.000 | 0.006 |
| $i = Q_0^2$ | −0.127 | 0.006 | 1.000 |

treatment.[8] The values of $\chi^2$/d.o.f. indicate an excellent consistency between the model and the data points for all nuclei.

The final values of $C_N$, $x_0$ and $Q_0^2$ obtained from a global fit to nuclear data are given in the last line of Table 2. The correlation between the parameters is small and mainly related to the normalization constant, as can be seen from Table 3.

Figures 1 and 2 show the excellent overall agreement between the calculation and the data points for many different nuclei. A few comments are in order. The region at $x > 0.75$ is characterized by a significant $Q^2$ dependence and therefore the calculation based upon the average $\bar{Q}^2$ provided by the experiments is approximate. It must also be noted that in some cases the data points from different experiments are not fully consistent. In particular, the data points on $^{12}$C/D and $^{40}$Ca/D ratios from E665 experiment [12] at low $x$ seem to be systematically above the corresponding NMC measurements, which have smaller uncertainties. Similarly, a normalization problem could be present for $^{207}$Pb/D data from E665. Assuming the effect is common to all heavy targets, in our fits we use instead the double ratios ($^{40}$Ca/D)/($^{12}$C/D) and ($^{207}$Pb/D)/($^{12}$C/D) and the E665 measurement of the ratio $^{207}$Pb/D. The double ratios are in good agreement with NMC data (noticed also in [5]) as well as with our predictions, while the $^{207}$Pb/D points lie slightly above our calculations. Futhermore, the ratio $^7$Li/D shown in Fig. 1 indicates a small excess in the region of $x$ between 0.01 and 0.03, which produces corresponding reductions in the ratios $^{12}$C/$^7$Li and $^{40}$Ca/$^7$Li. The effect is much larger than the quoted systematic uncertainties. For instance, the exclusion of three points at $x = 0.0125, 0.0175, 0.0250$ from

[8] Unfortunately it is not possible to have data points covering both the high and low $x$ regions for all nuclei. This can result in a small sensitivity to some of the parameters for specific nuclei, as can be seen from the uncertainties in Table 2.

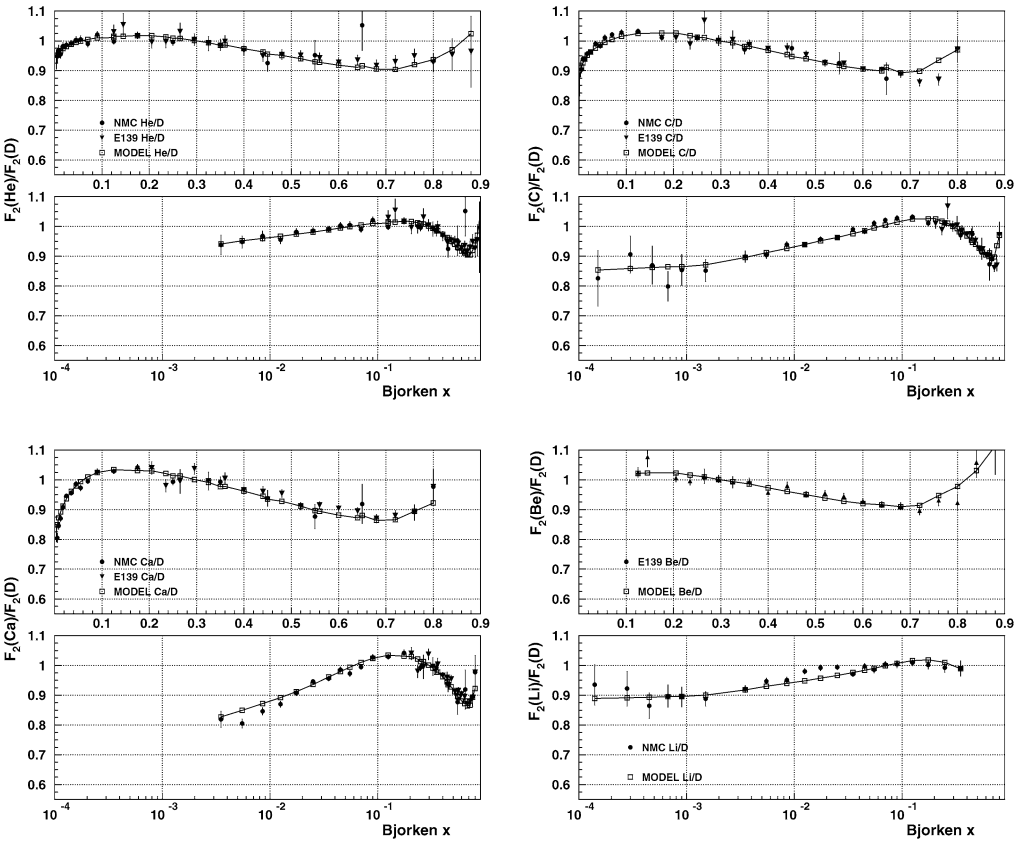


Fig. 1. Ratios $\mathcal{R}_2(x, A'/A)$ for $^4$He/D, $^{12}$C/D, $^{40}$Ca/D, $^7$Li/D and $^9$Be/D (left to right and top to bottom). The curves with open squares show the corresponding model calculations with the parameters specified in the last line of Table 2. For data points the error bars correspond to the sum in quadrature of statistical and systematic uncertainties, while the normalization uncertainty is not shown.

our fit leads to the reduction of overall $\chi^2$/d.o.f. for the ratio $^7$Li/D from 1.95 to 0.72.[9] We also comment that the value of the $^{207}$Pb/$^{12}$C ratio at $x = 0.7$ from NMC (Fig. 2) is marginally compatible with the corresponding value of $^{197}$Au/D ratio from E139 experiment.

It should be emphasized that at low $x$ there is an interplay between the off-shell function, the pion contribution and the coherent nuclear effects. This results in significant correlations between the corresponding parameterizations and does not allow an unambiguous extraction of individual components without external constraints. In our approach the pion (meson) excess in nuclei is calculated as described in Section 5.3. In order to disentangle the actual off-shell function from the remaining coherent correction, we use additional information from photoproduction experiments (Section 5.7.1). The agreement between our independent extraction of the average VMD parameters and the photoproduction limit makes us confident in the deconvolution of different components.

[9] The comment is only intended to quantify the effect. We keep all data in our fits, regardless of the inconsistencies described above.

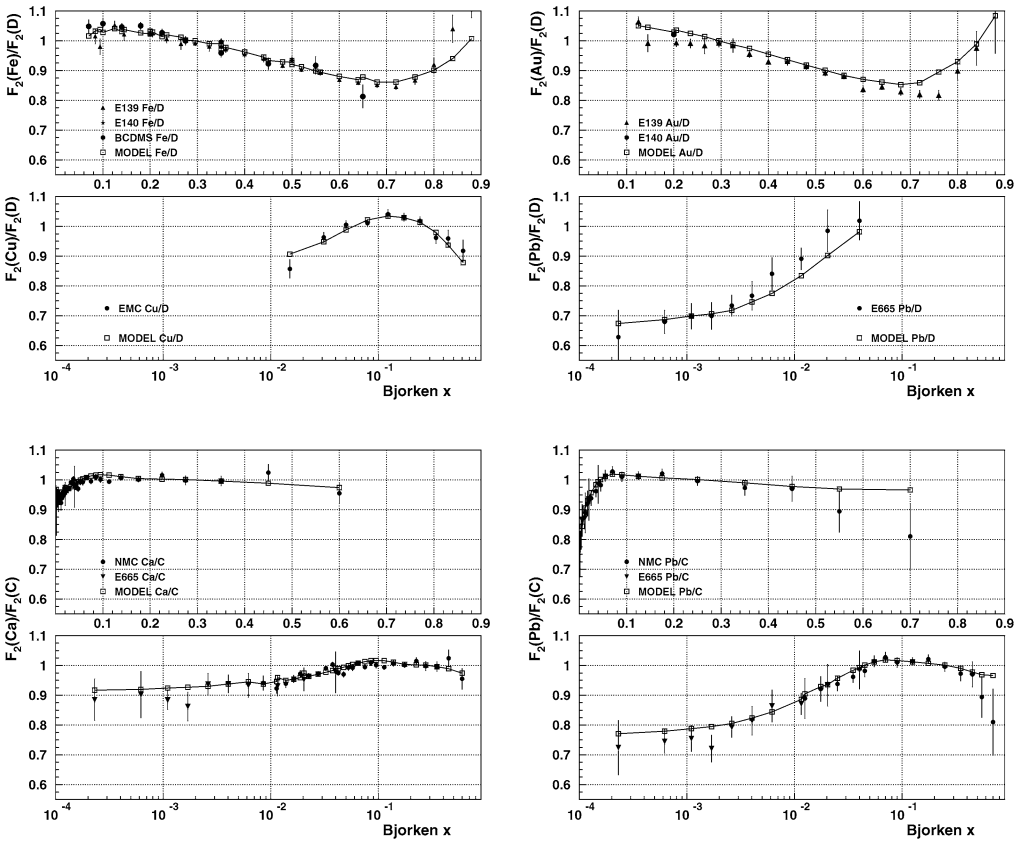


Fig. 2. Ratios $\mathcal{R}_2(x, A'/A)$ for $^{56}$Fe/D, $^{63}$Cu/D, $^{197}$Au/D, $^{207}$Pb/D, $^{40}$Ca/$^{12}$C and $^{207}$Pb/$^{12}$C (left to right and top to bottom). The curves with open squares show the corresponding model calculations with the parameters specified in the last line of Table 2. For data points the error bars correspond to the sum in quadrature of statistical and systematic uncertainties, while the normalization uncertainty is not shown.

We further check the interplay between nuclear pion excess and off-shell effects in our analysis by fitting our model without pion correction to $\mathcal{R}_2$ data. In this case the effective off-shell function $\delta f_2'$ absorbs the nuclear pion contribution to nuclear $F_2$. We use for this test a higher order polynomial with respect to Eq. (91), without any fixed parameter. This is intended to avoid biases from the functional form used to model the off-shell function. The results obtained for the effective $\delta f_2'$ are consistent with the following estimate which can be obtained by explicitly separating the nuclear pion contribution to nuclear $F_2$

$$\delta f_2' = \delta f_2 + \frac{\delta F_2^{\pi/A}(x)}{\langle v \rangle F_2^N(x)}, \tag{94}$$

where $\delta F_2^{\pi/A}$ is the nuclear pion correction calculated as described in Section 5.3 and $\langle v \rangle$ denotes the nucleon virtuality $v = (p^2 - M^2)/M^2$ averaged over the nuclear spectral function. Moreover, the best fit corresponds to a value of $Q_0^2$ which is in agreement with our fit with explicit treatment of nuclear pion correction.

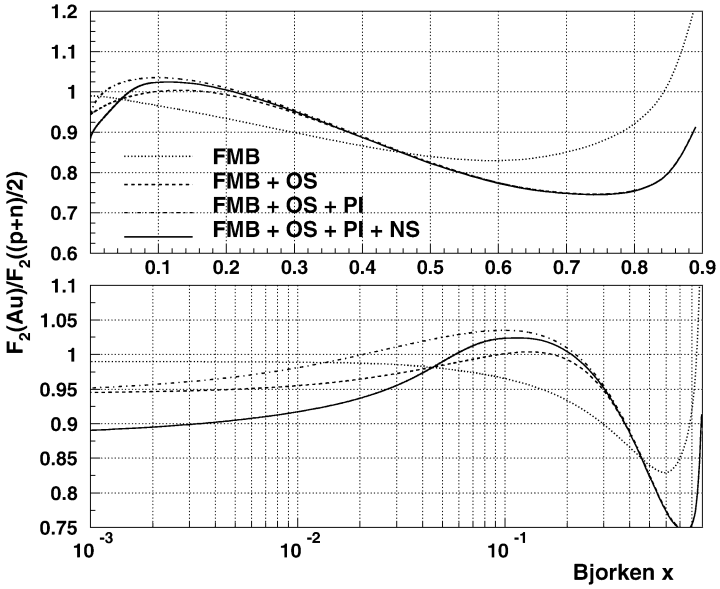


Fig. 3. Different nuclear effects on the ratio of $^{197}$Au to isoscalar nucleon for $F_2$ at $Q^2 = 10$ GeV$^2$. The labels on the curves correspond to effects due to Fermi motion and nuclear binding (FMB), off-shell correction (OS), nuclear pion excess (PI) and coherent nuclear processes (NS). Target mass and the neutron excess corrections are included.

Fig. 3 illustrates different nuclear corrections to the ratio of $F_2$ of $^{197}$Au to that of the isoscalar nucleon $F_2^N = \frac{1}{2}(F_2^p + F_2^n)$ calculated in our model using the final parameters shown in the last line of Table 2. As follows from comparison of Fig. 3 and the results of our fit displayed in Figs. 1 and 2 the standard Fermi motion and nuclear binding effect treated in impulse approximation does not quantitatively explain data at large $x$. The off-shell effect is therefore an important correction which modifies the structure functions of bound nucleon and affects the slope and the magnitude of the ratio $\mathcal{R}_2$ at large $x$. As discussed above, we extract this correction from inclusive nuclear DIS data. The disscussion of off-shell correction in terms of a scale characterizing valence quark distribution and its modification in nuclear environment is presented in Section 6.3.

*5.7.3. Systematic uncertainties*

Systematic uncertainties of the model are evaluated by varying each of the contributions from the deuterium wave function, the spectral function, the parton distributions, the pion structure function and the functional forms of $\delta f_2(x)$ and $\bar{\sigma}_T(Q^2)$. New fits are then performed and systematics are defined from the corresponding variation of the nuclear parameters and from the global $\chi^2$ values. Results are listed in Table 4.

Although we do not use directly deuterium data for the fits, most of the data points come from the ratios $\mathcal{R}_2$ of a heavy target to deuterium. In order to study the sensitivity of our result to the choice of the deuteron wave function we performed independent fits with two different choices of the deuteron wave function: the one which corresponds to the Bonn potential [62] and the Paris wave function [63]. These two wave functions have different high-momentum component and in this respect represent two extreme situations.

Table 4
The estimate of systematic uncertainties on the extraction of nuclear parameters. See text for a detailed explanation

| Systematics | $\delta C_N$ | $\delta x_0$ | $\delta Q_0^2$ [GeV$^2$] |
|---|---|---|---|
| Deuteron wave function | 0.238 | 0.0016 | 0.026 |
| Nuclear spectral function | 0.451 | 0.0046 | 0.021 |
| Parton distributions | 0.005 | 0.0007 | 0.023 |
| Pion structure function | 0.050 | 0.0020 | 0.065 |
| Functional form | 0.120 | 0.0040 | 0.070 |
| Cross sections $\sigma_0$ and $\sigma_1$ | 0.015 | 0.0005 | 0.165 |
| Total | 0.526 | 0.0067 | 0.195 |

Similarly, we modify the high-momentum component of the momentum distribution $n_{\rm cor}(\boldsymbol{p})$ in nuclei by multiplying it by the ratio of the Bonn and Paris deuteron wave functions squared. This is motivated by the observation [67,68] that the momentum distribution of finite nuclei and nuclear matter at high momenta are proportional to that of the deuteron. We then repeat our fits with modified spectral functions in order to estimate the corresponding variations of the parameters of the model.

The systematic uncertainty related to the parton distributions is estimated by varying the PDFs within their uncertainty ($\pm 1\sigma$). In addition, we also use different sets of parton distributions, extracted from fits to different data samples, with different $Q^2$ boundaries and different parameterization for the low $Q^2$ extrapolation.

For the pion structure function, we repeat our fits by using both the LO and the NLO approximations of the pionic parton distributions from [42]. We also arbitrarily change the parameterizations [42] within $\pm 10\%$.

We tried different functional forms in Eqs. (91) and (92) to parameterize $\delta f_2$ and $\bar{\sigma}_T$. In particular, for the off-shell function $\delta f_2$ we have tried a generic higher order polinomial parameterization in Eq. (91) and also used a parametrization with an additional $x^k$ term, with free parameter $k$. In spite of the new parameters, all acceptable results (i.e. with the values of $\chi^2$ comparable to our best fit solution) extracted from fits to data were very similar to the ones obtained with parametrization (91). We emphasize that the behaviour of the function $\delta f_2(x)$ for $x < 0.70$ is well constrained by data and only small variations on both the shape and the position of the zero $x_0$ are allowed. This observation in turn results in reduced systematic uncertainties of the model.

For the coherent nuclear effects, we varied $\sigma_0$ within the uncertainty estimated by averaging over $\rho^0$, $\omega$ and $\phi$ mesons, $\pm 3$ mb (Section 5.5). As explained in Section 5.7.1, this parameter is strongly correlated with $\alpha_T$ and $Q_0^2$. Similarly, we varied $\sigma_1$ within the $1\sigma$ allowed range (Section 5.7.1). We also tried to change the exponent controlling $Q^2$ dependence in Eq. (92). We obtained almost equally good fits with the dipole and monopole forms in Eq. (92). The monopole form of Eq. (92) had lower $\chi^2$/d.o.f. for the overall data set.

Fig. 4 shows the off-shell function $\delta f_2(x)$ and the effective cross section $\bar{\sigma}_T(Q^2)$ obtained in Section 5.7.2, together with the corresponding total uncertainty bands (including both statistical and systematic uncertainties). We comment that in our analysis the off-shell correction is treated as the first order correction in the parameter $v = (p^2 - M^2)/M^2$. At large $x > 0.7$ the off-shell correction can be as large as 25% for heavy nuclei (see also Fig. 3) indicating that higher-order terms in $v$ might not be negligible. This can also be a source of systematic uncertainty. However, going beyond the first order in $v$ requires the consideration of higher-order relativistic corrections

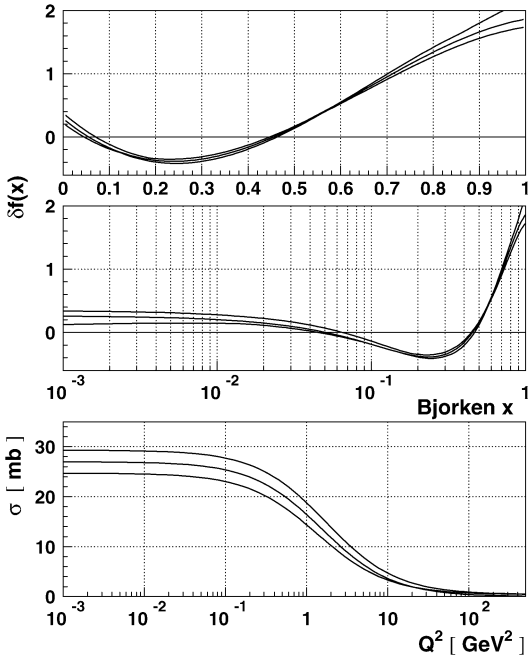


Fig. 4. Off-shell function $\delta f_2(x)$ and effective cross section $\bar{\sigma}_T(Q^2)$ corresponding to the parameters from Table 2. The curves show the size of the uncertainty bands ($\pm 1\sigma$), including both statistical and systematic (Table 4) uncertainties. The effect of different functional forms is also included, as explained in Section 5.7.3.

to nuclear wave and spectral functions (see discussion in Section 4.1.1) that would also affect the treatment of "standard" FMB effect. This goes beyond the scope of the present analysis. We also note that our phenomenological function $\delta f_2$ is extracted from nuclear data and hence it effectively incorporates additional contributions from missing terms.

The final results are dominated by systematic uncertainties, as can be seen from Tables 2 and 4. However, we note that the magnitude of systematic uncertainties is constrained by the value of $\chi^2$ of a global fit to data, as explained above. Therefore, the availability of more accurate (or with wider coverage of kinematics and nuclei) experimental measurements would significantly improve our results.

## 6. Discussion

We now discuss the results obtained from our fit to nuclear data in Section 5.7. In Section 6.1 we address the problem of the normalization of the nuclear valence quark distribution and Section 6.2 is focused on the implication of this constraint for our analysis. Section 6.4 is devoted to the $Q^2$ and $A$ dependence of nuclear effects predicted by our model. In Section 6.5 we discuss nuclear effects on the deuteron structure functions.

### *6.1. Nuclear valence quark number*

It is instructive to study the contributions due to different nuclear effects to the normalization of valence quark distribution in a nucleus. Common wisdom is that this quantity should not be

corrected by nuclear effects since it counts the baryon number of the system. Therefore, it is important to verify if different nuclear effects cancel out in the normalization. In the impulse approximation, i.e. if no shadowing and off-shell effects are taken into account, the cancellation of nuclear binding and Fermi motion effects in the normalization is explicit and it is guaranteed by the normalization of nucleon distribution function (30) to the number of nucleons. It should be also noted that nuclear pions do not contribute to nuclear valence distribution. In the presence of off-shell (OS) and nuclear shadowing (NS) effects different contributions to the valence quark normalization per one nucleon can be written as

$$N_{\mathrm{val}/A} = \int_0^A \mathrm{d}x\, q_{\mathrm{val}/A}(x) = N_{\mathrm{val}/N} + \delta N_{\mathrm{val}}^{\mathrm{OS}} + \delta N_{\mathrm{val}}^{\mathrm{NS}}, \tag{95}$$

where $N_{\mathrm{val}/N} = 3$ is the number of valence quarks in the nucleon and

$$\delta N_{\mathrm{val}}^{\mathrm{OS}} = \langle v\rangle \int_0^1 \mathrm{d}x \sum_{i=u,d} \big(q_{i/N}(x)\delta f_q(x) - \bar{q}_{i/N}(x)\delta f_{\bar{q}}(x)\big), \tag{96}$$

$$\delta N_{\mathrm{val}}^{\mathrm{NS}} = \int_0^1 \mathrm{d}x\, q_{\mathrm{val}/N}(x)\delta\mathcal{R}_{\mathrm{val}}(x). \tag{97}$$

Here $q_{\mathrm{val}/N} = u - \bar{u} + d - \bar{d}$ is the nucleon valence quark distribution, $\delta f_q$ and $\delta f_{\bar{q}}$ are off-shell correction functions for quark and antiquark distributions, $\delta\mathcal{R}_{\mathrm{val}}(x)$ is the shadowing correction to the valence quark distribution and $\langle v\rangle = \langle p^2 - M^2\rangle/M^2$ is the bound nucleon off-shellness averaged over nuclear spectral function (for more details see Section 7.1).[10]

In general, the off-shell corrections $\delta f_q$ and $\delta f_{\bar{q}}$ could be different. Since we phenomenologically extract the off-shell correction $\delta f_2$ from a study of $\mathcal{R}_2$ data it is difficult to unambiguously disentangle off-shell effects for quark and antiquark distributions. The analysis of additional data from either Drell–Yan production or neutrino scattering would be therefore important. While we defer a detailed analysis of the existing Drell–Yan data from nuclear targets [14] to a future publication, no sensitive neutrino data about nuclear effects on structure functions are currently available (see also the discussion in Section 7.2). In this paper we rather try to use simple considerations on the nuclear valence quark number in order to test the hypothesis of a single universal off-shell correction for all partons in the bound nucleon against the case of different corrections $\delta f_q$ and $\delta f_{\bar{q}}$. For this purpose it is enough to focus on the high $Q^2$ region, where we can use Eq. (47).

Let us first assume $\delta f_q(x) = \delta f_{\bar{q}}(x)$. From Eq. (47) we then also have $\delta f_2(x) = \delta f_q(x)$, that implies that we have a universal off-shell function for both quark (valence) and antiquark (sea) distributions. We evaluate $\delta N_{\mathrm{val}}^{\mathrm{OS}}$ by Eq. (96) as a function of $Q^2$ using the parameters of $\delta f(x)$ from Table 2 and the nucleon valence distribution of [39]. The results for iron and lead are reported in Fig. 5, indicating a positive off-shell correction of about 1.5–2% that decreases with $Q^2$. We then compute the shadowing correction $\delta N_{\mathrm{val}}^{\mathrm{NS}}$ by Eq. (106b) using the effective cross section

[10] Note that the normalization of valence quark distribution is not affected by the order of perturbation theory analysis and therefore Eq. (95) holds to any order in $\alpha_S$, unlike the Gross–Llewellyn-Smith sum rule [90] which is corrected by both perturbative [91] and non-perturbative effects.

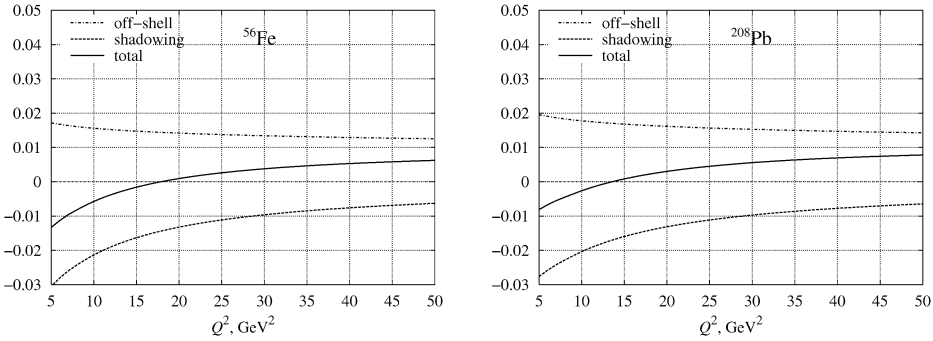


Fig. 5. Relative off-shell ($\delta N_{\rm val}^{\rm OS}/3$) and nuclear shadowing ($\delta N_{\rm val}^{\rm NS}/3$) corrections to the normalization of the valence quark distribution for $^{56}$Fe and $^{207}$Pb nuclei (left and right panel, respectively) computed as described in Section 6.1. The solid curve shows the sum of the off-shell and the nuclear shadowing corrections.

extracted from our fits (see Section 5.5). The results are shown in Fig. 5. It is important to observe that $\delta N_{\rm val}^{\rm NS}$ is negative and there is large cancellation between off-shell and shadowing effects in the normalization over a wide range of $Q^2$.

Let us now test a different hypothesis, namely no off-shell effect in the sea of bound nucleon $\delta f_{\bar q} = 0$. From Eq. (47) we then have for the isoscalar nucleon $(u+d)\delta f_q = \frac{18}{5} F_2 \delta f_2$. In this case the off-shell correction to valence quark number is dominated by the small $x$ region and even becomes divergent.[11] Therefore, this assumption leads to unphysical results and we have to rule out this case.

### *6.2. Normalization constraints*

In the following we will favor the assumption of a single universal off-shell function $\delta f(x)$, according to the discussion of the previous section. This is supported by the existing $\mathcal{R}_2$ data we used to extract the phenomenological off-shell function. The universality of $\delta f(x)$ should be further verified with both Drell–Yan data and future precise neutrino data. In our analysis we use the normalization condition in order to fix parameters of the function $\delta f(x)$, in particular the parameter $x_1$. As explained in Section 5.7.2, within all possible values of $x_1$ providing comparable descriptions of data ($\chi^2$) we selected the one minimizing the overall correction $\delta N_{\rm val}^{\rm OS} + \delta N_{\rm val}^{\rm NS}$.

The function $\delta f(x)$ measures the change in the quark–gluon structure of the nucleon in nuclear environment. This function is not accessible in experiments with isolated proton and/or neutron but can generally be probed in nuclear reactions. The results described in Section 5.7.2 demonstrate that inclusive DIS data have a good sensitivity to off-shell effects, allowing a precise determination of this correction.

The phenomenological cross section in Eq. (92) effectively incorporates contributions to structure functions due to all twists since it is extracted from data. Higher twists are known to be important at low and intermediate $Q^2$ and for this reason we should not expect an exact cancellation between $\delta N_{\rm val}^{\rm OS}$ and $\delta N_{\rm val}^{\rm NS}$ calculated with phenomenological cross section. Nevertheless, we observe from Fig. 5 that the cancellation becomes more accurate at higher $Q^2$ indicating transi-

[11] We obtain $\delta N_{\rm val}^{\rm os}/3 \approx -0.5$ for iron if we cut off the contribution of the region $x < 10^{-5}$. Changing the lower limit to $x = 10^{-6}$ increases the magnitude of this correction by about factor of 2.

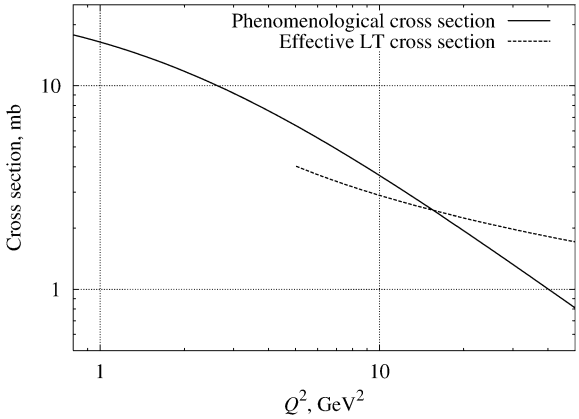


Fig. 6. Phenomenological cross section $\bar{\sigma}_T$ extracted from our fits (solid curve) and effective LT cross section (dashed curves) computed for iron and lead nuclei as described in Section 6.1.

tion to the leading twist regime. In particular, the exact cancellation takes place at $Q^2 \approx 15\,\mathrm{GeV}^2$. We performed similar calculation for several nuclei and we thus verified that this effect is independent of the choice of the nucleus.

It should be noted that the nuclear data available in the shadowing region are limited to relatively low $Q^2$ and for this reason the phenomenological cross section (92) is not constrained at high $Q^2$. In this work we evaluate the effective cross section at high $Q^2$ by treating the condition $\delta N_{\rm val}^{\rm OS} + \delta N_{\rm val}^{\rm NS} = 0$ as an equation on the cross section. We solve this equation numerically using the off-shell function $\delta f_2(x)$ from Section 5.7.2. The resulting cross section is presented in Fig. 6 together with phenomenological cross section extracted from our fits. In this paper we use the following simple model for the effective cross section. For $Q^2$ below the crossing point in Fig. 6 we use phenomenological cross section (92) extracted form the fits, and for higher $Q^2$ we use the cross section calculated from the normalization condition. The difference between the two curves in Fig. 6 below the crossing point is attributed to high-twist effects.

The function $\delta f(x)$ is positive for $x < x_1$ (see Fig. 4). This implies a negative off-shell correction to the structure functions at small Bjorken $x$ because the offshellness $v$ of a bound nucleon is negative. Thus the off-shell correction at small $x$ appears as a leading twist shadowing correction. Therefore, in this region there is a certain interplay between nuclear effects due to coherent nuclear interactions and off-shell effect. In the region $x_1 < x < x_0$ the function $\delta f(x)$ is negative that provides an enhancement of bound nucleon structure functions. Thus in our approach the antishadowing at $x \sim 0.1$ is linked to off-shell effects. It is important to note that for the valence distributions there is additional antishadowing mechanism due to coherent nuclear interactions. Indeed, the presence of substantial real part in the $C$-odd channel ($\alpha_\Delta = 1$) results in the constructive interference of multiple scattering interactions at $x \sim 0.1$ for valence distributions as will be discussed in more detail in Section 7.1.

### *6.3. Off-shell effect and modification of the nucleon size in nuclei*

From our analysis we obtain a positive off-shell correction at large $x > x_0$. Since the virtuality $p^2 - M^2$ of the bound nucleon is negative this leads to the suppression of valence distribution in the bound nucleon at large $x$. In order to give a qualitative interpretation to this result we consider a simple model of the valence distribution in the nucleon and we argue that the behavior of $\delta f_2$

at large $x$ observed in data can be related to the increase of the nucleon core radius in nuclear environment.

Let us consider the valence quark distribution in terms of spectral representation Eq. (48). We will consider a simple model in which the spectrum of spectator states is approximated by a single mass $\bar{s}$ [48,50]

$$D_{q/N} = \delta(s - \bar{s})\Phi\big(t, p^2\big), \tag{98}$$

where the function $\Phi(t, p^2)$ describes the distribution of valence quarks over $t = k^2$ in the nucleon with the invariant mass $p^2$. For the on-shell nucleon the distribution $\Phi(t)$ is characterized by a scale $\Lambda_v^2$. In configuration space this scale should be related to the size of the valence quark confinement region $r_c \sim \Lambda_v^{-1}$ (the nucleon core radius). From dimensional analysis one can write $\Phi(t) = C_v \Lambda_v^{-2} \phi(t/\Lambda_v^2)$ where $\phi$ and $C_v$ are dimensionless profile function and normalization constant. We found that a simple pole model $\phi(z) = (1-z)^{-n}$ results in a reasonable description of the nucleon valence distribution at large $x$ and high $Q^2$. In particular, we obtain a reasonable fit to valence distribution of [39] at $Q^2 = 15$ GeV$^2$ and $x \geqslant 0.2$ by taking $\bar{s} = 2.1$ GeV$^2$, $\Lambda_v^2 = 1.2$ GeV$^2$ and $n = 4.4$.

In order to model off-shell dependence of parton distributions we assume that the normalization constant $C_v$ and the scale $\Lambda_v$ become functions of $p^2$ while the profile function $\phi$ and the average mass of spectator states $\bar{s}$ do not change off-shell. We use Eq. (48) in order to calculate the off-shell modification of the quark distribution $\delta f_q$. The $\delta$-function in Eq. (98) allows us to integrate over the spectrum of residual system. Inspecting the resulting expression we observe a relation between the derivatives of the quark distribution with respect to $x$ and $p^2$. After some algebra we obtain

$$\delta f_q = c + \big[\ln q_{\rm val}(x)\big]' x(1-x)h(x), \tag{99}$$

$$h(x) = \frac{(1-\lambda)(1-x) + \lambda\bar{s}/M^2}{(1-x)^2 - \bar{s}/M^2}, \tag{100}$$

where $c = \partial \ln C_v / \partial \ln p^2$ and $\lambda = \partial \ln \Lambda_v^2 / \partial \ln p^2$ taken at $p^2 = M^2$. It should be noted that Eq. (99) is independent of the specific choice of the profile function $\phi$.

We use Eq. (99) in order to reproduce phenomenological function $\delta f_2$ at large $x$. In particular, we fix the parameters $c$ and $\lambda$ in order to reproduce the zero of $\delta f_2$ at large $x$ ($x_0$) and the slope $\delta f_2'(x_0)$. Using $\bar{s} = 2.1$ GeV$^2$ we obtain $\lambda = 1.03$ and $c = -2.31$. The function $\delta f_q(x)$ by Eq. (99) is shown in Fig. 7 together with the phenomenological function $\delta f_2(x)$. One observes that this simple model agrees with phenomenology at large $x$ but not at small $x$ at which effect of the nucleon sea is important.

The positive sign of the parameter $\lambda$ suggests that the scale parameter $\Lambda_v$ decreases in nuclear environment since $p^2 < M^2$ for bound nucleon. This in turn indicates the increase in the nucleon core $r_c$ in nuclear environment ("swelling" of bound nucleon). In order to quantitatively estimate this effect we consider the relative change in the nucleon radius $\delta r_c / r_c$. We have $\delta r_c / r_c \sim -\frac{1}{2}\delta\Lambda_v^2/\Lambda_v^2$. The relative change in the scale $\Lambda_v$ can be estimated as $\delta\Lambda_v^2/\Lambda_v^2 = \lambda\langle p^2 - M^2\rangle/M^2$, where averaging is taken over bound nucleons. We evaluate this quantity using our model spectral function for iron and obtain $\sim 9\%$ increase in $r_c$.

To conclude this section we remark that the swelling of bound nucleons was discussed in the context of quenching of nuclear longitudinal response function in [73]. The change of confinement scale in nuclei in terms of a different approach was discussed in the context of the EMC effect in [27,74]. The swelling effect was experimentally constrained to $< 30\%$ from the analysis of Coulomb sum in [75].

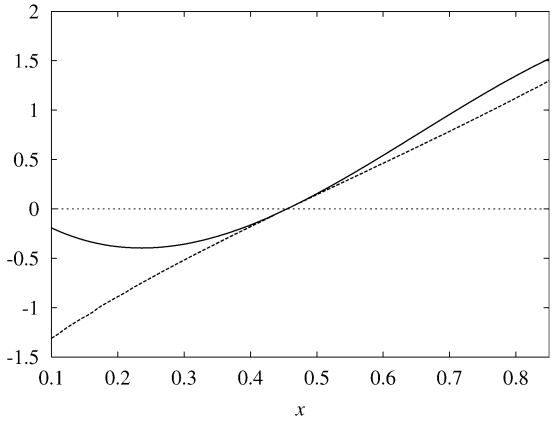


Fig. 7. Phenomenological off-shell function $\delta f_2(x)$ (solid) in comparison with $\delta f_q(x)$ (dashed) computed using Eq. (99) as described in text.

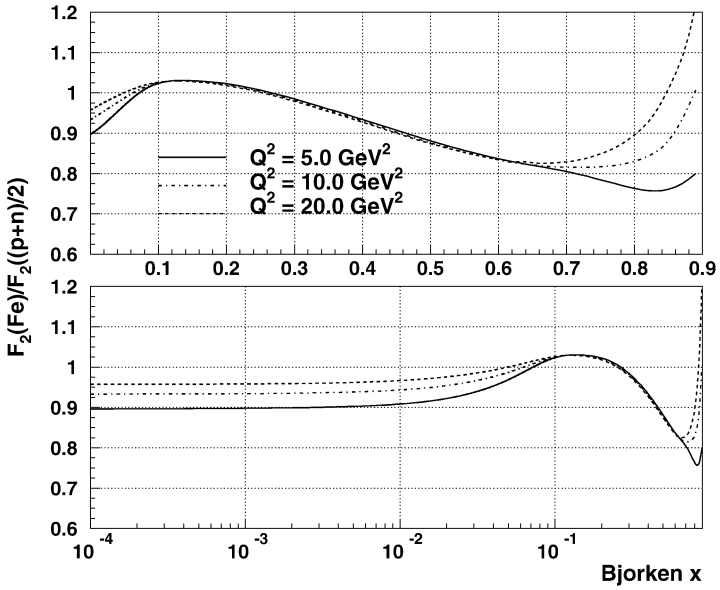


Fig. 8. Our predictions for the ratio of $^{56}$Fe and isoscalar nucleon structure functions calculated for $Q^2 = 5, 10, 20\ \mathrm{GeV}^2$. The calculation takes into account the non-isoscalarity correction for iron by Eq. (43).

### *6.4. The $Q^2$ and A dependence*

In order to illustrate the $Q^2$ dependence of $\mathcal{R}_2$ calculated in our approach, in Fig. 8 we plot the ratio $\mathcal{R}_2(\mathrm{Fe}/N)$, where $N$ is isoscalar nucleon $(p+n)/2$, as a function of $x$ for a few fixed $Q^2$. We observe from Fig. 8 significant variations of the ratio $\mathcal{R}_2$ with $Q^2$ at small $x < 0.1$ and large $x > 0.65$. This $Q^2$ dependence can be attributed to several effects. In the nuclear shadowing region at small $x$ the $Q^2$ dependence of the ratio $\mathcal{R}_2$ is due to the corresponding dependence of effective cross section $\bar{\sigma}_T$ (see Eq. (92) and Fig. 4). It must be also noted that in the region of $x$ between 0.01 and 0.1 the $Q^2$ dependence of $\mathcal{R}_2$ is affected by the $Q^2$ dependence of longitudinal

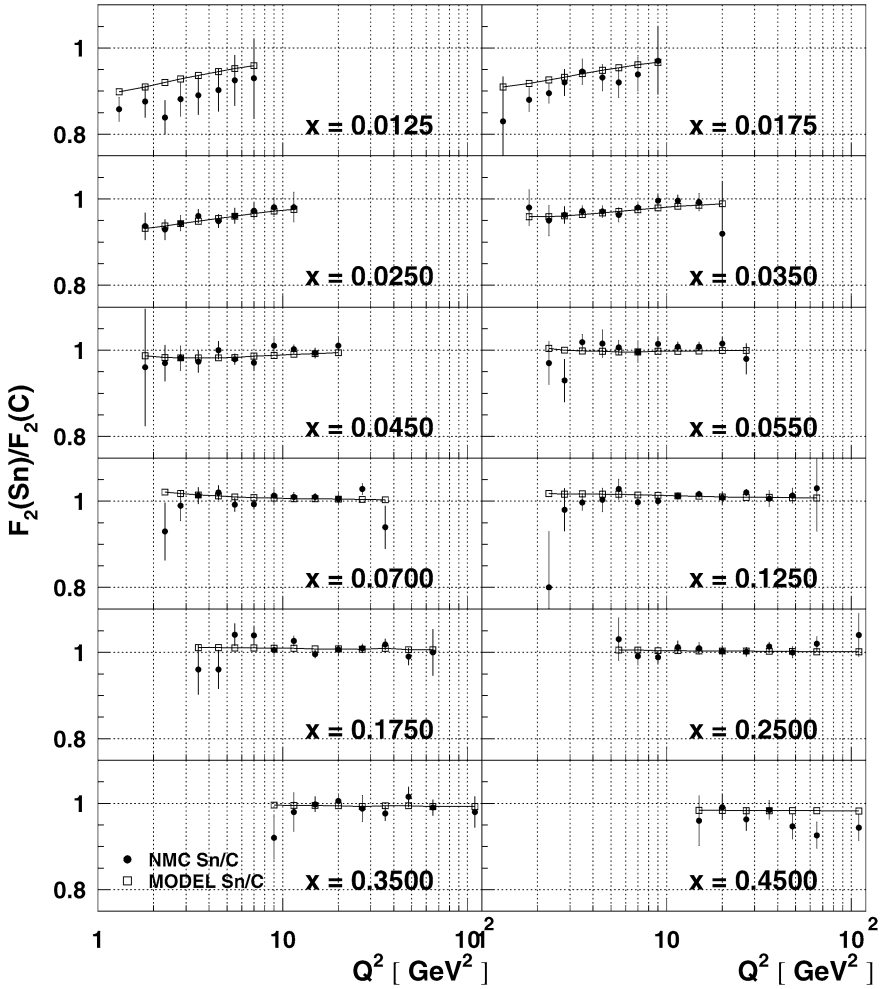


Fig. 9. The $Q^2$ dependence of the ratio $\mathcal{R}_2$(Sn/C) for different values of $x$ as measured by the NMC [5]. The curves with open squares show the corresponding model calculations. For data points the error bars correspond to the sum in quadrature of statistical and systematic uncertainties, while the normalization uncertainty is not shown.

correlation length $1/k_L$ (see Section 4.2 and Eqs. (53) and (62)). For $0.1 < x < 0.65$ the $Q^2$ dependence of $\mathcal{R}_2$ is negligible. At large $x$ the $Q^2$ dependence is due to the target mass correction effect by Eq. (11) in convolution equations.

In Fig. 9 we compare the NMC data on $Q^2$ dependence of the ratio $\mathcal{R}_2$(Sn/C) with our calculations. We observe an overall good agreement between data and model calculations for all values of $x$ within available region of $Q^2$. However, it should be remarked that available data on $Q^2$ dependence of nuclear effects are still too scarce to make thorough phenomenological studies of this effect. In particular, the correlation between $x$ and $Q^2$ for fixed target experiments and the lack of information about the $Q^2$ distributions of data in each of the $x$ bins used (typically only the average $Q^2$ is provided) can potentially bias the calculations where a significant $Q^2$ dependence is expected.

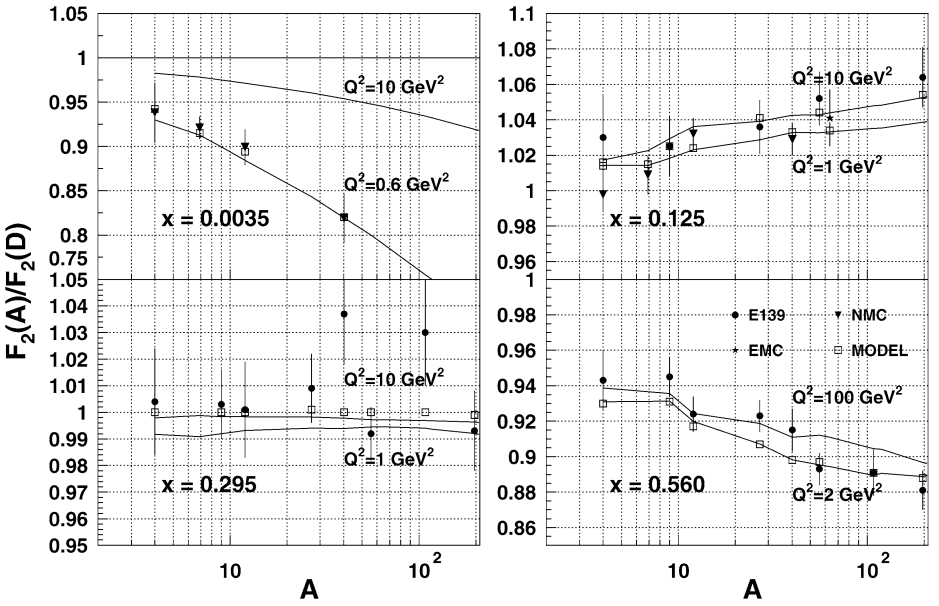


Fig. 10. The ratio $\mathcal{R}_2(A/\mathrm{D})$ as a function of $A$ for different values of $x$. The open squares show the model calculations corresponding to the average $Q^2$ of the data points. For data points the error bars correspond to the sum in quadrature of statistical and systematic uncertainties, while the normalization uncertainty is not shown. Two curves calculated at constant $Q^2$ values are also shown for comparison.

Figs. 1 and 2 show that the model reproduces correctly the ratios $\mathcal{R}_2$ over a wide range of nuclei and kinematic regions. The $A$ dependence of the ratio $\mathcal{R}_2$ is illustrated in Fig. 10 for a few fixed values of $x$. At small $x$ the $A$ dependence is related to the multiple scattering coefficients in Eqs. (62) and (67), through the nucleon number density distributions. The increase in the nuclear shadowing effect with $A$ has "geometrical" origin and can be attributed to the rising size of heavy nuclei. At large $x$ the $A$ dependence of the ratio $\mathcal{R}_2$ is determined by the corresponding dependence of parameters of nuclear spectral function. The slope of $\mathcal{R}_2$ as a function of $x$ at intermediate $x = 0.5$–$0.6$ increases with $A$ because of the corresponding increase in the average separation and kinetic energy of bound nucleons. It is interesting to note that at $x \approx 0.3$ the ratio $\mathcal{R}_2$ depends on neither $A$ nor $Q^2$.

### *6.5. Nuclear effects in deuterium*

Understanding of nuclear effects in deuterium is an important issue since deuterium data are often used as the source of information on the neutron structure functions. As explained in Section 5.7, the determination of $d$ and $u$ parton distributions is sensitive to nuclear corrections to deuterium data (Section 3.2). In this section we apply our model with the parameters fixed from fit to data from heavy nuclei (see Table 2) in order to calculate nuclear modifications in deuterium and compare our predictions with data. We take into account nuclear binding, Fermi motion, off-shell, nuclear pion and shadowing corrections as explained in Section 4. It should be emphasized that our approach does not require any extrapolation from heavy nuclei to deuterium.

The ratio of the deuteron and the proton structure functions $\mathcal{R}_2(\mathrm{D}/p) = F_2^{\mathrm{D}}/F_2^p$ was measured by the E665 and NMC collaborations [2,11] in a wide kinematical region of $x$ and $Q^2$.

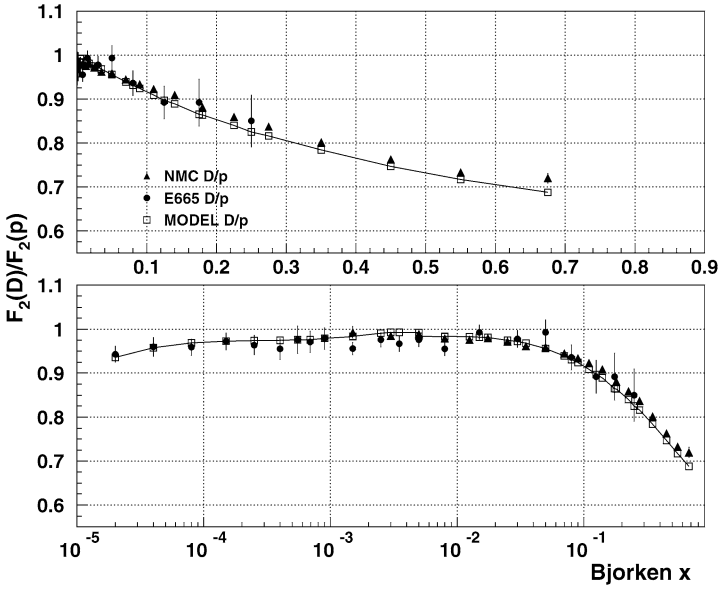


Fig. 11. Comparison of E665 and NMC data to our calculations (curve with open squares) for the ratio $\mathcal{R}_2(x, \mathrm{D}/p)$. For data points the error bars correspond to the sum in quadrature of statistical and systematic uncertainties, while the normalization uncertainty is not shown.

A comparison with these data provide a good test of the applicability of our model to D, since these data were not used in the fits described in Section 5.7. In Fig. 11 we show the E665 and NMC data together with the results of our calculations. A good agreement is found between data and the model described in this paper. In particular, our prediction of a small shadowing effect in D seems to be supported by the measured values of $\mathcal{R}_2(\mathrm{D}/p)$ at small values of $x$. We note that the ratio $\mathcal{R}_2(\mathrm{D}/p)$ also provides a test of the parton distributions used in our calculation and in particular of the difference between $d$ and $u$ quark contents. This was not the case for all the remaining data listed in Table 1 which were corrected by experiments for the neutron excess, thus providing an effective cancellation of PDFs in the ratios $\mathcal{R}_2(A'/A)$ (Section 5.7).

Unlike the ratio $\mathcal{R}_2(\mathrm{D}/p)$ the ratio $\mathcal{R}_2(\mathrm{D}/N) = F_2^D/F_2^{p+n}$ cannot be measured directly because a free neutron target is not available. The extraction of $\mathcal{R}_2(\mathrm{D}/N)$ from SLAC data was discussed in Ref. [10] in terms of a phenomenological model of the EMC effect in the deuterium. In Ref. [10] the ratio $\mathcal{R}_2(\mathrm{D}/N)$ was extracted by extrapolating the measured ratios $\mathcal{R}_2(A/\mathrm{D})$ using the nuclear density model of Ref. [27]. The key assumption was made that the quantity $\mathcal{R}_2(A/N) - 1$ scales as nuclear number density and it was also assumed that this ratio is independent of $Q^2$. The values of $\mathcal{R}_2(\mathrm{D}/N)$ were given in [10] for $x$ corresponding to the $x$ bins of SLAC data. The results are shown in Fig. 12 together with our calculation of the ratio $\mathcal{R}_2(\mathrm{D}/N)$ for the same kinematics of the points presented in [10].[12] In Fig. 13 we show our prediction for the ratio $\mathcal{R}_2(\mathrm{D}/N)$ at fixed $Q^2 = 10$ GeV$^2$ and the corresponding uncertainty band ($\pm 1\sigma$), including model systematics.

[12] The theoretical uncertainties of such extrapolation were not estimated in [10]. See also discussion of these points in [53].

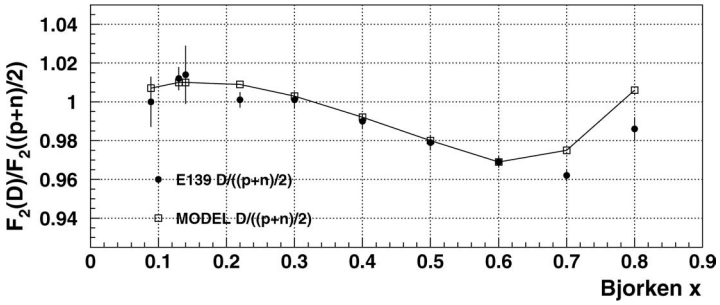


Fig. 12. Comparison of the extrapolations of E139 nuclear data within the nuclear density model of Ref. [10] to our calculations (curve with open squares) for the ratio $\mathcal{R}_2(x, \mathrm{D}/N)$. The error bars of the E139 data points correspond to the sum in quadrature of statistical and systematic uncertainties. For each $x$ value, the model calculation was performed at the average $Q^2$ of the experimental points quoted in Ref. [10].

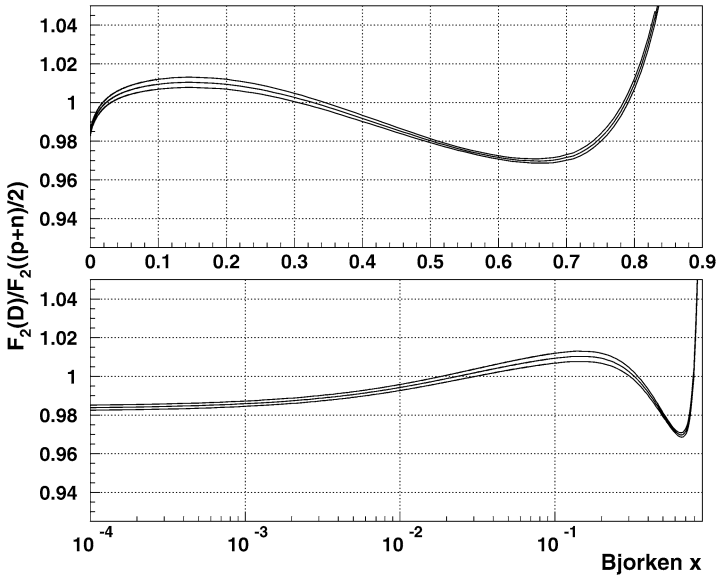


Fig. 13. Our predictions for the ratio $\mathcal{R}_2(x, \mathrm{D}/N)$ of deuterium to isoscalar nucleon at a fixed $Q^2 = 10\ \mathrm{GeV}^2$. The $\pm 1\sigma$ band is also given, including both statistical and systematic uncertainties.

## 7. Applications

In this section we apply our results to evaluate nuclear parton distributions (Section 7.1) and make the predictions of nuclear effects for neutrino structure functions (Section 7.2).

### *7.1. Nuclear parton distributions*

The parton distributions are process-independent characteristics of the target in high-energy processes. Different phenomenological approaches to the extraction of nuclear PDFs (nPDFs) can be found in Refs. [76–79]. It should be remarked at this point that physics observables are the cross sections and the structure functions, which include contributions from all twists. The

higher-twist terms are generally process-dependent, can be essential in the region of relatively low $Q^2$, and, furthermore, can be substantially affected by nuclear environment. Therefore, the applicability of the leading twist approximation must be considered in comparison with data as well as in any attempt to extract nPDFs. In our approach we derive nPDFs from the analysis of nuclear structure functions (Sections 5.7.2 and 6.2) that allows us to determine both nPDFs and their uncertainties from existing data. However, this paper is not aimed at the full nPDF analysis, which will be published elsewhere [80]. We rather want to discuss a few different effects which cause modifications of nuclear quark distributions. The numerical results shown in this section were obtained using the NNLO proton and neutron PDFs described in Section 3.2.

*7.1.1. Nuclear convolution*

As discussed in Section 4, in the region of high $Q^2$ and large $x$ the nuclear structure functions can be approximated by incoherent contributions from different nuclear constituents which can be presented in a convolution form (see Eqs. (29) and (37)). The convolution formulas look similar for all type of nuclear structure functions suggesting that the convolution equations hold for the parton distributions. We denote $q_{a/T}(x, Q^2)$ the distribution of quarks of type $a$ in a target $T$. Then the quark distribution in a nucleus can be written as

$$q_{a/A}\big(x, Q^2\big) = \sum_{c=p,n,\pi} f_{c/A} \otimes q_{a/c}, \tag{101}$$

where the function $f_{c/A}(y, v)$ can be interpreted as the distribution of particles of type $c$ in a nucleus over light-cone momentum $y$ and invariant mass (virtuality) $v$ (for bound nucleons and nuclear pions see Eqs. (30) and (38), respectively). The operation $f \otimes q$ denotes the convolution

$$f \otimes q = \int\limits_{x<y} \frac{\mathrm{d}y\,\mathrm{d}v}{y} f(y, v) q\big(x/y, Q^2, v\big). \tag{102}$$

Equations similar to (101) can be written for antiquark and gluon distributions in nuclei. Note also that the distribution functions are independent of $Q^2$ and, therefore, the $Q^2$ evolution of nuclear PDFs is goverened by the evolution of PDFs of nuclear constituents.

In view of applications to complex nuclei with different number of protons and neutrons, it is usefull to sort out the contributions to the convolution equation according to *isospin*. Let us consider the isoscalar and isovector quark distributions, $q_0 = u + d$ and $q_1 = u - d$. We first address the contributions from bound protons and neutrons to nuclear quark distributions. Assuming exact isospin invariance of PDFs in the proton and neutron we have simple relations between the isoscalar and the isovector distributions in the proton and the neutron

$$q_{0/p}\big(x, Q^2\big) = q_{0/n}\big(x, Q^2\big), \tag{103a}$$

$$q_{1/p}\big(x, Q^2\big) = -q_{1/n}\big(x, Q^2\big). \tag{103b}$$

Using these relations we observe that the quark distributions with different isospin decouple in the convolution equation. In particular, for the isoscalar ($q_{0/A}$) and the isovector ($q_{1/A}$) nuclear quark distributions we have

$$q_{0/A}\big(x, Q^2\big) = A\, f_0 \otimes q_{0/p}, \tag{104a}$$

$$q_{1/A}\big(x, Q^2\big) = (Z - N)\, f_1 \otimes q_{1/p}, \tag{104b}$$

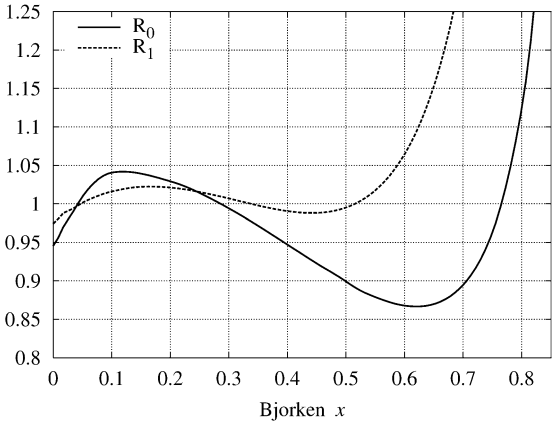


Fig. 14. Nuclear effects for the isoscalar and the isovector quark distributions in $^{56}$Fe. The ratios $\mathcal{R}_0$ and $\mathcal{R}_1$ (see text) were calculated for the valence quark distributions at $Q^2 = 20$ GeV$^2$. Nuclear shadowing and pion corrections are also included for the isoscalar distribution.

where $f_0$ and $f_1$ are the isoscalar and the isovector nucleon distributions in a nucleus. These distributions are given by Eq. (30) with the spectral functions $\mathcal{P}_0$ and $\mathcal{P}_1$ defined by Eq. (42). Note that the distributions $f_0$ and $f_1$ are normalized to unity.

Let us now discuss the pion contribution to Eq. (101). Similar to the nucleon case, we assume the isospin relations for quark distributions in the pion: $q_{0/\pi^+} = q_{0/\pi^-} = q_{0/\pi^0}$ and $q_{1/\pi^+} = -q_{1/\pi^-}$ and $q_{1/\pi^0} = 0$. Using these relations we have for the pion correction to the isoscalar and isovector nuclear quark distributions

$$q^{\pi}_{0/A}\big(x, Q^2\big) = f_{\pi/A} \otimes q_{0/\pi}, \tag{105a}$$

$$q^{\pi}_{1/A}\big(x, Q^2\big) = (f_{\pi^+/A} - f_{\pi^-/A}) \otimes q_{1/\pi}. \tag{105b}$$

Here in the first equation $f_{\pi/A}$ is the sum of the distributions over all pion states. It should be emphasized that in Eqs. (105) the pion distributions refer to nuclear pion excess, since scattering off virtual pions emitted and absorbed by same nucleon (nucleon pion cloud) are accounted in the proton and neutron PDFs. For the calculation of nuclear pion distributions in our model see Section 5.3.

The isovector component should vanish in isoscalar nuclei with $Z = N$.[13] However, for a generic nucleus with different number of protons and neutrons both the isoscalar and the isovector distributions are present. Heavy nuclei typically have a small excess of neutrons over the protons and the distributions $f_0$ and $f_1$ are quite different in such nuclei, as discussed in Section 4.1.5. For this reason nuclear corrections depend on the isospin (quark flavour). In order to illustrate this statement we calculate the ratios $\mathcal{R}_0 = q_{0/A}(x)/(A\, q_{0/p}(x))$ and $\mathcal{R}_1 = q_{1/A}(x)/[(Z-N)q_{1/p}(x)]$ for the iron nucleus using the proton PDFs of Ref. [39]. The results are shown in Fig. 14. We note that the full nuclear correction is shown in case of $q_{0/A}$, i.e. the calculation includes effect of nuclear spectral function, off-shell correction, nuclear pion

[13] It should be remarked that this statement applies to nuclear states with the total nuclear isospin 0. If higher-isospin states are present for a $Z = N$ nucleus, then the isovector distribution $q_{1/A}$ may be non-zero. The discussion of these issues is postponed for future studies.

and shadowing effects. However, for the isovector quark distribution $q_{1/A}$ we neglect possible nuclear pion and shadowing effects.

*7.1.2. Nuclear shadowing*

In this section we discuss coherent nuclear effects in the context of parton distributions. To this end we want to apply the approach discusses in Section 4.2.2. The multiple scattering effects are generally different for different PDFs. We specify this statement by considering nuclear effects for quark distributions of different $C$ parity, $q^{(\pm)}(x) = q(x) \pm \bar{q}(x)$. In order to simplify discussion we consider the isoscalar (anti)quark distributions, $q = u + d$ and $\bar{q} = \bar{u} + \bar{d}$. The $C$-odd distribution is in fact the valence quark distribution in the target $q^{(-)} = q_{\rm val}$. The $C$-even distribution at small $x$ describes the target quark sea.

In order to bridge between Section 4.2 and the present discussion we recall that the structure function $F_1$ in the LT approximation is given by $C$-even distribution $q^{(+)}$. The structure function $F_1$ is transverse helicity structure function (more precise, the average over left- and right-polarized transverse helicity structure function, see Eq. (9)). At small $x$, as discussed in Section 4.2, nuclear effects are described by the propagation of hadronic component of virtual boson with the proper helicity state in nuclear environment. Eq. (63) applies in the case of $q^{(+)}$.

Similarly, the structure function $F_3$ in the LT approximation is given by $C$-odd (valence) distribution $q^{(-)}$. In terms of helicity structure functions this is the asymmetry between left- and right-polarized states. Therefore, nuclear corrections to $q^{(-)}$ at small $x$ can be described by Eq. (66). We have for coherent nuclear corrections to $q^{(+)}$ and $q^{(-)}$ quark distributions

$$\delta\mathcal{R}^{(+)} = \frac{\delta q_A^{(+)}(x)}{q_N^{(+)}(x)} = \mathrm{Re}\big(a_T^2 \mathcal{C}_2^A\big)/\,\mathrm{Im}\, a_T, \tag{106a}$$

$$\delta\mathcal{R}^{(-)} = \frac{\delta q_A^{(-)}(x)}{q_N^{(-)}(x)} = \big[2\,\mathrm{Re}\big(\Delta a\, a_T \mathcal{C}_2^A\big) - \mathrm{Im}\big(\Delta a\, a_T^2 \mathcal{C}_3^A\big)\big]/\,\mathrm{Im}\,\Delta a, \tag{106b}$$

where $\mathcal{C}_2^A$ and $\mathcal{C}_3^A$ are given by Eqs. (62) and (67) with effective transverse scattering amplitude $a_T = (i + \alpha_T)\bar{\sigma}_T/2$. Eq. (106b) determines the nuclear shadowing effect for valence quark distribution $\delta\mathcal{R}_{\rm val} = \delta\mathcal{R}^{(-)}$. The amplitude $\Delta a$ describes the left–right asymmetry in the transverse amplitude. In other terms $\Delta a$ can be interpreted as the difference between $\bar{q}N$ and $qN$ scattering amplitudes [61]. As discussed in Section 4.2.2 the correction $\delta\mathcal{R}^{(-)}$ does not depend on the specific value of the cross section asymmetry $\Delta\sigma$ but does depend on $\alpha_\Delta = \mathrm{Re}\,\Delta a/\,\mathrm{Im}\,\Delta a$. The rate of nuclear effects for both $C$-even and $C$-odd distributions is determined by transverse amplitude $a_T$. Nuclear shadowing effect for antiquark distributions can readily be derived from Eqs. (106a) and (106b) and we have

$$\delta\mathcal{R}_{\rm sea} = \frac{\delta\bar{q}_A(x)}{\bar{q}_N(x)} = \delta\mathcal{R}^{(+)} + \frac{q_{{\rm val}/N}(x)}{2\bar{q}_N(x)}\big(\delta\mathcal{R}^{(+)} - \delta\mathcal{R}^{(-)}\big). \tag{107}$$

The results of calculation of nuclear effects for valence quark and antiquark distributions are reported in Fig. 15. The calculations account of the effects of smearing with nuclear spectral function (FMB), off-shell corrections (OS), nuclear shadowing (NS), and nuclear pion (PI) corrections. The FMB, OS, and PI corrections have been computed as discussed in Section 7.1.1 using our model spectral function, pion distribution function and off-shell correction described in Section 5. The NS correction for valence and sea distributions are computed by Eqs. (106b) and (107) using the parameters of effective scattering amplitude derived from our fits (see Sections 5.7.2 and 6.2).

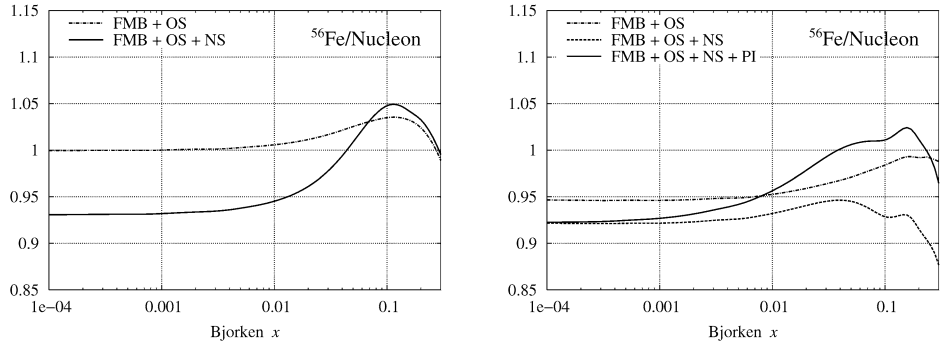


Fig. 15. Nuclear effects for isoscalar valence and sea quark distributions calculated for iron nucleus at $Q^2 = 20$ GeV$^2$ (see text). The left panel displays different contributions to $\mathcal{R}_{\rm val}$: the dot-dashed curve if only the effect of nuclear spectral function (FMB) and off-shell (OS) corrections are taken into account, the full curve is overall nuclear correction including nuclear shadowing effect (NS). The right panel displays similar contributions to $\mathcal{R}_{\rm sea}$. The full curve also includes the nuclear pion effect (PI), which is absent for the valence quark distribution.

A few remarks are in order. At small $x < 0.01$ the NS effect for valence quark distribution is enhanced relative to that for nuclear sea. The underlying reason for that is the enhancement of multiple scattering corrections for the cross section asymmetry as discussed in Section 4.2.2. If we keep only the double scattering correction then the ratio $\delta\mathcal{R}_{\rm val}/\delta\mathcal{R}_{\rm sea}$ is given by Eq. (60). The OS correction is negative in this region. However, the combined effect of FMB and OS is somewhat different for valence and sea distributions as displayed in Fig. 15. This is attributed to different $x$ dependence of valence and sea in the nucleon which affect the result of the averaging with nuclear spectral function. Nevertheless, in spite of these differences, the overall nuclear corrections are similar for valence and sea for $x < 0.01$.[14]

One observes that nuclear corrections for valence and sea distributions are different in the antishadowing region. The antishadowing effect for valence (i.e. positive nuclear correction) is a joint effect of two corrections both of which are positive: (1) the FMB and OS corrections and (2) the constructive interference in the multiple scattering effect which is due to a finite real part $\alpha_\Delta$ of the effective scattering amplitude in the $C$-odd channel (for this reason shadowing becomes antishadowing, see the left panel of Fig. 15). For sea-quark distribution in the antishadowing region we observe a cancellation between different effects. In this respect we remark that the contribution of the last term in Eq. (107) becomes increasingly important at $x > 0.05$, because of the ratio $q_{{\rm val}/N}(x)/\bar{q}_N(x)$. This term is negative in this region and cancels a positive nuclear pion contribution. As a result the overall nuclear correction to antiquark distribution is small for $0.02 < x < 0.2$. Note that this agrees with the results of E772 experiment, in which no enhancement of nuclear sea was observed in DY nuclear processes [14].

It should be noted that the calculation of the relative nuclear correction for valence quark distribution is stable with respect to the choice of the PDF set for entire region of $x$ (see also Fig. 14 for nuclear correction to valence distributions). Nuclear effects for sea quarks also depend weakly on the particular choice of PDF for small $x$. However, at high $x$ the calculation of nuclear effects for antiquark distributions has larger uncertainties and the result is sensitive to both the shape and the magnitude of the nucleon antiquark distribution (note the val/sea ratio in Eq. (107)).

[14] Note that this discussion refers to a high $Q^2 \sim 20$ GeV$^2$. At lower $Q^2$ the balance between different nuclear effects change.

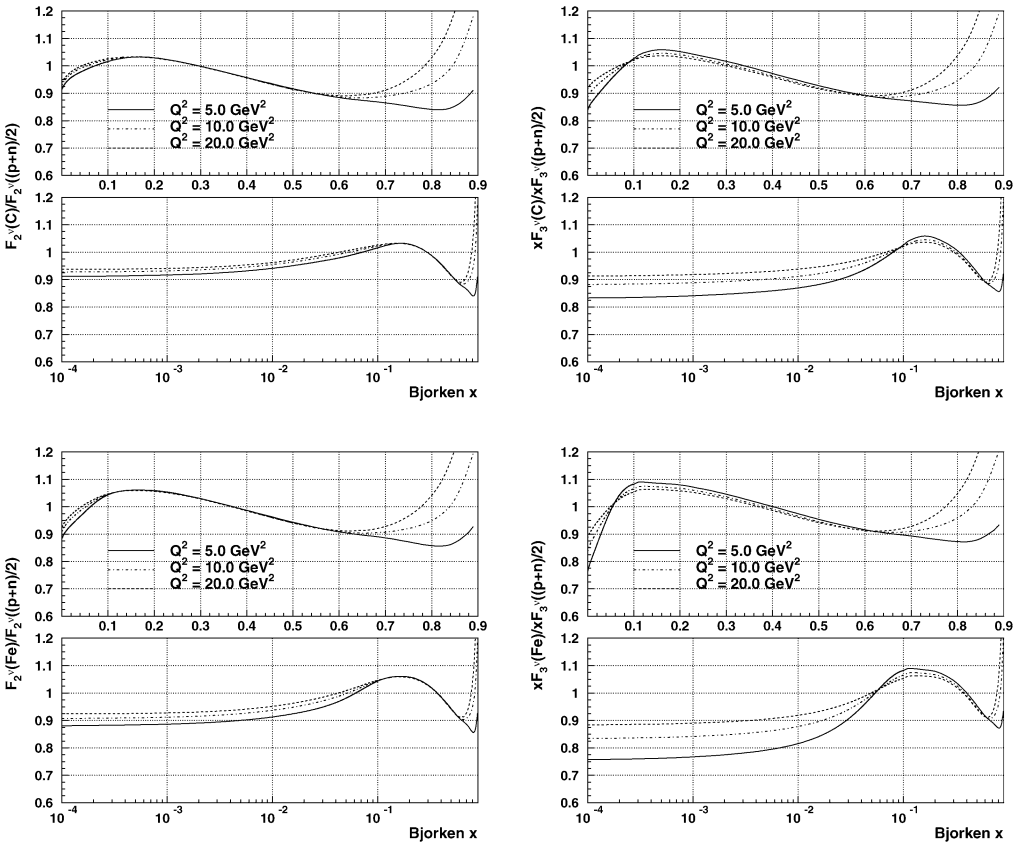


Fig. 16. Our predictions for the ratios $\mathcal{R}_2$ (left plots) and $\mathcal{R}_3$ (right plots) for neutrino scattering on $^{12}$C and $^{56}$Fe (see text). The curves are drawn for $Q^2 = 5$, 10, 20 GeV$^2$.

### *7.2. Neutrino interactions with nuclei*

In this section we calculate nuclear effects for neutrino charged-current structure functions using the approach developed in the previous sections. The study of neutrino interactions is particularly interesting to this end since they are flavour sensitive and they are strongly influenced by the structure function $F_3$, which is not present in the electromagnetic case. We also note that due to the low interaction probability in practice the detection of neutrinos always requires heavy nuclear targets. Therefore, the knowledge of nuclear effects is crucial for understanding of neutrino cross sections.

In order to compute corrections to $F_2^\nu$ and $F_3^\nu$ related to the averaging with nuclear spectral function (FMB and OS effects) we apply Eqs. (27) and (28) and use the off-shell function $\delta f_2$ extracted from the analysis of Section 5.7.2 for both $F_2$ and $F_3$. Nuclear shadowing/antishadowing corrections are computed as discussed in Section 4.2.

We focus here on the region of relatively high momentum transfer $Q^2 > 5$ GeV$^2$ and assume that coherent nuclear interactions driven by axial current are similar to those of vector current at large $Q^2$ and that they can be described by the effective amplitude extracted from the analysis of

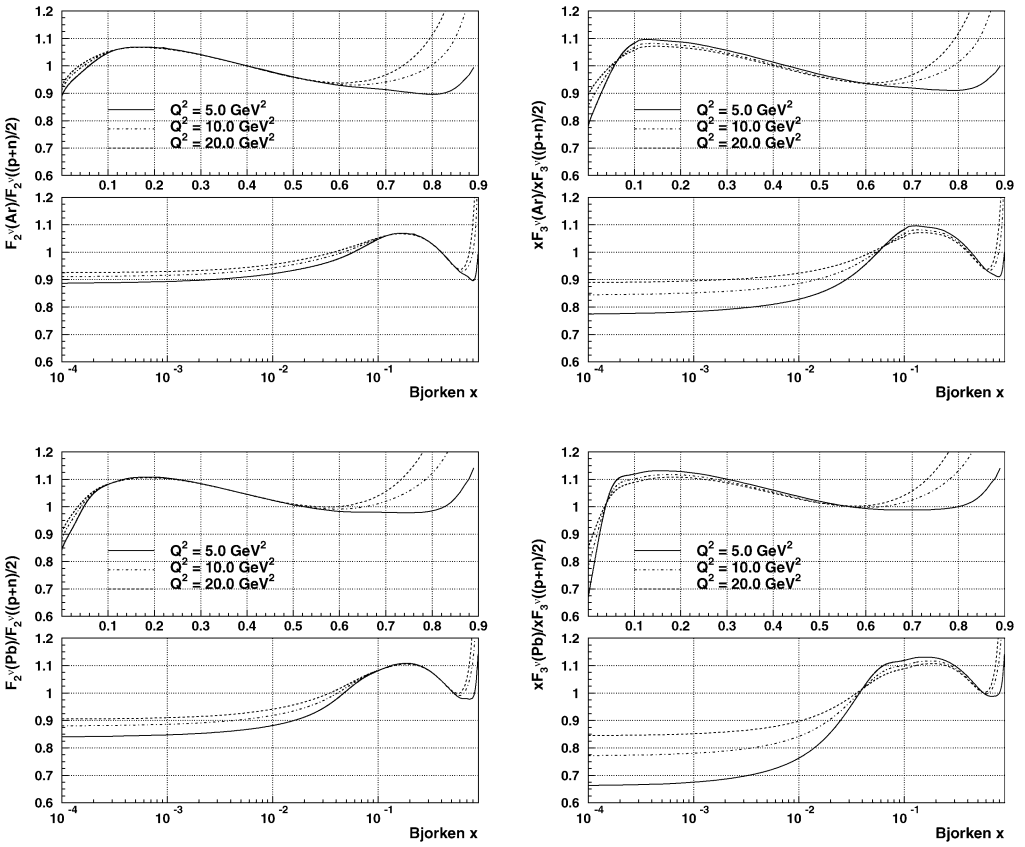


Fig. 17. Our predictions for the ratios $\mathcal{R}_2$ (left plots) and $\mathcal{R}_3$ (right plots) for neutrino scattering on $^{40}$Ar and $^{208}$Pb (see text). The curves are drawn for $Q^2 = 5$, 10, 20 GeV$^2$.

Sections 5.5 to 5.7.3.[15] A detailed study of nuclear effects in (anti)neutrino interactions including the low $Q^2$ region will be the subject of a future publication [80].

We calculate the ratios $\mathcal{R}_2^{\nu} = F_2^{\nu A}/(A F_2^{\nu N})$ and $\mathcal{R}_3^{\nu} = x F_3^{\nu A}/(A x F_3^{\nu N})$, where $N$ denotes the isoscalar nucleon (averaged over proton and neutron), for the most common nuclear targets used by recent neutrino experiments: $^{12}$C (NOMAD [81]), $^{56}$Fe (NuTeV [82], MINOS [83]), $^{40}$Ar (ICARUS [84]) and $^{207}$Pb (OPERA [85], CHORUS [89]). Our results for both $F_2$ and $xF_3$ are shown in Figs. 16 and 17 for different values of $Q^2$. We briefly comment on the main features that distinguish the nuclear corrections in neutrino DIS from the ones in charged-lepton DIS ($F_2^{\mu}$). By comparing Figs. 8 and 16 we observe that nuclear effects for $F_2^{\nu}$ and $F_2^{\mu}$ in the coherent region are similar (note that we restrict the present discussion to relatively high $Q^2$). However, at large $x$ nuclear effects for $F_2^{\nu}$ and $F_2^{\mu}$ are somewhat different. In particular, we note that $\mathcal{R}_2^{\nu} > \mathcal{R}_2^{\mu}$ in the dip region of $x \sim 0.6$–$0.8$. This is because the neutron excess correction is positive for $F_2^{\nu}$, while it is negative for $F_2^{\mu}$. From Figs. 16 and 17 one can also observe that nuclear effects at

[15] Note that the interactions of the axial-vector current at low $Q^2$ are essentially different from those of the vector current. This region requires a special analysis which goes beyond the scope of the present paper.

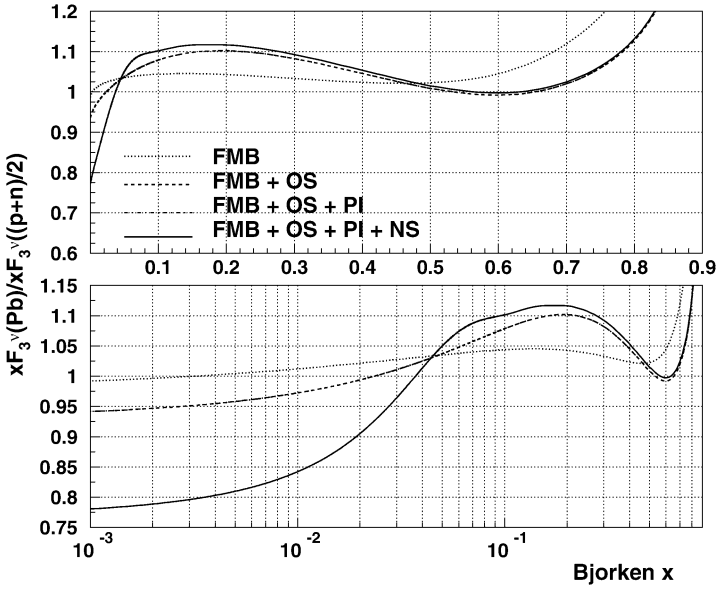


Fig. 18. Comparison of different nuclear effects calculated for neutrino $xF_3$ at $Q^2 = 10$ GeV$^2$ for $^{207}$Pb target. The labels on the curves correspond to the effects included in turn: the averaging with nuclear spectral function (FMB), off-shell correction (OS), nuclear pion excess (PI) and coherent multiple-scattering correction (NS). The calculation takes into account the target mass and the neutron excess corrections. Note that $xF_3$ is not corrected for pion excess effect (overlapping dashed and dashed-dotted curves).

large $x$ are similar for neutrino $F_2$ and $xF_3$. However, at small $x$ the nuclear shadowing effect for $xF_3$ is systematically larger as follows from Eq. (60).

Fig. 18 illustrates different nuclear corrections to $xF_3^\nu$ for $^{207}$Pb target computed at fixed $Q^2$. The enhancement at intermediate $x$ values is a joined effect of all considered nuclear correction (see also Fig. 15 and discussion in Section 7.1.2). In the case of $F_2$ the "antishadowing" at $x \sim 0.1$ is due to off-shell and nuclear pion corrections.[16] Note that the nuclear pion excess effect can be neglected in the case of $xF_3$, in contrast to the case of $F_2$. Indeed, in the isoscalar nucleus the pion correction depends on pion structure functions averaged over different pion states and $F_3^\pi$ vanishes after such averaging. A small isovector correction which is proportional to $\pi^+ - \pi^-$ asymmetry in the nuclear pion distribution functions (see Eq. (105)) is also neglected.

The study of $xF_3$ is particularly important since it allows to test the normalization of nuclear valence quark number. As discussed in Sections 6.1 and 6.2 the conservation of the nuclear valence quark number was used in our analysis in order to test the balance between nuclear shadowing and off-shell effects. The valence quark (baryon) number of the target is related to the integral of neutrino and antineutrino averaged $F_3$, the Gross–Llewellyn-Smith (GLS) sum rule [90]. We remark, however, that in QCD this relation is not exact and only holds in the leading twist and the leading order in $\alpha_S$ and is corrected by both the radiative [91] and the higher-twist effects. It would be interesting to experimentally address the question of nuclear modification of the GLS sum rule. New measurements of $xF_3$ from neutrino and antineutrino scattering off

[16] See also Fig. 3 for $F_2^\mu$. Note, however, that the neutron excess correction has a different sign for $F_2^\mu$ and $F_2^\nu$ that explains the differences between the magnitude of nuclear effects in Figs. 3 and 17.

Table 5
List of recent nuclear data which can be used to study nuclear effects on neutrino structure functions

| Experiment | Targets | CC statistics ($\times 10^6$) | Data taking | Reference |
|---|---|---|---|---|
| NOMAD | $^{12}$C | 1.3(0.06) $\nu(\bar{\nu})$ | 1995–1998 | [81] |
| | $^{27}$Al | 1.5(0.07) $\nu(\bar{\nu})$ | | |
| | $^{56}$Fe | 12.5(0.6) $\nu(\bar{\nu})$ | | |
| CHORUS | $^{207}$Pb | 1.3(0.3) $\nu(\bar{\nu})$ | 1998 | [89] |
| NuTeV | $^{56}$Fe | 2.7(1.2) $\nu(\bar{\nu})$ | 1996–1997 | [82] |

different nuclei would help to clarify this issue, provided they can reach a precision comparable to the size of the effects we observe in our analysis (typically 1%, see Fig. 5).

We conclude this section by remarking that in spite of the major interest of neutrinos as a probe for nuclear effects, virtually no precise experimental information is available so far in DIS region. The only direct measurements of nuclear effects on neutrino DIS cross sections were performed by BEBC [86] ($^{20}$Ne/D) and CDHSW [87] ($^{56}$Fe/$p$). However, these results are affected by large statistical and systematic uncertainties. It should be emphasized that neutrino DIS provides information complementary to that of the charged-lepton scattering and, therefore, the completion of new high-statistics measurements would have a large impact on our understanding of nuclear effects. The NOMAD experiment [81] collected large neutrino samples on $^{12}$C, $^{27}$Al and $^{56}$Fe targets allowing a study of nuclear effects from $^{27}$Al/$^{12}$C and $^{56}$Fe/$^{12}$C ratios [19]. The recent NuTeV cross section data [88] also provide information on nuclear effects in $^{56}$Fe. In addition, the CHORUS experiment [89] is extracting neutrino cross sections from the interactions collected on $^{207}$Pb. Table 5 summarizes the various (anti)neutrino data samples.

## 8. Summary

We presented a detailed phenomenological study of unpolarized nuclear structure functions for a wide kinematical region of $x$ and $Q^2$. A general approach was developed which, on one side, includes the main nuclear corrections and, on the other side, provides a good description of data on nuclear structure functions. We take into account the QCD treatment of the nucleon structure functions and address a number of nuclear effects including nuclear shadowing, Fermi motion and nuclear binding, nuclear pions and off-shell corrections to bound nucleon structure functions.

Starting from a relativistic approach in the description of nuclear DIS we then exploited the fact that characteristic energy and momentum of bound nucleon are small compared to the nucleon mass. This allowed us to compute nuclear corrections in terms of non-relativistic nuclear spectral function, the quantity which is well constrained by data at low- and intermediate-energy regions. Our analysis suggested that data cannot be quantitatively explained in impulse approximation by applying "standard" Fermi motion and nuclear binding corrections even at large $x$. This motivated us to address the off-shell effect in bound nucleon structure functions. This correction was parametrized in terms of a few parameters which were extracted from data, together with their uncertainties. The effective scattering amplitude which determines the magnitude of nuclear shadowing effect was also addressed phenomenologically.

It should be emphasized that the phenomenological parameters of our model refer to the nucleon structure and for this reason they are common to all nuclei. We verified this hypothesis by extracting them from different subsets of nuclei. Overall, we obtained an excellent agreement between our calculations and data by using only three independent parameters. Our results show

that inclusive nuclear DIS data have a good sensitivity to off-shell effects, allowing a precise determination of this correction. We also note that the study of semi-inclusive nuclear DIS in which the kinematics of the active nucleon can be controlled by selecting certain final states would provide additional information on the off-shell effect.

The off-shell effect is related to the modification of the nucleon structure in nuclear environment. This relation was discussed in terms of a simple model in which the off-shell effect at large $x$ was linked to the modification of the bound nucleon core radius. We found that the off-shell correction derived from our analysis favours the increase in the nucleon core radius in nuclear environment.

We studied in detail the $Q^2$ and $A$ dependencies of nuclear corrections. One important application was the calculation of nuclear effects for deuterium, which is of primary interest for the problem of the extraction of the neutron structure functions. We also applied our model to study nuclear valence and sea quark distributions, as well as the flavour (isospin) dependence of nuclear effects.

Another important application was the calculation of nuclear structure functions for neutrino scattering. In the present paper we evaluated nuclear corrections for charged-current neutrino structure functions for relatively high $Q^2$, which are relevant for the analysis of existing DIS neutrino data. More detailed studies of neutrino and antineutrino interactions for both charged-current and neutral-current scattering are planned in future publications.

**Acknowledgements**

We would like to thank M. Arneodo for useful information on NMC data, S. Alekhin, A. Butkevich and A. Kataev for fruitful discussions on different stages of this work. The work of S.K. was partially supported by the Russian Foundation for Basic Research grant 03-02-17177 and by INTAS project 03-51-4007.

## Appendix A. Integration in nuclear convolution

The integration in convolution formulas is constrained by the requirement that the invariant mass of bound nucleon and the virtual photon is high enough for producing physical final states. In particular, for the region of invariant masses of final states larger than a given mass $M_X$ the required relation is

$$W^2 \geqslant M_X^2, \tag{A.1}$$

where $W^2 = (p+q)^2$ and $p$ the four-momentum of the bound nucleon. The threshold of inelastic channels corresponds to pion production and $M_X = M + m_\pi$ and by setting $M_X = M$ we include the elastic channel. Here we discuss in detail the constraints on the integration region in the convolution formulas due to Eq. (A.1). Note that Eq. (A.1) is equivalent to

$$p_0 + q_0 \geqslant E_X, \tag{A.2}$$

where $E_X = (M_X^2 + (\boldsymbol{p}+\boldsymbol{q})^2)^{1/2}$ and $p_0 = M + \varepsilon$. Using this equation we can write the integral over the bound nucleon four-momentum in convolution formulas as

$$\int \mathrm{d}^4 p\, \theta\big(W^2 - M_X^2\big) = \int \mathrm{d}^3 \boldsymbol{p} \int\limits_{E_X - q_0 - M} \mathrm{d}\varepsilon. \tag{A.3}$$

This equation should be applied together with the nuclear spectral function and other functions in the convolution formulas. The energy integration in Eq. (A.3) corresponds to the integration over the excitation energies of the residual nucleus.

We first consider the spectral function

$$\mathcal{P}(\varepsilon, \boldsymbol{p}) = 2\pi\delta(\varepsilon - \varepsilon_{\boldsymbol{p}})n(\boldsymbol{p}), \tag{A.4}$$

$$\varepsilon_{\boldsymbol{p}} = \varepsilon_0 - \boldsymbol{p}^2/(2m_0). \tag{A.5}$$

This is the relevant case for the deuterium, for which $\varepsilon_0 = \varepsilon_D$ and $m_0 = M$ (see Eq. (39)), and also for the model spectral function $\mathcal{P}_{\rm MF}$ with $m_0 = M_{A-1}$ the mass of the residual nucleus and $\varepsilon_0 = -E^{(1)}$ the nucleon separation energy averaged over mean-field configurations of the residual nucleus (see Eq. (74) and the discussion thereafter).

The energy integration in Eq. (A.3) can easily be performed and inequality (A.2) then becomes

$$q_0 + M + \varepsilon_{\boldsymbol{p}} \geqslant E_X. \tag{A.6}$$

This inequality provides the constraints on the momentum space in Eq. (A.3). In order to solve it explicitly we chose the coordinate system such that the momentum transfer has only longitudinal component $q = (q_0, \boldsymbol{0}_\perp, -|\boldsymbol{q}|)$. Then after some algebra (A.6) can be written as (we retain only the terms linear in $\varepsilon_{\boldsymbol{p}}$)

$$\boldsymbol{p}^2/(2m_*) - p_z - p_* \leqslant 0, \tag{A.7}$$

where the notations are

$$\gamma p_* = M\left[1 - x\left(1 + \frac{\Delta}{Q^2}\right) + \frac{\varepsilon_0\gamma_2}{M}\right], \tag{A.8a}$$

$$m_* = \frac{m_0|\boldsymbol{q}|}{m_0 + q_0 + M}, \tag{A.8b}$$

and $\Delta = M_X^2 - M^2$, $\gamma = |\boldsymbol{q}|/q_0$, and $\gamma_2 = 1 + M/q_0$.

Inequality (A.7) is most easily solved in terms of *longitudinal* and *transverse coordinates*, $\boldsymbol{p} = (\boldsymbol{p}_\perp, p_z)$. In this case, the solution to (A.7) can be written as

$$\begin{cases} p_z^- \leqslant p_z \leqslant p_z^+, \\ 0 \leqslant \boldsymbol{p}_\perp^2 \leqslant T^2, \end{cases} \tag{A.9}$$

where $T^2 = m_*^2 + 2m_* p_*$ is maximum transverse momentum squared of the bound nucleon (for the given kinematical conditions) and $p_z^\pm$ correspond to those longitudinal momenta at which the left side of (A.7) is 0,

$$p_z^\pm = m_* \pm \left(T^2 - \boldsymbol{p}_\perp^2\right)^{1/2}. \tag{A.10}$$

The momentum integral in Eq. (A.3) in terms of these variables is

$$\int\limits_{W^2 \geqslant M_X^2} \mathrm{d}^3\boldsymbol{p} = \pi\,\theta(T) \int\limits_0^{T^2} \mathrm{d}p_\perp^2 \int\limits_{p_z^-}^{p_z^+} \mathrm{d}p_z. \tag{A.11}$$

The requirement $T^2 \geqslant 0$ gives the constraint on possible $x$ and $Q^2$ in inelastic scattering off bound nucleon.[17]

In *spherical coordinates* we introduce the azimuthal angle $\theta$ between the $z$-axis and the direction of the momentum $p_z = p\cos\theta$ (here $p = |\boldsymbol{p}|$). The solution to (A.7) splits into two different regions with respect to the sign of $p_*$ and the momentum integral in convolution formula can be written as

$$\int\limits_{W^2\geqslant M_X^2} \mathrm{d}^3\boldsymbol{p} = \begin{cases} 2\pi \int_{-1}^{1} \mathrm{d}\cos\theta \int_0^{p_+(\cos\theta)} \mathrm{d}p\; p^2, & \text{if } p_* > 0, \\ 2\pi \int_{c_*}^{1} \mathrm{d}\cos\theta \int_{p_-(\cos\theta)}^{p_+(\cos\theta)} \mathrm{d}p\; p^2, & \text{if } -\frac{m_*}{2} \leqslant p_* \leqslant 0, \end{cases} \tag{A.12}$$

where $p_\pm(\cos\theta)$ are the values of $p$ at which the left side of (A.7) is 0

$$p_\pm(\cos\theta) = m_*\cos\theta \pm \sqrt{(m_*\cos\theta)^2 + 2m_* p_*} \tag{A.13}$$

and $c_* = (2|p_*|/m_*)^{1/2}$. The first case in (A.12) applies if $x < 1$ as can be readily seen from Eqs. (A.8), while the last case concerns the regions $x \sim 1$ and $x > 1$.

We now consider generic spectrum in Eq. (A.3). The upper limit of energy integration is determined by the threshold separation energy $\varepsilon_{\rm th}$. We recall that in our notations the separation energy $\varepsilon = E_0^A - E^{A-1}$, where $E_0^A$ is the ground state energy of the target nucleus and $E^{A-1}$ is the energy of the residual nucleus including the recoil energy. Therefore, for the given recoil momentum $\varepsilon_{\rm th} = \varepsilon_0 - \boldsymbol{p}^2/(2m_0)$, where $\varepsilon_0 = E_0^A - E_0^{A-1}$ is the difference of the ground state energies of the target and the residual nucleus and $m_0 = M_{A-1}$ is the mass of the residual nucleus. The constraints on the momentum space in Eq. (A.3) directly follow from

$$E_X - q_0 - M \leqslant \varepsilon_{\rm th}. \tag{A.14}$$

This inequality, written in terms of $\varepsilon_0$ and $m_0$, is equivalent to (A.6). Therefore, the discussion of (A.6) can be taken over (A.14). In particular, the solutions to (A.14) in terms of the longitudinal and transverse momentum are given by Eqs. (A.9) and (A.10). The integration in (A.3) in terms of these variables can be written as

$$\int\limits_{W^2\geqslant M_X^2} \mathrm{d}^4 p = \pi\,\theta\big(T^2\big) \int\limits_0^{T^2} \mathrm{d}p_\perp^2 \int\limits_{p_z^-}^{p_z^+} \mathrm{d}p_z \int\limits_{E_X - q_0 - M}^{\varepsilon_{\rm th}} \mathrm{d}\varepsilon, \tag{A.15}$$

where the limits of integration are similar to those in Eq. (A.11) and given by (A.8)–(A.10).

The integration in spherical coordinates is

$$\int\limits_{W^2\geqslant M_X^2} \mathrm{d}^4 p = \begin{cases} 2\pi \int_{-1}^{1} \mathrm{d}\cos\theta \int_0^{p_+(\cos\theta)} \mathrm{d}p\; p^2 \int_{E_X-q_0-M}^{\varepsilon_{\rm th}} \mathrm{d}\varepsilon, & \text{if } p_* > 0, \\ 2\pi \int_{c_*}^{1} \mathrm{d}\cos\theta \int_{p_-(\cos\theta)}^{p_+(\cos\theta)} \mathrm{d}p\; p^2 \int_{E_X-q_0-M}^{\varepsilon_{\rm th}} \mathrm{d}\varepsilon, & \text{if } -\frac{m_*}{2} \leqslant p_* \leqslant 0, \end{cases} \tag{A.16}$$

where the notations are similar to those in Eq. (A.12).

[17] The equation $T^2 = 0$ determines the maximum possible $x$ which can be achieved in DIS from bound nucleon. In application to the deuteron this gives $x = 3/2$ (neglecting $Q^{-2}$ terms and $\varepsilon_d/M$ corrections in Eq. (A.8)). This is different from the kinematical maximum $x = M_D/M \approx 2$, which corresponds to elastic scattering from the deuteron as a whole. We comment that the limit $x = 3/2$ was derived keeping linear terms in $\varepsilon/M$. However, the events with such large $x$ are due to high-momentum configurations $p \sim M$ in the wave function and, therefore, require fully relativistic description.

## Appendix B. Multiple scattering coefficients for uniform nuclear density

The magnitude of coherent nuclear effects in the $C$-even and $C$-odd structure functions $F_2$ and $F_3$ is determined by the terms $\mathcal{C}_2^A$ and $\mathcal{C}_3^A$ (see Eqs. (62) and (67)). These quantities can be computed analytically for uniform density distribution with a sharp edge (square well model), $\rho_A(\boldsymbol{r}) = \rho_0\theta(R_A - |\boldsymbol{r}|)$, which is a reasonable approximation for large nuclei [65]. The nuclear radius $R_A$ in this model is related to the r.m.s. nuclear radius as $R_A^2 = \frac{5}{3}\langle r^2\rangle$ and the central nuclear density is $\rho_0 = A/(\frac{4\pi}{3}R_A^3)$ with $A$ the number of nucleons. The coefficients $\mathcal{C}_2^A$ and $\mathcal{C}_3^A$ are

$$\mathcal{C}_2^A = A\rho_0 R_A\,\varphi_2^{\rm SW}(y), \tag{B.1a}$$

$$\mathcal{C}_3^A = A(\rho_0 R_A)^2\varphi_3^{\rm SW}(y), \tag{B.1b}$$

where $\varphi_{2,3}^{\rm SW}$ are the functions of dimensionless and complex variable $y = 2i(\rho_0 a - k_L)R_A$

$$\varphi_2^{\rm SW}(y) = \big[6 - 3y^2 - 2y^3 + 6(y-1)\exp(y)\big]/y^4, \tag{B.2a}$$

$$\varphi_3^{\rm SW}(y) = 12\big[-4 + y^2 + y^3/3 + (2-y)^2\exp(y)\big]/y^5. \tag{B.2b}$$

If the real part of the amplitude $a$ and $k_L$ can be neglected (which is a reasonable approximation for $x \ll 0.1$), then $y = R_A/l_f$ with $l_f = (\rho_0\sigma)^{-1}$ the mean free path of the particle in a nucleus.

## References


[1] J.J. Aubert, et al., Phys. Lett. B 123 (1983) 275.
[2] M. Arneodo, et al., New Muon Collaboration, Nucl. Phys. B 487 (1997) 3.
[3] M. Arneodo, et al., New Muon Collaboration, Nucl. Phys. B 441 (1995) 12, hep-ex/9504002.
[4] P. Amaudruz, et al., New Muon Collaboration, Nucl. Phys. B 441 (1995) 3, hep-ph/9503291.
[5] M. Arneodo, et al., New Muon Collaboration, Nucl. Phys. B 481 (1996) 3.
[6] M. Arneodo, et al., New Muon Collaboration, Nucl. Phys. B 481 (1996) 23.
[7] J. Ashman, et al., European Muon Collaboration, Z. Phys. C 57 (1993) 211.
[8] G. Bari, et al., BCDMS Collaboration, Phys. Lett. B 163 (1985) 282.
[9] S. Dasu, et al., Phys. Rev. Lett. 60 (1988) 2591.
[10] J. Gomez, et al., Phys. Rev. D 49 (1994) 4348.
[11] M.R. Adams, et al., E665 Collaboration, Phys. Rev. Lett. 75 (1995) 1466.
[12] M.R. Adams, et al., E665 Collaboration, Z. Phys. C 67 (1995) 403, hep-ex/9505006.
[13] J. Arrington, R. Ent, C.E. Keppel, J. Mammei, I. Niculescu, nucl-ex/0307012.
[14] D.M. Alde, et al., Phys. Rev. Lett. 64 (1990) 2479;
M.A. Vasilev, et al., FNAL E866 Collaboration, Phys. Rev. Lett. 83 (1999) 2304, hep-ex/9906010;
G. Moreno, et al., Phys. Rev. D 43 (1991) 2815.
[15] K.H. Ackermann, et al., STAR Collaboration, Nucl. Instrum. Methods A 499 (2003) 624;
M. Adamczyk, et al., BRAHMS Collaboration, Nucl. Instrum. Methods A 499 (2003) 437;
K. Adcox, et al., PHENIX Collaboration, Nucl. Instrum. Methods A 499 (2003) 469;
B.B. Back, et al., PHOBOS Collaboration, Nucl. Instrum. Methods A 499 (2003) 603.
[16] F. Carminati, et al., ALICE Collaboration, J. Phys. G 30 (2004) 1517;
ATLAS Collaboration, CERN/LHCC/2004-009, LHCC I-013;
P.P. Yepes, CMS Collaboration, Nucl. Phys. A 698 (2002) 456, nucl-ex/0104026.
[17] G.A. Miller, A.W. Thomas, hep-ex/0204007;
S. Kovalenko, I. Schmidt, J.J. Yang, Phys. Lett. B 546 (2002) 68, hep-ph/0207158;
S. Kumano, Phys. Rev. D 66 (2002) 111301, hep-ph/0209200;
S.A. Kulagin, Phys. Rev. D 67 (2003) 091301, hep-ph/0301045;
S. Kumano, hep-ph/0307105;
S.A. Kulagin, hep-ph/0406220;
S.A. Kulagin, Nucl. Phys. B. (Proc. Suppl.) 139 (2005) 213, hep-ph/0409057;
S.J. Brodsky, I. Schmidt, J.J. Yang, Phys. Rev. D 70 (2004) 116003, hep-ph/0409279.

[18] G.P. Zeller, et al., Phys. Rev. Lett. 88 (2002) 091802, hep-ex/0110059.
[19] R. Petti, hep-ex/0411032.
[20] J. Hylen, et al., Fermilab Report No. TM-2018 (1997);
L. Bartoszek, et al., hep-ex/0408121;
D. Drakoulakos, et al., hep-ex/0405002.
[21] Japan Proton Accelerator Research Complex, Tokai, Japan, URL: http://jkj.tokai.jaeri.go.jp/.
[22] M.L. Mangano, et al., hep-ph/0105155;
A. Blondel, et al., CERN-2004-002;
M.M. Alsharoa, et al., Muon Collider/Neutrino Factory Collaboration, Phys. Rev. ST Accel. Beams 6 (2003) 081001, hep-ex/0207031.
[23] Jefferson Laboratory, Newport News, USA, URL: http://www.jlab.org/.
[24] G. Piller, W. Weise, Phys. Rep. 330 (2000) 1, hep-ph/9908230.
[25] D.F. Geesaman, K. Saito, A.W. Thomas, Annu. Rev. Nucl. Part. Sci. 45 (1995) 337.
[26] M. Arneodo, Phys. Rep. 240 (1994) 301.
[27] L.L. Frankfurt, M.I. Strikman, Phys. Rep. 160 (1988) 235.
[28] B.L. Ioffe, V.A. Khoze, L.N. Lipatov, Hard Processes. Vol. 1: Phenomenology, Quark Parton Model, Elsevier, North-Holland, 1984.
[29] C.H. Albright, C. Jarlskog, Nucl. Phys. B 84 (1975) 467.
[30] S. Kretzer, M.H. Reno, Phys. Rev. D 66 (2002) 113007, hep-ph/0208187.
[31] K.G. Wilson, Phys. Rev. 179 (1969) 1499;
E.V. Shuryak, A.I. Vainshtein, Nucl. Phys. B 199 (1982) 451.
[32] R. Brock, et al., CTEQ Collaboration, Rev. Mod. Phys. 67 (1995) 157.
[33] L.N. Lipatov, Sov. J. Nucl. Phys. 20 (1975) 94, Yad. Fiz. 20 (1974) 181;
G. Altarelli, G. Parisi, Nucl. Phys. B 126 (1977) 298;
Yu.L. Dokshitzer, Sov. Phys. JETP 46 (1977) 641, Zh. Eksp. Teor. Fiz. 73 (1977) 1216.
[34] W. Furmanski, R. Petronzio, Z. Phys. C 11 (1982) 293.
[35] W.L. van Neerven, E.B. Zijlstra, Phys. Lett. B 272 (1991) 127;
W.L. van Neerven, E.B. Zijlstra, Nucl. Phys. B 383 (1992) 525;
D.I. Kazakov, A.V. Kotikov, Phys. Lett. B 291 (1992) 171.
[36] S. Moch, J.A.M. Vermaseren, A. Vogt, Nucl. Phys. B 688 (2004) 101, hep-ph/0403192;
A. Vogt, S. Moch, J.A.M. Vermaseren, Nucl. Phys. B 691 (2004) 129, hep-ph/0404111.
[37] H. Georgi, H.D. Politzer, Phys. Rev. D 14 (1976) 1829.
[38] O. Nachtmann, Nucl. Phys. B 63 (1973) 237.
[39] S.I. Alekhin, Phys. Rev. D 68 (2003) 014002, hep-ph/0211096.
[40] J. Pumplin, D.R. Stump, J. Huston, H.L. Lai, P. Nadolsky, W.K. Tung, JHEP 0207 (2002) 012, hep-ph/0201195.
[41] A.D. Martin, R.G. Roberts, W.J. Stirling, R.S. Thorne, Eur. Phys. J. C 23 (2002) 73, hep-ph/0110215.
[42] M. Gluck, E. Reya, I. Schienbein, Eur. Phys. J. C 10 (1999) 313, hep-ph/9903288.
[43] G.B. West, Ann. Phys. 74 (1972) 464;
D. Kusno, M.J. Moravcsik, Phys. Rev. D 20 (1979) 2734;
A. Bodek, J.L. Ritchie, Phys. Rev. D 23 (1981) 1070.
[44] S.V. Akulinichev, S.A. Kulagin, G.M. Vagradov, Phys. Lett. B 158 (1985) 485;
S.V. Akulinichev, S. Shlomo, S.A. Kulagin, G.M. Vagradov, Phys. Rev. Lett. 55 (1985) 2239;
B.L. Birbrair, A.B. Gridnev, M.B. Zhalov, E.M. Levin, V.E. Starodubsky, Phys. Lett. B 166 (1986) 119;
H. Jung, G.A. Miller, Phys. Lett. B 200 (1988) 351;
C. Ciofi degli Atti, S. Liuti, Phys. Rev. C 41 (1990) 1100;
P.J. Mulders, A.W. Schreiber, H. Meyer, Nucl. Phys. A 549 (1992) 498;
V. Barone, M. Genovese, N.N. Nikolaev, E. Predazzi, B.G. Zakharov, Z. Phys. C 58 (1993) 541;
V.V. Burov, A.V. Molochkov, G.I. Smirnov, Phys. Lett. B 466 (1999) 1, nucl-th/9904050;
S.A. Gurvitz, A.S. Rinat, Phys. Rev. C 65 (2002) 024310, nucl-th/0106032.
[45] G.V. Dunne, A.W. Thomas, Phys. Rev. D 33 (1986) 2061.
[46] F. Gross, S. Liuti, Phys. Rev. C 45 (1992) 1374.
[47] S.A. Kulagin, Nucl. Phys. A 500 (1989) 653.
[48] S.A. Kulagin, G. Piller, W. Weise, Phys. Rev. C 50 (1994) 1154, nucl-th/9402015.
[49] S.A. Kulagin, W. Melnitchouk, G. Piller, W. Weise, Phys. Rev. C 52 (1995) 932, hep-ph/9504377.
[50] S.A. Kulagin, Nucl. Phys. A 640 (1998) 435, nucl-th/9801039.
[51] W. Melnitchouk, A.W. Schreiber, A.W. Thomas, Phys. Rev. D 49 (1994) 1183, nucl-th/9311008.

[52] M. Ericson, S. Kumano, Phys. Rev. C 67 (2003) 022201, hep-ph/0212001.
[53] S.I. Alekhin, S.A. Kulagin, S. Liuti, Phys. Rev. D 69 (2004) 114009, hep-ph/0304210.
[54] J.D. Sullivan, Phys. Rev. D 5 (1972) 1732.
[55] C.H. Llewellyn Smith, Phys. Lett. B 128 (1983) 107;
M. Ericson, A.W. Thomas, Phys. Lett. B 128 (1983) 112;
E.L. Berger, F. Coester, Phys. Rev. D 32 (1985) 1071;
B.L. Friman, V.R. Pandharipande, R.B. Wiringa, Phys. Rev. Lett. 51 (1983) 763;
E.E. Sapershtein, M.Z. Shmatikov, JETP Lett. 41 (1985) 53, Pis'ma Zh. Eksp. Teor. Fiz. 41 (1985) 44;
L.P. Kaptari, A.I. Titov, E.L. Bratkovskaya, A.Y. Umnikov, Nucl. Phys. A 512 (1990) 684;
H. Jung, G.A. Miller, Phys. Rev. C 41 (1990) 659;
D.S. Koltun, Phys. Rev. C 57 (1998) 1210, nucl-th/9709033.
[56] R.J. Glauber, Phys. Rev. 100 (1955) 242.
[57] V.N. Gribov, Sov. Phys. JETP 30 (1970) 709, Zh. Eksp. Teor. Fiz. 57 (1969) 1306.
[58] T.H. Bauer, R.D. Spital, D.R. Yennie, F.M. Pipkin, Rev. Mod. Phys. 50 (1978) 261;
T.H. Bauer, R.D. Spital, D.R. Yennie, F.M. Pipkin, Rev. Mod. Phys. 51 (1979) 407, Erratum.
[59] R.D. Spital, D.R. Yennie, Phys. Rev. D 9 (1974) 128.
[60] J. Kwiecinski, B. Badelek, Phys. Lett. B 208 (1988) 508;
N.N. Nikolaev, B.G. Zakharov, Z. Phys. C 49 (1991) 607;
S.J. Brodsky, H.J. Lu, Phys. Rev. Lett. 64 (1990) 1342;
G. Shaw, Phys. Rev. D 47 (1993) 3676;
W. Melnitchouk, A.W. Thomas, Phys. Lett. B 317 (1993) 437, nucl-th/9310005;
G. Piller, W. Ratzka, W. Weise, Z. Phys. A 352 (1995) 427, hep-ph/9504407;
A. Capella, A. Kaidalov, C. Merino, D. Pertermann, J. Tran Thanh Van, Eur. Phys. J. C 5 (1998) 111, hep-ph/9707466;
B.Z. Kopeliovich, J. Raufeisen, A.V. Tarasov, Phys. Lett. B 440 (1998) 151, hep-ph/9807211;
L. Frankfurt, V. Guzey, M. McDermott, M. Strikman, JHEP 0202 (2002) 027, hep-ph/0201230;
J.W. Qiu, I. Vitev, Phys. Lett. B 587 (2004) 52, hep-ph/0401062.
[61] S.A. Kulagin, hep-ph/9812532.
[62] R. Machleidt, K. Holinde, C. Elster, Phys. Rep. 149 (1987) 1.
[63] M. Lacombe, B. Loiseau, J.M. Richard, R. Vinh Mau, J. Cote, P. Pires, R. De Tourreil, Phys. Rev. C 21 (1980) 861.
[64] S. Frullani, J. Mougey, Adv. Nucl. Phys. 14 (1984) 1.
[65] A. deShalit, H. Feshbach, Theoretical Nuclear Physics, Vol. 1: Nuclear Structure, Wiley, 1974.
[66] H. Muther, A. Polls, Prog. Part. Nucl. Phys. 45 (2000) 243, nucl-th/0001007.
[67] C. Ciofi degli Atti, S. Simula, Phys. Rev. C 53 (1996) 1689, nucl-th/9507024.
[68] J.G. Zabolitsky, W. Ey, Phys. Lett. B 76 (1978) 527.
[69] S.A. Kulagin, A.V. Sidorov, Eur. Phys. J. A 9 (2000) 261, hep-ph/0009150.
[70] D.S. Koltun, Phys. Rev. C 9 (1974) 484.
[71] P.D.B. Collins, An Introduction To Regge Theory And High-Energy Physics, Cambridge Univ. Press, Cambridge, 1977.
[72] MINUIT, Function minimization and error analysis, CERN Long Writeup D506.
[73] J.V. Noble, Phys. Rev. Lett. 46 (1981) 412.
[74] F.E. Close, R.L. Jaffe, R.G. Roberts, G.G. Ross, Phys. Rev. D 31 (1985) 1004.
[75] J.P. Chen, et al., Phys. Rev. Lett. 66 (1991) 1283.
[76] K.J. Eskola, V.J. Kolhinen, P.V. Ruuskanen, Nucl. Phys. B 535 (1998) 351, hep-ph/9802350;
K.J. Eskola, V.J. Kolhinen, C.A. Salgado, Eur. Phys. J. C 9 (1999) 61, hep-ph/9807297.
[77] M. Hirai, S. Kumano, M. Miyama, Phys. Rev. D 64 (2001) 034003, hep-ph/0103208;
M. Hirai, S. Kumano, T.H. Nagai, Phys. Rev. C 70 (2004) 044905, hep-ph/0404093.
[78] S.y. Li, X.N. Wang, Phys. Lett. B 527 (2002) 85, nucl-th/0110075.
[79] D. de Florian, R. Sassot, Phys. Rev. D 69 (2004) 074028, hep-ph/0311227.
[80] S.A. Kulagin, R. Petti, in preparation.
[81] J. Altegoer, et al., NOMAD Collaboration, Nucl. Instrum. Methods A 404 (1998) 96.
[82] D.A. Harris, et al., NuTeV Collaboration, Nucl. Instrum. Methods A 447 (2000) 377, hep-ex/9908056.
[83] MINOS Collaboration, Fermilab Report Nos. NuMI-L-337 (1998), NuMI-L-726 (2001).
[84] S. Amerio, et al., ICARUS Collaboration, Nucl. Instrum. Methods A 527 (2004) 329.
[85] M. Guler, et al., CERN/SPSC 2000-028, SPSC/P318, LNGS P25/2000.
[86] P.P. Allport, et al., BEBC WA59 Collaboration, Phys. Lett. B 232 (1989) 417.

[87] H. Abramowicz, et al., Z. Phys. C 25 (1984) 29.
[88] V.A. Radescu, NuTeV Collaboration, hep-ex/0408006.
[89] E. Eskut, et al., CHORUS Collaboration, Nucl. Instrum. Methods A 401 (1997) 7.
[90] D.J. Gross, C.H. Llewellyn Smith, Nucl. Phys. B 14 (1969) 337.
[91] S.G. Gorishnii, S.A. Larin, Phys. Lett. B 172 (1986) 109;
S.A. Larin, J.A.M. Vermaseren, Phys. Lett. B 259 (1991) 345.